USGS
science for a changing world

Groundwater Resources Program

Numerical Simulation of Groundwater Flow in the Columbia Plateau Regional Aquifer System, Idaho, Oregon, and Washington

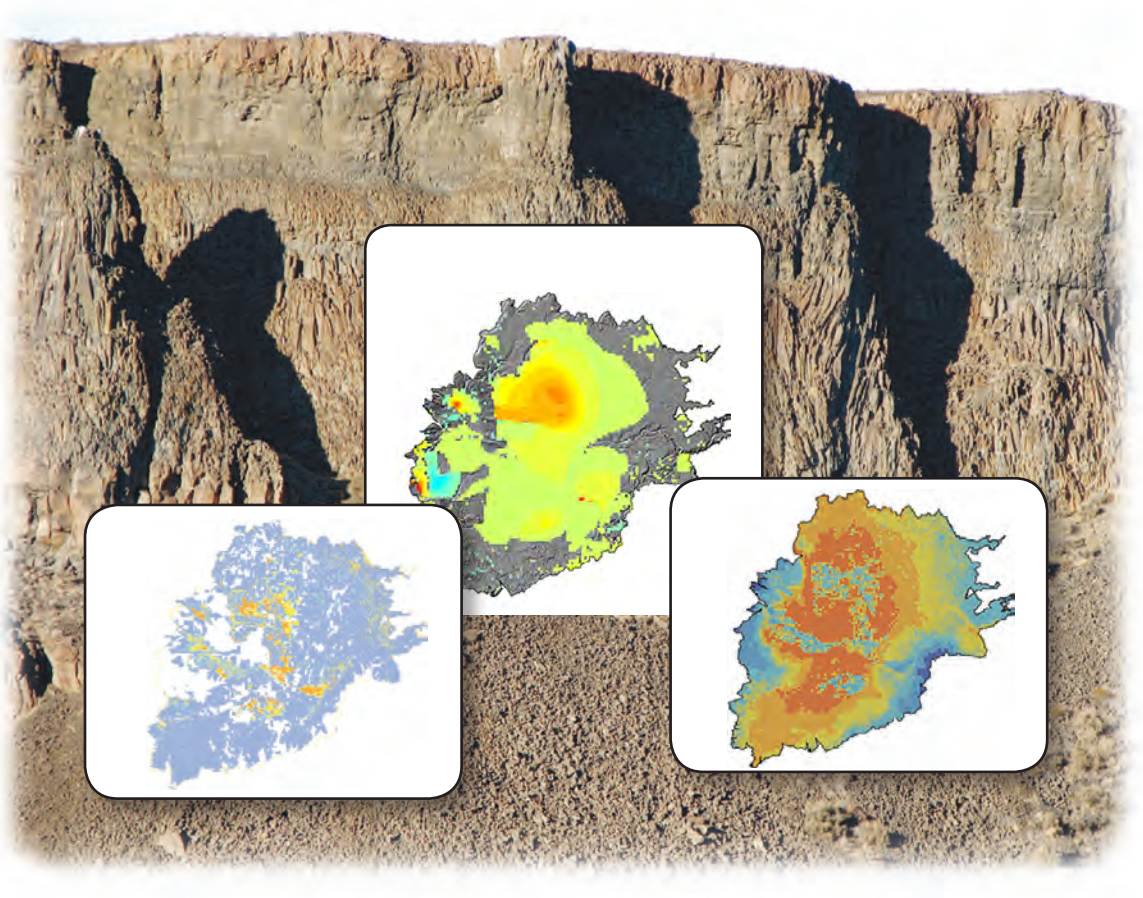

Scientific Investigations Report 2014–5127
Version 1.1, January 2015

U.S. Department of the Interior
U.S. Geological Survey

Cover: Lower left: Mean annual groundwater pumpage for current conditions (2000–2007).

Center foreground: Model-generated upper Grande Ronde unit composite drawdowns from predevelopment to current conditions (2000–2007).

Lower right: Mean annual groundwater recharge for current conditions (2000–2007).

Background: Photograph of Frenchman's Coulee in the vicinity of Quincy, Washington. (Photograph taken by Peter Prehn, private citizen, 2008. Used with permission.)

Numerical Simulation of Groundwater Flow in the Columbia Plateau Regional Aquifer System, Idaho, Oregon, and Washington

By D. Matthew Ely, Erick R. Burns, David S. Morgan, and John J. Vaccaro

Groundwater Resources Program

Scientific Investigations Report 2014–5127
Version 1.1, January 2015

U.S. Department of the Interior
U.S. Geological Survey

U.S. Department of the Interior
SALLY JEWELL, Secretary

U.S. Geological Survey
Suzette M. Kimball, Acting Director

U.S. Geological Survey, Reston, Virginia
First release: 2014
Revised January 2015 (ver. 1.1)

Suggested citation:
Ely, D.M., Burns, E.R., Morgan, D.S., and Vaccaro, J.J., 2014, Numerical simulation of groundwater flow in the Columbia Plateau Regional Aquifer System, Idaho, Oregon, and Washington (ver. 1.1, January 2015): U.S. Geological Survey Scientific Investigations Report 2014–5127, 90 p., *http://dx.doi.org/10.3133/sir20145127*.

ISSN 2328-0328 (online)

Contents

Contents—Continued

Figures

Figures—Continued

Figures—Continued

Tables

Conversion Factors, Datums, and Abbreviations and Acronyms

Conversion Factors

Inch/Pound to SI

Multiply	By	To obtain
	Length	
inch (in.)	2.54	centimeter (cm)
foot (ft)	0.3048	meter (m)
mile (mi)	1.609	kilometer (km)
	Area	
acre	4,047	square meter (m^2)
square mile (mi^2)	2.590	square kilometer (km^2)
	Volume	
cubic mile (mi^3)	4.168	cubic kilometer (km^3)
acre-foot (acre-ft)	1,233	cubic meter (m^3)
	Flow rate	
acre-foot per year (acre-ft/yr)	1,233	cubic meter per year (m^3/yr)
foot per day (ft/d)	0.3048	meter per day (m/d)
cubic foot per second (ft^3/s)	0.02832	cubic meter per second (m^3/s)
inch per year (in/yr)	25.4	millimeter per year (mm/yr)
	Hydraulic conductivity	
foot per day (ft/d)	0.3048	meter per day (m/d)
	Transmissivity*	
foot squared per day (ft^2/d)	0.09290	meter squared per day (m^2/d)

SI to Inch/Pound

Multiply	By	To obtain
	Length	
kilometer (km)	0.6214	mile (mi)

*Transmissivity: The standard unit for transmissivity is cubic foot per day per square foot times foot of aquifer thickness [(ft^3/d)/ft^2]ft. In this report, the mathematically reduced form, foot squared per day (ft^2/d), is used for convenience.

Datums

Vertical coordinate information is referenced to North American Vertical Datum of 1988 (NAVD 88).

Horizontal coordinate information is referenced to the North American Datum of 1983 (NAD 83).

Altitude, as used in this report, refers to distance above the vertical datum.

Conversion Factors, Datums, and Abbreviations and Acronyms

Abbreviations and Acronyms

BCF	Block-Centered Flow package in MODFLOW
CBIP	Columbia Basin Irrigation Project
CONDFACT	conductance factor
CPRAS	Columbia Plateau Regional Aquifer System
CRBG	Columbia River Basalt Group
DRN	Drain package in MODFLOW
ELEVATION	drain elevation
ET	evapotranspiration
GWMA	Ground Water Management Area
HFB	Horizontal-Flow Barrier
HUF	Hydrogeologic-Unit Flow package in MODFLOW
HYSEP	hydrograph separation technique
Kh	horizontal hydraulic conductivity
Kv	vertical hydraulic conductivity
LPF	Layer Property Flow package in MODFLOW
MNW2	Multi-Node Well package in MODFLOW
NHD	National Hydrography Dataset
MODFLOW	USGS modular three-dimensional finite-difference groundwater-flow model
NWT	Newton Solver package in MODFLOW
PEST	parameter estimation software package
PRISM	Parameter-elevation Regressions on Independent Slopes Model
RASA	Regional Aquifer-System Analysis program
RBOT	river bottom elevation
RIV	River package in MODFLOW
RMS	root-mean-square error
SOWAT	SOil WATer balance
Ss	specific storage
STAGE	river stage
Sy	specific yield
UPW	Upstream Weighting package in MODFLOW-2005
USGS	U.S. Geological Survey

Numerical Simulation of Groundwater Flow in the Columbia Plateau Regional Aquifer System, Idaho, Oregon, and Washington

By D. Matthew Ely, Erick R. Burns, David S. Morgan, and John J. Vaccaro

Abstract

A three-dimensional numerical model of groundwater flow was constructed for the Columbia Plateau Regional Aquifer System (CPRAS), Idaho, Oregon, and Washington, to evaluate and test the conceptual model of the system and to evaluate groundwater availability. The model described in this report can be used as a tool by water-resource managers and other stakeholders to quantitatively evaluate proposed alternative management strategies and assess the long-term availability of groundwater. The numerical simulation of groundwater flow in the CPRAS was completed with support from the Groundwater Resources Program of the U.S. Geological Survey Office of Groundwater.

The model was constructed using the U.S. Geological Survey modular three-dimensional finite-difference groundwater-flow model, MODFLOW-NWT. The model uses 3-kilometer (9,842.5 feet) grid cells that subdivide the model domain by 126 rows and 131 columns. Vertically, the model domain was subdivided into six geologic model units. From youngest to oldest, the units are the Overburden, the Saddle Mountains Basalt, the Mabton Interbed, the Wanapum Basalt, the Vantage Interbed, and the Grande Ronde Basalt.

Natural recharge was estimated using gridded historical estimates of annual precipitation for the period 1895–2007. Pre-development recharge was estimated to be the average natural recharge for this period. Irrigation recharge and irrigation pumping were estimated using a remote-sensing based soil-water balance model for the period 1985–2007. Pre-1985 irrigation recharge and pumping were estimated using previously published compilation maps and the history of large-scale irrigation projects. Pumping estimates for municipal, industrial, rural, residential, and all other uses were estimated using reported values and census data. Pumping was assumed to be negligible prior to 1920.

Two models were constructed to simulate groundwater flow in the CPRAS: a steady-state predevelopment model representing conditions before large-scale pumping and irrigation altered the system, and a transient model representing the period 1900–2007. Automated parameter-estimation techniques (steady-state predevelopment model) and traditional trial-and-error (transient model) methods were used for calibration. To calibrate the steady-state and transient models, 10,525 and 46,460 water level measurements, respectively, and 50 base-flow estimates were used.

The steady-state model simulated the shape, slope, and trends of a potentiometric surface that was generally consistent with mapped water levels. For the transient model, the mean and median difference between simulated and measured hydraulic heads is -10 and 4 ft, respectively, with a standard deviation of 164 ft over a 5,648 ft range of measured heads. The residuals for the simulation period show that 52 percent of the simulated heads exceeded measured heads with a median residual value of 43 ft, and 48 percent were less than measured heads with a median residual value of -76 ft.

The CPRAS model was constructed to derive components of the groundwater budget and help understand the interactions of stresses, such as recharge, groundwater pumping, and commingling wells on the groundwater and surface-water system. Through these applications, the model can be used to identify trends in groundwater storage and use, and quantify groundwater availability. The annual groundwater budgets showed several patterns of change over the simulation period. Groundwater pumping was negligible until the 1950s and began to increase significantly during the 1970s and 1980s. Recharge was highly variable due to the interannual variability of precipitation, but began to increase in the late 1940s due to the increase in surface-water irrigation projects. Groundwater contributions to streamflow (base flow) followed recharge closely. However, in areas of significant groundwater-level decline, base flow is reduced.

Groundwater pumping had the greatest effect on water levels, followed by irrigation enhanced recharge. Commingling was a larger factor in structurally complex upland areas where hydraulic-head gradients are naturally high.

Groundwater pumping has increased substantially over the past 40–50 years; this increase resulted in declining water levels at depth and decreased base flows over much of the study area. The effects of pumping are mitigated somewhat by the increase of surface-water irrigation, especially in the shallow Overburden unit, and commingling wells in some areas. During dry to average years, groundwater pumping causes a net loss of groundwater in storage and current condition (2000–2007) groundwater pumping exceeds recharge in all but the wettest of years.

Introduction

The Columbia Plateau Regional Aquifer System (CPRAS) covers approximately 44,000 mi^2 of northeastern Oregon, southeastern Washington, and western Idaho (fig. 1). The area supports a $6 billion-per-year agricultural industry, leading the Nation in production of apples and nine other commodities (State of Washington Office of Financial Management, 2014; U.S. Department of Agriculture, 2007). Groundwater availability in the area is a critical water-resource management issue due to the large water demand for agriculture, economic development, and ecological needs.

The primary aquifers of the CPRAS are basalts of the Columbia River Basalt Group (CRBG) and in places, overlying basin-fill sediments (Overburden). Water-resources issues that have implications for current (2013) and future groundwater availability in the region include (1) widespread water-level declines associated with withdrawals of groundwater for irrigation and other uses, (2) decreases in base flow to rivers and the associated effects on river temperature and water quality, and (3) current and potential effects of global climate change on recharge, base flow, and ultimately, groundwater availability.

The U.S. Geological Survey (USGS) Groundwater Resources Program began a study of the CPRAS in 2007 with the broad goals of (1) characterizing the hydrologic status of the system, (2) identifying trends in groundwater storage and use, and (3) quantifying groundwater availability. The study approach included updating and refining the regional hydrogeologic framework, documenting changes in the status of the system, quantifying the hydrologic budget, and developing a groundwater-flow model for the system. The simulation model, presented here, was used to evaluate and test the conceptual model of the system and to evaluate groundwater availability. Groundwater availability is not only a function of the quantity and quality of water in an aquifer system, but also the physical structures, laws, regulations, and socioeconomic factors that control its demand and use (Reilly and others, 2008). This report discusses the physical characteristics that are important as indicators of groundwater availability.

Purpose and Scope

This report describes the construction, calibration, and application of a numerical model of groundwater flow in the Columbia Plateau Regional Aquifer system. The hydrogeologic framework for constructing the model was documented in a previous report (Kahle and others, 2011) as part of this study. The purposes for constructing the model were to test the conceptual model and to provide an improved understanding of the groundwater-flow system and groundwater availability. The model development is presented and described, and includes information on the spatial and temporal discretization of the aquifer system, boundary conditions, stresses, and hydraulic properties of the hydrogeologic units constituting the aquifer system. Predevelopment and 1900–2007 conditions were simulated to provide a better understanding of current demands on groundwater in the study area.

Previous Investigations

Numerous geologic, hydrologic, and hydrogeologic studies of or within the CPRAS have been done. The earliest works of Smith (1901), Calkins (1905), Waring (1913), Schwennsen and Meinzer (1918), Piper (1932), and Taylor (1948) formed the foundation of our current understanding of the water resources of the Columbia Plateau. A substantial body of work on the geology and hydrology of the CPRAS was produced as part of the USGS Regional Aquifer-System Analysis (RASA) Program of the 1980s and 1990s. A description of the hydrogeologic framework, characteristics of the hydrogeologic units, water budget components, geochemistry of the aquifer system, and regional groundwater-flow system are provided in Whiteman and others (1994).

As part of the USGS groundwater availability study, aspects of the CPRAS, such as the hydrogeology and water-budget components, have been investigated and provided the basis for much of the updated information incorporated in the groundwater-flow model. The model presented in this report is based on the existing USGS groundwater-flow model (CP-RASA) developed by Hansen and others (1994) for the RASA program. The boundaries and much of the initial conceptual understanding of the current model is based on the CP-RASA model. Groundwater-flow models exist for subareas of the CPRAS, including the Columbia Basin Irrigation Project (CBIP) area (Tanaka and others, 1974), Umatilla and Horse Heaven Hills (Davies-Smith and others, 1988), Pullman-Moscow (Barker, 1979; Lum and others, 1990), Horse Heaven Hills (Packard and others, 1996), Hanford Site (Bergeron and others, 1986; Wurstner and others, 1995; Vermeul and others, 2001 and 2003), Yakima River Basin (Ely and others, 2011), Mosier, Oregon (Burns, 2012a), and the Columbia Basin Ground Water Management Area (GWMA) Adams, Franklin, Grant, and Lincoln Counties, Washington (Porcello and others, 2010).

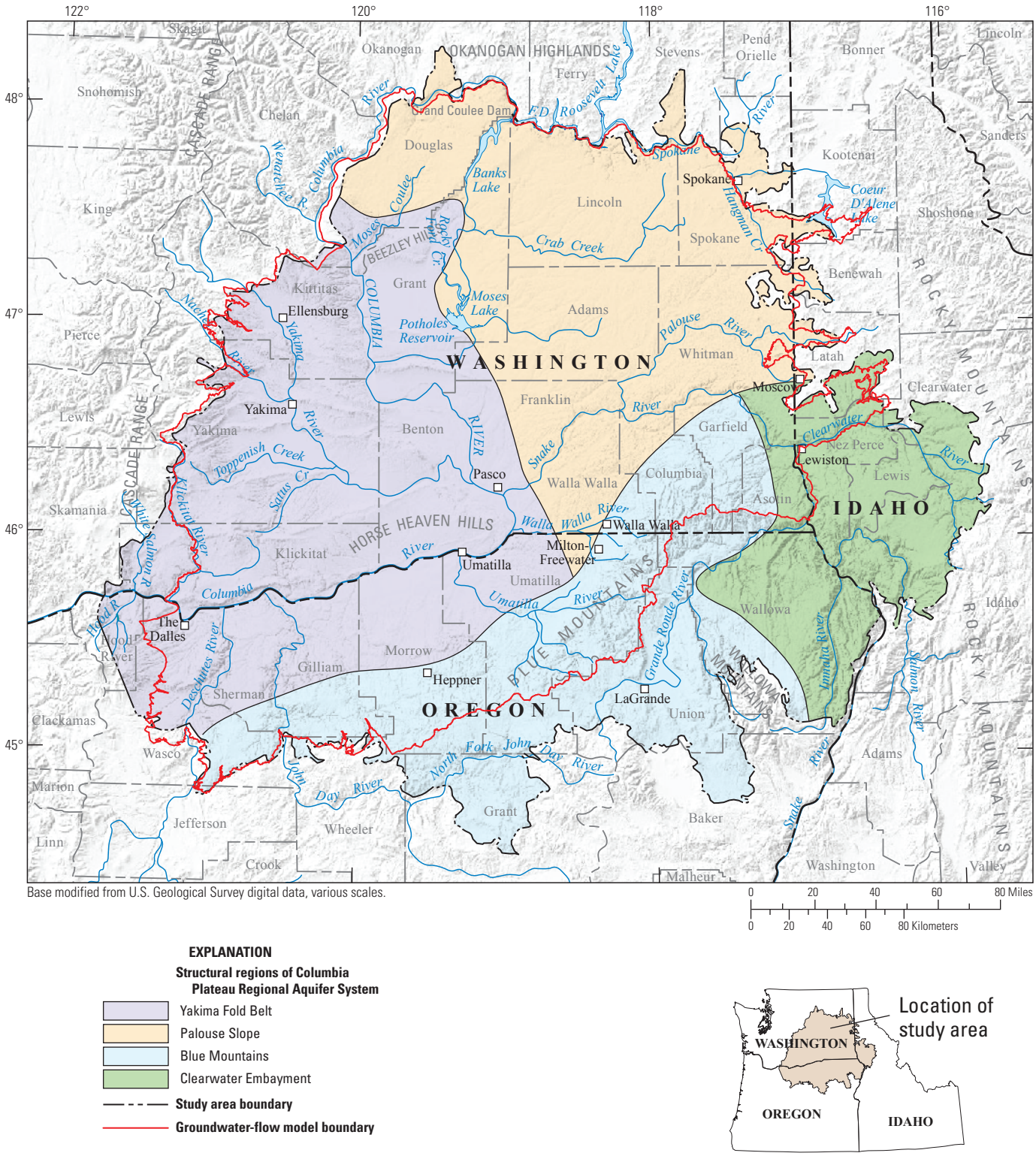

Figure 1. Columbia Plateau Regional Aquifer System study area and structural regions, Idaho, Oregon, and Washington. Structural regions modified from Reidel and others (2002).

Description of Study Area

A complete description of the Columbia Plateau is available in Kahle and others (2011), parts of which are presented here.

Location and Setting

The Columbia Plateau is a structural and topographic basin within the drainage of the Columbia River (fig. 1). It is bounded on the west by the Cascade Range, on the east by the Rocky Mountains, and on the north by the Okanogan Highlands. Its southern boundary corresponds to the mapped extent of the CRBG. The Columbia Plateau is underlain by massive basalt flows having an estimated composite thickness of at least 14,000 ft at one of the lowest points of the plateau near Pasco, Washington (Drost and others, 1990; Reidel and others, 2002). Sedimentary deposits overlie the basalt over large areas of the plateau, and may exceed 2,000 ft in thickness in places.

The Columbia Plateau was divided into four informal structural regions—the Yakima Fold Belt, Palouse Slope, Blue Mountains, and the Clearwater Embayment (fig. 1). The Yakima Fold Belt includes most of the western half of the plateau and is characterized by a series of east-west trending anticlinal ridges and synclinal basins. The Palouse Slope, in the northeast quarter of the plateau, is much less deformed and has a gently southwestward dipping slope. The other structural regions within the CPRAS are the Blue Mountains, a composite anticlinal structure that forms the southern extent of the Columbia River Basin, and the Clearwater Embayment, which marks the eastward extent of the CPRAS along the foothills of the Rocky Mountains and includes a series of folds extending into Idaho. The geologic and hydraulic properties of these structural regions may influence groundwater flow owing to flow barriers which may impede flow or to compartmentalization (the creation of distinct zones within an aquifer with limited interconnectivity) of the hydrogeologic units. The presence and importance of flow barriers and compartments in the CPRAS have been recognized and discussed in numerous studies (for example, Newcomb, 1969; Porcello and others, 2010).

Much of the Columbia Plateau is semiarid, the mean annual precipitation for 1895–2007 is about 17 in. (about 40 million acre-ft) and ranges from about 7 in. in the center of the study area to more than 60 in. in the northwestern-most extent of the study area (PRISM Climate Group, 2004; calculated from annual values). The types and amounts of natural vegetation on the Columbia Plateau vary according to precipitation and land-surface altitudes. The vegetation ranges from sagebrush and grasslands at lower altitudes to grasslands and forest at mid-altitudes to barren rock and conifer forests that are representative of the mountainous topography at the upper altitudes. Dry land agriculture mostly includes winter and spring wheat and lentils. Irrigated agriculture includes apples, hops, and other crops.

Overviews of the geology and hydrology of the CPRAS presented in this report summarize detailed descriptions in reports by (1) Kahle and others (2009), who discuss the geologic framework used in this report; (2) Burns and others (2011), who describe the three-dimensional characteristics of the geology of the CPRAS; and (3) Kahle and others (2011), who discuss the hydrogeologic framework and the hydrologic budget components of the CPRAS.

History of Water Resource Development

The cultural and economic development of the Columbia Plateau has depended heavily on the availability of water and the ability to store and redistribute water from the Columbia River and its major tributaries. Irrigation began as early as the 1840s and 1850s at missions in Walla Walla, Lewiston, and the Yakima Valley. In the early 1900s, the lumber and agricultural industries grew steadily and small-grain production on dryland farms and dairy and poultry farming were especially profitable because these enterprises did not need large quantities of water.

The dry summer climate in the region forced the early settlers to develop water supplies for irrigation wherever possible. By the 1930s, economic growth was relatively slow because of the 1929 depression and severe droughts that occurred after 1919. Those who survived these hardships lived along surface-water bodies or in areas where groundwater was available at shallow depths. A notable exception to this pattern was the Yakima River Basin, where reservoirs, diversion dams, and canals were constructed during 1892–1933. By 1902, about 120,000 acres were under mostly surface-water irrigation in the Yakima River basin (Parker and Storey, 1916; Bureau of Reclamation, 1999). Irrigation water projects by the Bureau of Reclamation (Reclamation) between 1910 and 1933 allowed the irrigated acreage to grow to more than 500,000 acres.

The start of Reclamation's CBIP (fig. 2) in 1933 and construction of the Hanford Site (between the Yakima and Columbia Rivers in Benton County, Washington [fig. 1]) in the 1940s brought a large influx of workers and associated service industries. By 1946, irrigation water was supplied to about 850,000 acres within the study area (Simons, 1953).

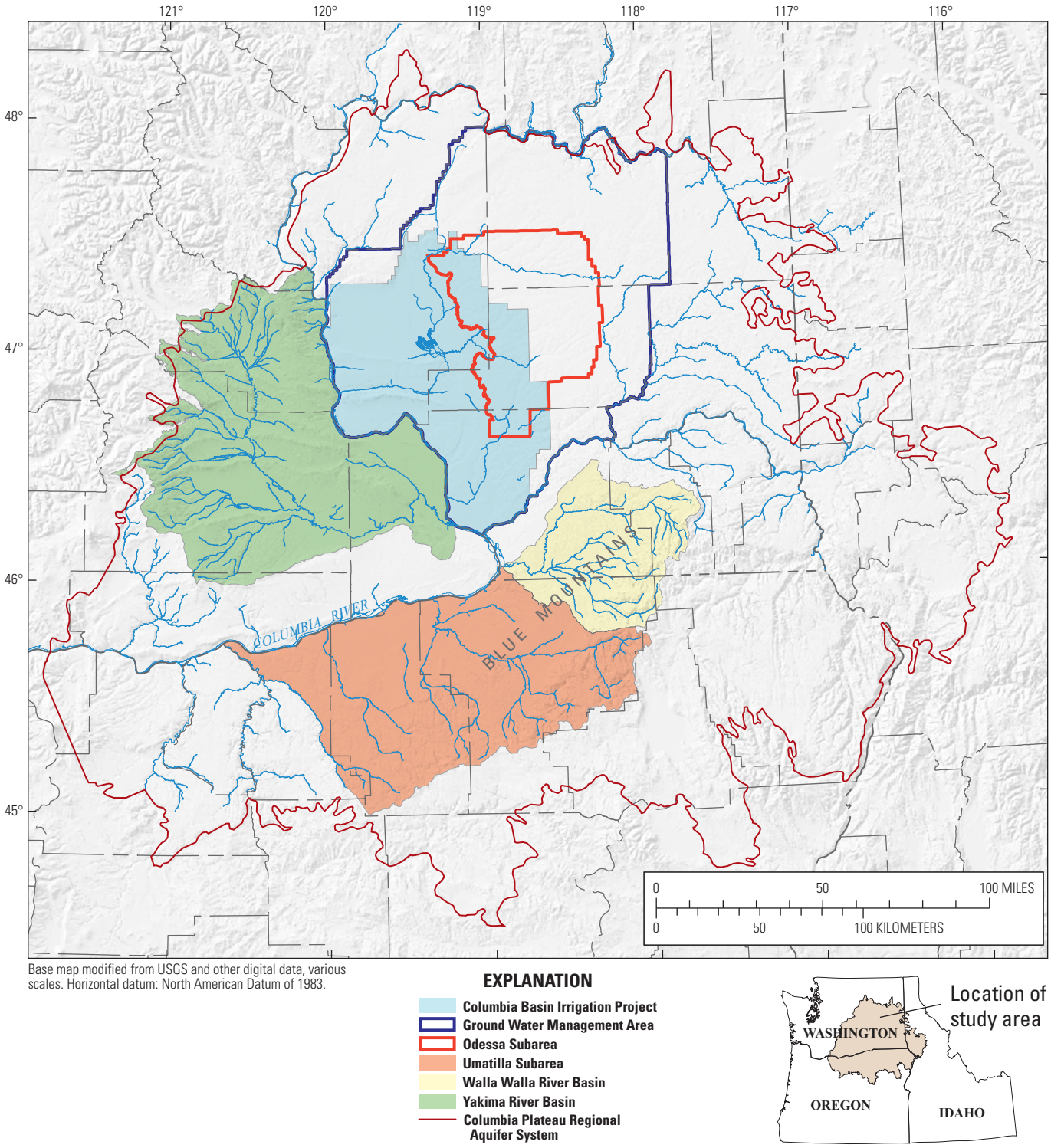

Figure 2. Location of major river basins and study subareas, Oregon and Washington.

Most of these acres were irrigated with water supplied by Reclamation projects created under the Federal Reclamation Act of 1902. Water from Franklin D. Roosevelt Lake, the reservoir formed by Grand Coulee Dam, became available in 1952, and by 1972 more than 0.5 million acres were being irrigated by this project in Washington, producing more than 60 crops. Currently (2013), about 2 million acres of croplands are irrigated with surface water and groundwater; much of the surface water is supplied by Reclamation projects. The surface-water withdrawals account for about 75 percent of the total irrigation water and groundwater withdrawals account for the remaining 25 percent (Kahle and others, 2011).

With the advent of new technology in about 1950, a rapid and intensive expansion of deep-well irrigation practices took place in areas not served by surface-water irrigation projects. These areas included parts of the Yakima, Pasco, Umatilla, The Dalles, and Walla Walla River Basins and the Odessa subarea in western Adams County, Washington. By 1984, about 0.5 million acres were irrigated with groundwater (Whiteman and others, 1994. By 2002, the total number of irrigated acres generally had stabilized (U.S. Department of Agriculture, 2007).

Hydrogeologic Setting

The Columbia Plateau is an intermontane basin between the Rocky Mountains and the Cascade Range that is filled with mostly Cenozoic basalt and sediment. Most rocks exposed in the region are the CRBG, intercalated sedimentary rocks, and younger sedimentary rocks and deposits that include Pleistocene cataclysmic flood deposits, eolian deposits, and terrace gravels of modern rivers. The CRBG consists of a series of more than 300 lava flows that erupted during various stages of the Miocene Age, 17 million to 6 million years ago. Individual flows range in thickness from 10 to more than 300 ft (Tolan and others, 1989; Drost and others, 1990) with a total thickness that might be greater than 14,000 ft in the central part of the study area near Pasco, Washington (Reidel and others, 2002). Soils derived from flows or sediments deposited on the surface of a flow were sometimes preserved, creating sedimentary interbeds between flows.

Generalized hydrogeologic units of the Overburden and CRBG, listed in order of generally increasing age, include Overburden, Saddle Mountains, Mabton Interbed, Wanapum, Vantage Interbed, and Grande Ronde (figs. 3 and 4; table 1). The Overburden unit consists predominantly of undivided, unconsolidated to semi-consolidated sedimentary deposits ranging from Pliocene to Holocene in age (Drost and others, 1990). These include many types of deposits of local and (or) regional extent including flood gravels and slack water sediments, terrace gravels of modern rivers, and eolian deposits that can range in thickness from 0 to 1,300 ft. The Saddle Mountains hydrogeologic unit consists mostly of the Saddle Mountains Basalt and interbed members and is the least extensive and youngest formation of the CRBG. Most of the unit is in the west-central part of the study area, with less continuous occurrences in the Blue Mountains and eastward into Idaho. Thickness of the Saddle Mountains unit can range from 0 to about 1,000 ft. The Wanapum hydrogeologic unit, composed mostly of basalt and interbed members of the Wanapum Basalt, mostly is in the north-central part of the study area. Much of the unit lies beneath the Overburden and Saddle Mountains units. Thickness of the Wanapum unit ranges from 0 to about 1,200 ft. The Grande Ronde hydrogeologic unit is the oldest and most extensive of the basalt units and constitutes the vast majority of the CRBG. This unit underlies most of the study area, except for an area along the southern boundary of the CPRAS in Oregon and along the eastern edge of the CPRAS in Idaho. The Grande Ronde unit contains the Grande Ronde Basalt and associated interbed members. Younger Wanapum and Saddle Mountains basalts were deposited in synclines and fault bounded valleys underlain by Grande Ronde basalts, indicating folding and faulting was active during CRBG deposition, continuing into the Quaternary. Distribution and thickness of younger basalt flows are determined by structurally controlled valleys. During the Pleistocene, the surface of the basalt units was modified greatly during repeated catastrophic outburst flooding, which caused erosion of vast channels as well as removal or deposition of overlying sediment. The basement confining unit, referred to as Older Bedrock, is composed of various rock types older than the CRBG (Kahle and others, 2009). In Washington and Idaho, the rocks bordering the CPRAS consist mostly of sedimentary and granitic rocks. In Oregon, the CPRAS is bordered by sedimentary, volcaniclastic, volcanic, plutonic, and metamorphic rocks (Drost and others, 1990). The bedrock unit generally has much lower permeabilities than the basalts and is considered the base of the regional flow system.

Hydrologic Budget Components

Discussion and estimates of the regional-scale hydrologic budget components for the CPRAS is from Kahle and others (2011). The extent of the study area used by Kahle and others (2011) differs from the model domain presented in this report; therefore, a direct comparison of budget component values with simulated values is not appropriate. The conceptual model for the aquifer system is that water (1) enters the system as recharge from precipitation (rainfall and snowmelt) and recharge from the delivery and application of surface-water and groundwater irrigation; and (2) exits the system as streamflow, evapotranspiration, and groundwater pumpage. A complete description of the budget components can be found in Kahle and others (2011).

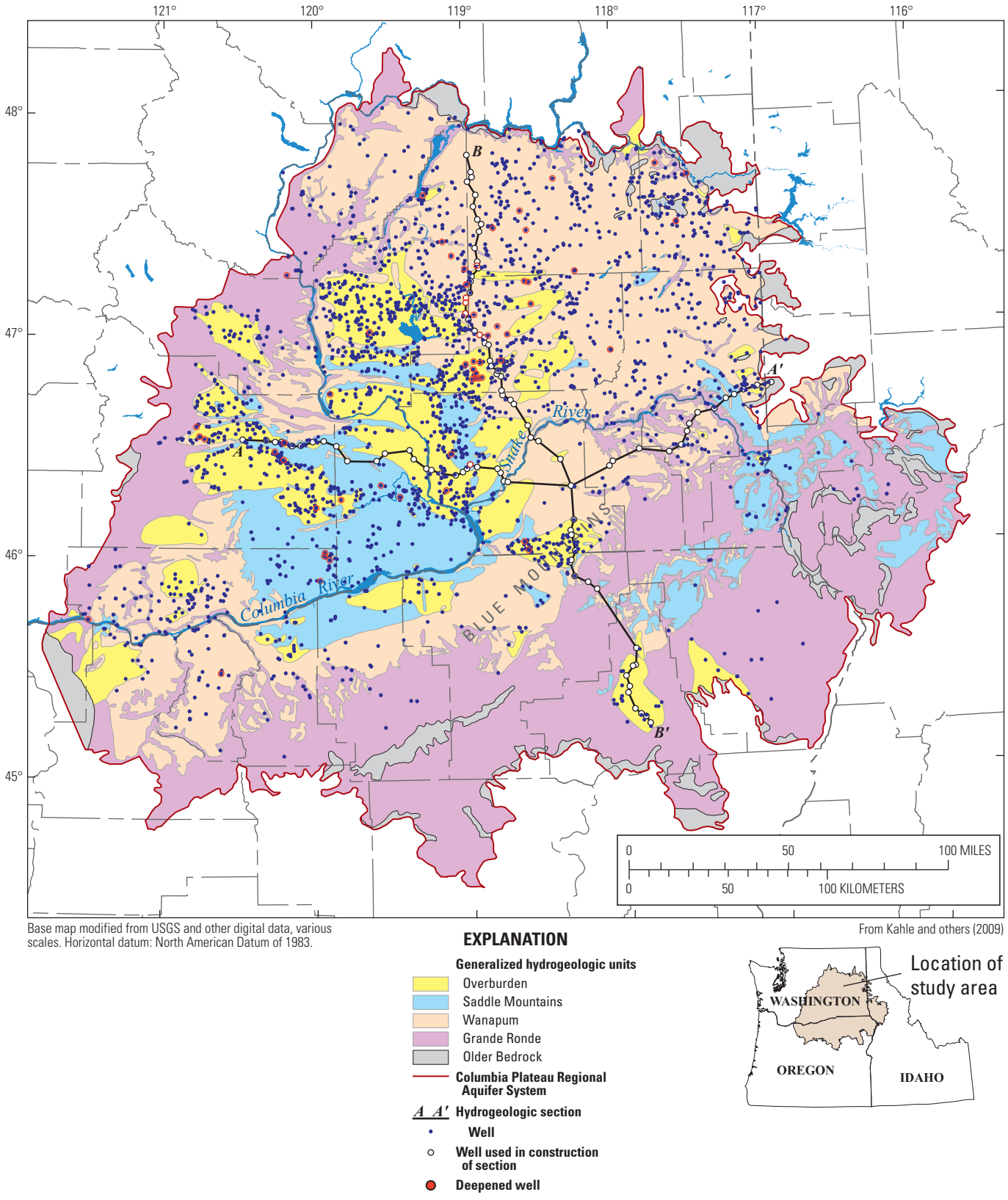

Figure 3. Surficial distribution of generalized hydrogeologic units and locations of hydrogeologic sections, Columbia Plateau Regional Aquifer System, Idaho, Oregon, and Washington. Hydrogeologic sections are shown in figure 4.

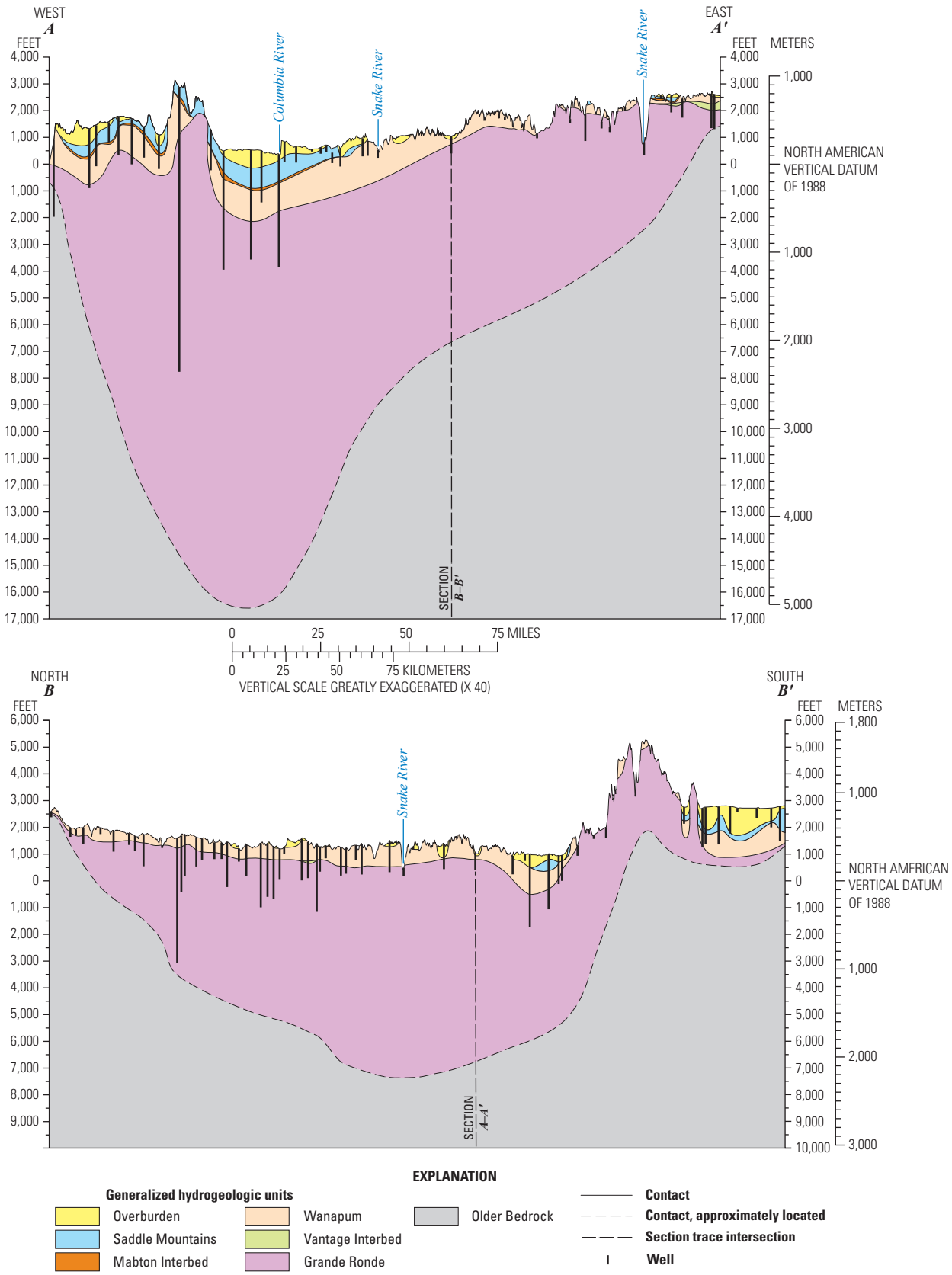

Figure 4. Generalized hydrogeologic sections of the Columbia Plateau Regional Aquifer System, Idaho, Oregon, and Washington. Adapted from Kahle and others (2009).

Table 1. Correlation chart showing relation between generalized stratigraphy and hydrogeologic units, Columbia Plateau Aquifer System, Idaho, Oregon, and Washington.

[From Kahle and others, 2009]

<table>
<tr><th>Era</th><th>Period</th><th>Epoch</th><th>Sediment stratigraphy</th><th colspan="3">Basalt stratigraphy</th><th>Hydrogeologic unit</th></tr>
<tr><td rowspan="11">Cenozoic</td><td rowspan="2">Quaternary</td><td>Holocene</td><td rowspan="2">Alluvial, colluvial, eolian, glacial, glacial outburst flood, lacustrine, landslide, terrace, and peat deposits; ash, debris-avalanche and debris-flow deposits, talus; Touchet Beds, Palouse Formation</td><td colspan="3" rowspan="2">Quaternary and Pliocene Basalts</td><td rowspan="2">Overburden</td></tr>
<tr><td>Pleistocene</td></tr>
<tr><td rowspan="9">Tertiary</td><td>Pliocene</td><td>Alluvial fan deposits; Alkali Canyon, Chenoweth, Deschutes, Madras and Ringold Formations; Dalles Group; Thorpe Gravel; and unknown continental sedimentary deposits</td></tr>
<tr><td rowspan="8">Miocene</td><td rowspan="8">Ellensburg, Deschutes, Latah, Madras, Payette, and Ringold Formations; Dalles Group; Snipes Mountain deposits; Deer Creek Beds; and unknown continental sedimentary deposits</td><td rowspan="8">Columbia River Basalt Group</td><td colspan="2">Saddle Mountains Basalt flow members and interbeds</td><td>Saddle Mountains unit</td></tr>
<tr><td colspan="2">Mabton interbed (Mabton Member of the Ellensburg Formation)</td><td>Mabton unit</td></tr>
<tr><td colspan="2">Wanapum Basalt Flow members and interbeds</td><td>Wanapum unit</td></tr>
<tr><td colspan="2">(Vantage Member of the Ellensburg Formation)</td><td>Vantage unit</td></tr>
<tr><td></td><td rowspan="4">Grande Ronde Basalt flow members and interbeds</td><td rowspan="5">Grande Ronde unit</td></tr>
<tr><td>Prineville Basalt</td></tr>
<tr><td></td></tr>
<tr><td>Picture Gorge Basalt</td></tr>
<tr><td colspan="2">Imnaha Basalt</td></tr>
<tr><td colspan="7">pre-Columbia River Basalt Group rocks, undivided</td><td>Older Bedrock</td></tr>
</table>

Mean annual recharge from infiltration of precipitation was estimated on the basis of annual precipitation and the results of previous modeling of recharge (Bauer and Vaccaro, 1990). The other budget components, excluding streamflow, were developed using estimates of actual evapotranspiration from a Simplified Surface Energy Balance method (Senay and others, 2007) and a monthly SOil WATer balance (SOWAT; Kahle and others, 2011) model that determined irrigation water demand, flux into and out of the groundwater system (recharge or discharge), direct runoff, and soil moisture in irrigated areas. The SOWAT model used simple relations among climatic, soils, land-cover, and irrigation data to compute monthly irrigation requirements and surplus moisture available for recharge. Estimates of groundwater pumping for irrigation and recharge from irrigation return flow from the application of the SOWAT model were refined as initial input to the groundwater-flow model.

The estimated mean annual recharge from infiltration of precipitation for the CPRAS was 4.6 in/yr (10.8 million acre-feet per year [acre-ft/yr]) for 1985–2007. The spatial distribution in recharge mirrors that of annual precipitation, with the highest mean annual recharge (more than 20 in.) occurring in the upper Yakima River Basin, the Blue Mountains southeast of Walla Walla, and adjacent to the Columbia River where it leaves the study area through the gorge in the Cascade Range. Mean annual recharge from infiltration of precipitation is less than 1 in. in a large part of the study area where precipitation is low, adjacent to the Columbia and Yakima Rivers.

Annual irrigation water use in the study area averaged 5.3 million acre-feet (acre-ft) during 1985–2007, with 1.4 million acre-ft (26 percent) supplied from groundwater and 3.9 million acre-ft (74 percent) supplied from surface water. Mean monthly irrigation throughout the study area peaks in July at 1.6 million acre-ft (1985–2007 average), of which, 0.45 and 1.15 million acre-ft is from groundwater and surface-water sources, respectively. Mean annual recharge from irrigation return flow in the study area was 4.2 million acre-ft (1985–2007) with 2.1 million acre-ft (50 percent) occurring within the predominately surface-water irrigated regions of the Yakima and Umatilla River Basins and Columbia Basin Irrigation Project. Annual recharge rates range from less than 5 in/yr in predominately sprinkler-irrigated areas where groundwater is the source to more than 20 in/yr in surface-water supplied areas where conveyance losses and less-efficient application methods are common.

Annual groundwater use (1985–2007) for purposes other than irrigation was estimated for the study area using information from multiple sources (Kahle and others, 2011). Public-supply groundwater use increased from about 201,500 acre-ft/yr in 1985 (12 percent of total groundwater use) to about 262,800 acre-ft/yr in 2007 (10 percent of total groundwater use). Domestic self-supplied groundwater use increased from about 54,600 acre-ft/yr in 1985 (3 percent of total groundwater use) to about 70,100 acre-ft/yr in 2007 (3 percent of total groundwater use). Industrial groundwater use decreased from about 53,400 acre-ft/yr in 1985 (3 percent of total groundwater use) to about 43,900 acre-ft/yr in 2007 (2 percent of total groundwater use). Other groundwater use, including water used for mining, thermoelectric needs, livestock, and aquaculture combined, increased from 16,900 acre-ft/yr (1 percent of total groundwater use) in 1985 to about 43,600 acre-ft/yr in 2007 (2 percent of total groundwater use).

Description of Groundwater-Flow System

Hydrogeologic Units

The conceptual groundwater model developed for the study area divides the aquifer system into seven hydrogeologic units (table 1)—the Overburden unit, three aquifer units in the permeable basalt rock, two sedimentary interbeds, and the basement confining unit (older bedrock) (Vaccaro, 1999). The three basalt hydrogeologic units are the Saddle Mountains, Wanapum, and Grande Ronde Basalts and their intercalated sediments. To distinguish these basalt hydrogeologic units from basalt formations in this study, they are referred to as "units." For example, the Wanapum Basalt and intercalated sediments are referred to as the Wanapum unit (Vaccaro, 1999). In the southeastern part of the study area, the Imnaha Basalt and any intercalated sediments are included with the Grande Ronde unit. Similarly, the Picture Gorge and Prineville Basalts in the southern part of the study area are included in the Grande Ronde unit. The interbeds between the Saddle Mountains and Wanapum basalt units, and between the Wanapum and Grande Ronde basalt units, are referred to in this study as the Mabton and Vantage Interbeds, respectively (Kahle and others, 2009, table 1). The interbed units are fairly extensive laterally, but are thin when compared with the thickness of the basalt units. The basement confining unit, referred to as "Older Bedrock," consists of pre-CRBG sedimentary, volcaniclastic, volcanic, plutonic, and metamorphic rocks that generally have much lower permeabilities than the overlying basalts and is considered the base of the regional flow system (Vaccaro, 1999; Kahle and others, 2009). The approximate surficial distribution of overburden and the three basalt hydrogeologic units are shown in figure 3. The approximate subsurface distribution of the CPRAS hydrogeologic units is shown in figure 4. Detailed descriptions of the units are available in Drost and others (1990), Whiteman and others (1994), Vaccaro (1999), and Jones and Vaccaro (2008), Kahle and others (2009), and Burns and others (2011).

Overburden Unit

The Overburden unit consists of undivided, unconsolidated to semi-consolidated sedimentary deposits and minor basalt and andesite, ranging from Pliocene to Holocene in age (Drost and others, 1990). The Overburden unit includes several formations of local or regional extent and numerous types of deposits including alluvial, colluvial, eolian, glacial, glacial outburst flood, lacustrine, landslide, terrace, and peat deposits; talus; and other continental sedimentary deposits of undetermined origin (table 1). Thickness of the Overburden unit ranges from 0 to 1,300 ft, with a median thickness of about 47 ft (Kahle and others, 2009).

Saddle Mountains Unit

The Saddle Mountains unit consists mostly of the Saddle Mountains Basalt and intercalated sediments. Most of the unit is in the west-central part of the study area, with less continuous occurrences in the Blue Mountains and eastward into Idaho (fig. 3). Kahle and others (2009) estimated an areal extent of about 8,000 mi^2, with a range in altitude of the unit top from about 4,000 to -280 ft relative to North American Vertical Datum of 1988 (NAVD 88). Thickness of the Saddle Mountains unit ranges from about 0 to 990 ft, with a median thickness of 280 ft (Kahle and others, 2009).

Mabton Interbed Unit

The Mabton unit is the sedimentary interbed between the overlying Saddle Mountains unit and the underlying Wanapum unit. The Mabton unit consists of the Mabton Member of the Ellensburg Formation and is mostly in the west-central part of the study area. Outcrops of the Mabton unit are scarce in the study area and the extent of the Mabton unit is assumed to be within the extent of the Saddle Mountains unit. The Mabton unit generally consists of clay, shale, claystone, clay with basalt, clay with sand, and sandstone. Thickness of the Mabton unit ranges from about 0 to 520 ft, with a median thickness of about 44 ft (Kahle and others, 2009).

Wanapum Unit

The Wanapum unit, composed mostly of basalt and intercalated sediments of the Wanapum Basalt, is in most of the north-central part of the study area (fig. 3) and has an estimated areal extent of about 25,000 mi^2 with the altitude of the top ranging from about 3,400 to -1,000 ft relative to NAVD 88 (Kahle and others, 2009). Much of the unit lies beneath the Overburden and Saddle Mountains units. Thickness of the Wanapum unit ranges from about 0 to 1,200 ft, with a median thickness of about 330 ft (Kahle and others, 2009).

Vantage Interbed Unit

The Vantage unit is the sedimentary interbed between the overlying Wanapum unit and the underlying Grande Ronde unit. Over most of the study area, this unit consists of the Vantage Member of the Ellensburg Formation; however, this unit includes sediment of the Latah Formation in the northeastern part of the study area. Outcrops of this unit are scarce in the study area and the extent is assumed to be within the extent of the Wanapum unit (fig. 3). The Vantage unit consists of clay, shale, sandstone, tuff with claystone, and clay with basalt, but also may contain small amounts of sand and sand-and-gravel. A few well logs also indicate that the Vantage unit is not present in the southeastern part of the Yakima River Basin and near the Cold Creek Syncline and Rattlesnake Hills Structure (Jones and Vaccaro, 2008). Thickness of the Vantage unit ranges from about 0 to 320 ft, with a median thickness of about 20 ft (Kahle and others, 2009).

Grande Ronde Unit

The Grande Ronde unit is the oldest and most extensive of the basalt units. This unit underlies most of the study area, except for an area along the southern boundary of the CPRAS in Oregon and along the eastern extent in Idaho (fig. 3). The estimated areal extent of the Grande Ronde unit is about 42,000 mi^2 (Kahle and others, 2009). The Grande Ronde unit predominantly contains the basalt and interbed members associated with the Grande Ronde Basalt. Sedimentary interbeds within the unit generally are rare and are only a few feet thick where present. The top of the Grande Ronde unit ranges from 4,300 to -2,100 ft relative to NAVD 88 based on Kahle and others (2009). Thickness of the unit is largely unknown, but is estimated to be greater than 14,000 ft near the central part of the basin.

Older Bedrock Unit

The Older Bedrock unit that borders and underlies the CPRAS is composed of various rock types older than the CRBG (Kahle and others, 2009). In Washington and Idaho, the rocks bordering the CPRAS consist mostly of sedimentary and granitic rocks. In Oregon, the CPRAS is bordered by sedimentary, volcaniclastic, volcanic, plutonic, and metamorphic rocks (Drost and others, 1990).

Hydraulic Characteristics of Hydrogeologic Units

The hydraulic characteristics of the aquifers determine how a groundwater-flow system functions and how it will respond to stresses such as pumping. These characteristics include horizontal and vertical hydraulic conductivity, porosity, and the storage coefficient. Because of the heterogeneity of the geologic materials that constitute the CPRAS, the hydraulic characteristics can vary widely. The overburden deposits are diverse in lithology and the large variation in grain size, depositional regimes, and age of the deposits account for the large range of their hydraulic characteristics (Kahle and others, 2011, p. 20). Hydraulic characteristics also vary greatly within and between the individual basalt flows and the basalt hydrogeologic units. Horizontal hydraulic conductivities generally are greatest in the interflow zones formed from the combination of basalt flow tops with the base of an overlying basalt flow (fig. 5), and an intervening sedimentary interbed, if present. The flow tops generally are brecciated and (or) vesicular, and the flow bases are brecciated and may contain pillow complexes if the basalt extruded within or flowed into water and exhibit high horizontal hydraulic conductivity (Lindholm and Vaccaro, 1988). The interflow zones commonly are separated by a less-transmissive flow interior (fig. 5) in which fractures typically are vertically oriented. The older bedrock generally has lower values of porosity and hydraulic conductivity than the overburden and CRBG units.

Kahle and others (2011, p. 21) estimated the median horizontal hydraulic conductivity values for the overburden, basalt units, and bedrock as 161, 70, and 6 ft/d, respectively, based on specific capacity data reported in previous studies. Vertical hydraulic conductivity of the hydrogeologic units in the CPRAS largely is unknown. Estimates of vertical hydraulic conductivity range from about 0.009 to 2 ft/d for the Overburden unit although values for some parts of this unit may be as low as 10^{-10} to 10^{-7} ft/d; values for the CRBG units range from 4×10^{-7} to 4 ft/d (Kahle and others, 2011, p. 57).

The storage characteristics of an aquifer are described by the storage coefficient, which is defined as the volume of water that an aquifer takes into or releases from storage per unit surface area, per unit change in head. The storage coefficient is expressed in units of cubic feet per cubic feet, a dimensionless quantity. Previous estimates of the storage coefficient in the CPRAS typically range from about 0.1 to 0.2 for the unconfined parts of the Overburden unit and from about 10^{-6} to 0.01 for the CRBG basalt units (Kahle and others, 2011, p. 26–27).

Groundwater Flow and Occurrence in Basalt Units

Groundwater moves through the regional aquifer system through preferential pathways (fig. 5) developed during lava deposition. Generally, each CRBG lava flow consists of a dense flow interior and irregular flow tops and flow bottoms with a variety of textures (Reidel and others, 2002). Although flow interiors have joints and fractures, they typically do not transmit water easily. Flow tops and bottoms commonly are vesicular or brecciated, and may or may not be permeable. Local permeability of flow tops and bottoms can be highly variable over short distances as a result of depositional processes, but tends to be high over long distances, resulting in highly transmissive aquifers at the regional scale. The CRBG thus comprises a stack of laterally extensive lava flows with relatively thin permeable productive zones at flow tops and flow bottoms separated by relatively thick dense flow interiors of low permeability. Thin permeable aquifers are estimated to occupy about 10 percent of the total flow thickness. Flow interiors have low permeability and low storage characteristics, so that they form effective confining units between permeable flow tops. As a result, the aquifer system is highly anisotropic, with effective horizontal hydraulic conductivity controlled by the fraction of the thickness occupied by thin aquifers, and the effective vertical hydraulic conductivity controlled by the dense flow interiors.

Except for groundwater flow in the deeply buried parts of the CPRAS, large-scale structural features compartmentalize the flow system in places (Kinnison and Sceva, 1963; Hansen and others, 1994; Bauer and Hansen, 2000; Vaccaro and others, 2009). The compartmentalization limits the length of the flow paths, resulting in relatively short paths for such a large aquifer system. Structural control is exerted primarily by the major ridges in the Yakima Fold Belt (fig. 1; Hansen and others, 1994; Reidel and others, 2002; Jones and others, 2006).

Groundwater flow in the Grande Ronde unit is compartmentalized, but not to the same extent as in the Saddle Mountains or Wanapum units. The large spatial extent of the Grande Ronde unit results in a large flow system with more interconnections than in the other two CRBG units. Where the unit outcrops, the water-level contours mimic land-surface topography and become a more subdued expression of topography as the unit becomes buried. In the more deeply buried parts of the Grande Ronde unit, the contours are smoother than contours for the other CRBG units. Similarly, water-level contours near geologic structures in the eastern part of the area are more subdued and smoother. The flow system in the Grande Ronde unit is controlled by the regional discharge locations along the Columbia River and major tributaries; that is, the hydraulic gradient in the Grande Ronde unit is toward the major streams (fig. 6). There may be a separate regional flow system in the deeper part of the unit, but data are insufficient to verify the presence of such a system.

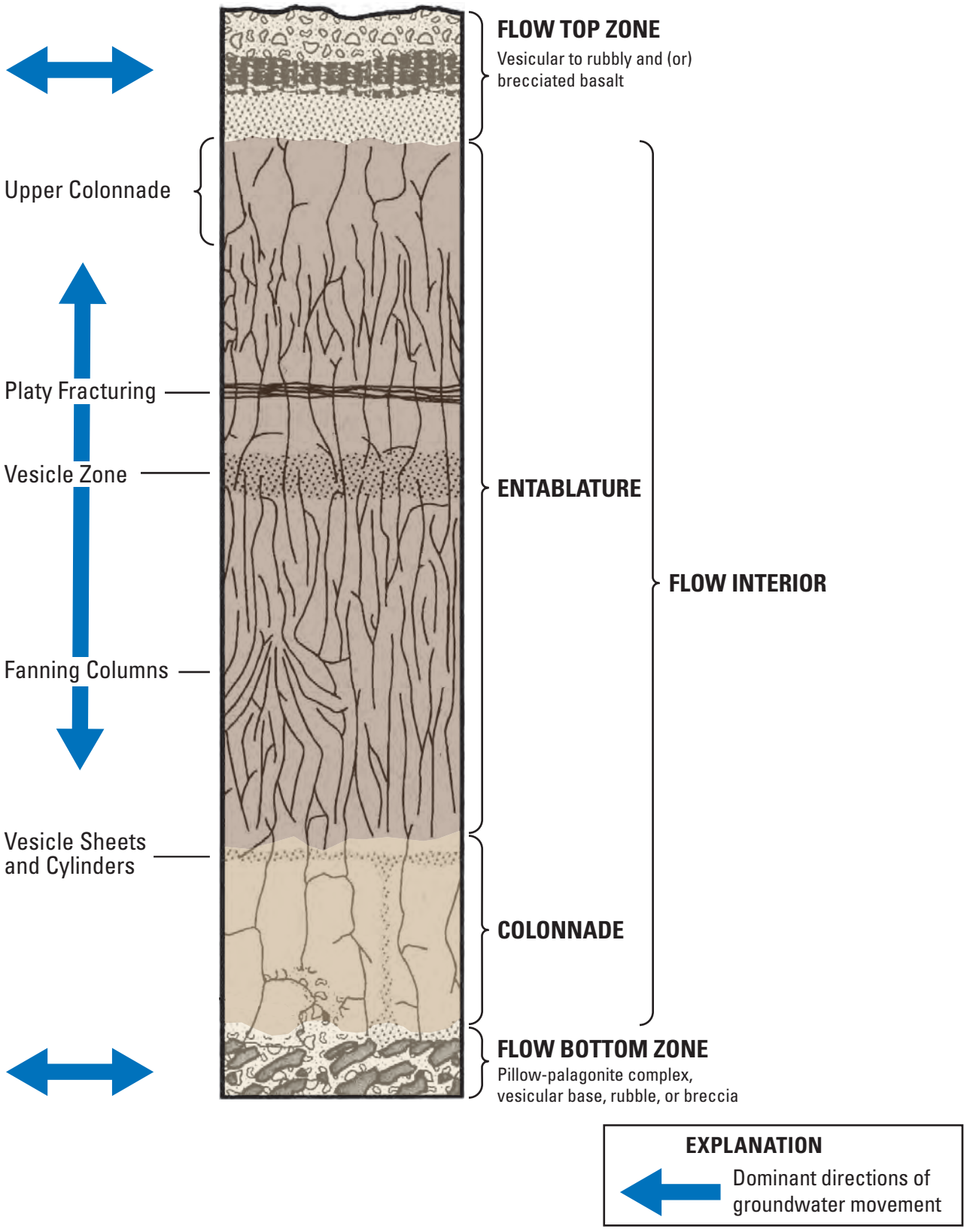

Figure 5. Features within a typical Columbia River Basalt Group flow. Modified from Vaccaro (1986) and Reidel and others (2002).

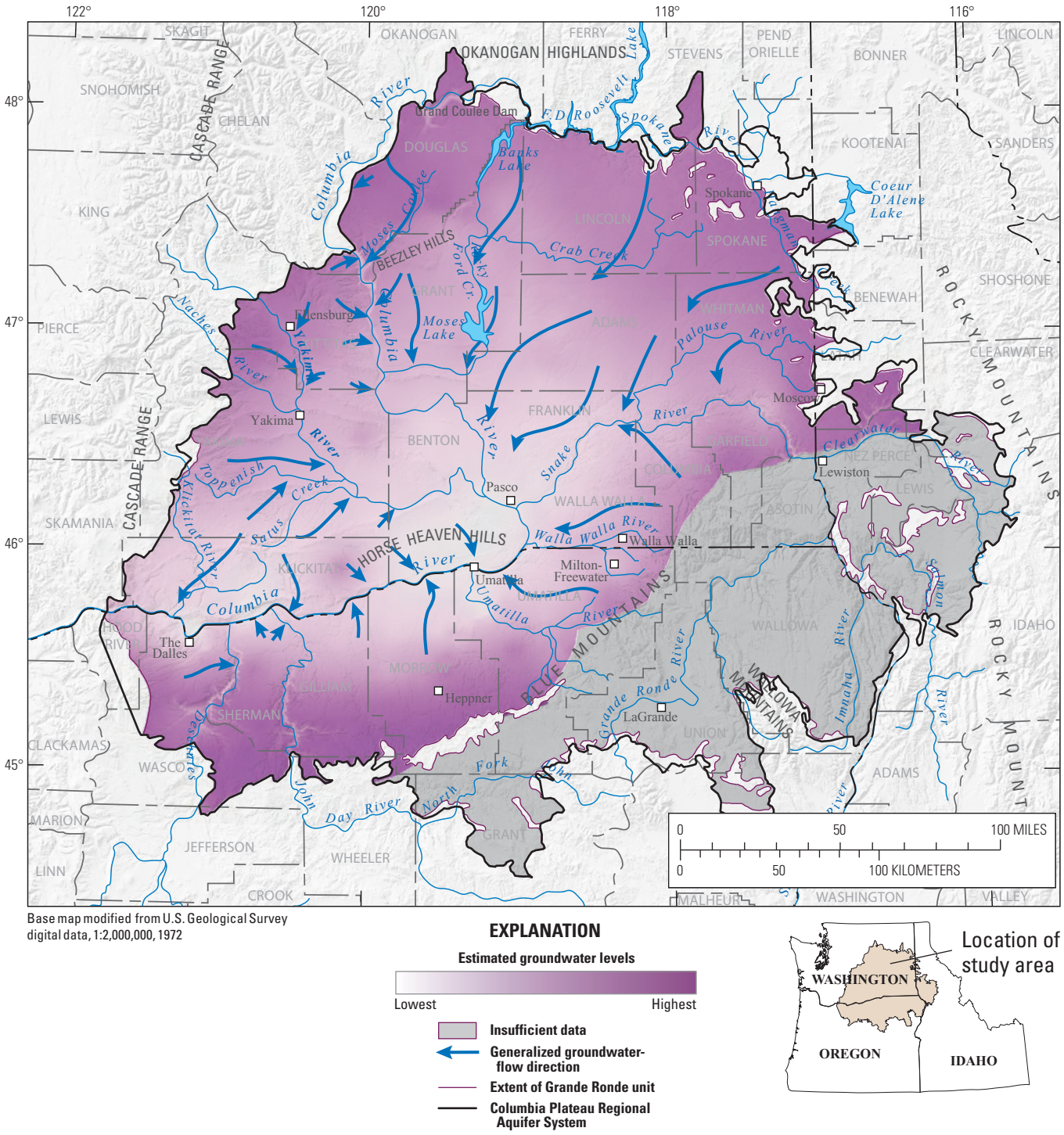

Figure 6. Estimated groundwater levels and directions of lateral groundwater movement for the Grande Ronde unit, Columbia Plateau Regional Aquifer System, Idaho, Oregon, and Washington (from Snyder and Haynes, 2010).

Numerical Simulation of Groundwater Flow

Development of a calibrated groundwater-flow model allows for simulation and analysis of the movement of water through the hydrogeologic units that constitute the CPRAS. The USGS modular three-dimensional finite-difference groundwater-flow model, MODFLOW-NWT (Niswonger and others, 2011), a standalone program that is intended for solving problems involving drying and rewetting nonlinearities of the unconfined groundwater-flow equation, was used to simulate groundwater flow in the overburden deposits, interbeds, and basalt units of the aquifer system, and the interaction of the groundwater-flow system with surface water.

Modeling Strategy

The groundwater-flow model was developed to improve understanding of the hydrogeologic system. The model was formulated to test processes or aspects of the geology that previously have been identified or hypothesized to be important for controlling the flow and storage of groundwater in parts of the CPRAS (see section, "Previous Investigations"). In particular, the model was designed to investigate:

- Quantification of groundwater pumping;
- Flow through wells that are open to multiple aquifers;
- Enhanced groundwater recharge due to anthropogenic activities, especially large-scale irrigation projects;
- Horizontal barriers to groundwater flow corresponding to geologic structure;
- The large number of barriers to vertical groundwater flow corresponding to hundreds of dense lava flow interiors; and
- The connection between the groundwater and surface-water systems.

The goal of the model is to help researchers understand the role of each of these mechanisms in producing observed long-term (decadal) changes in groundwater (Snyder and Haynes, 2010; Burns and others, 2012b) and changes to base flow in rivers and streams.

Because there is strong correlation of hydraulic measurements over tens of miles (Burns and others, 2012b) and steep vertical hydraulic gradients are present in the CPRAS, a coarse horizontal grid and fine vertical grid was created. Representation of appropriate horizontal hydraulic connectivity was achieved by designing the grid to follow the general pattern of hydrogeologic deposits by using the geologic model of Burns and others (2011), and using vertically thin cells to approximate typical basalt flow thicknesses of about 100 ft (Burns and others, 2011, 2012a). Using thin cells allowed the horizontal permeability of each layer to represent the transmissivity of individual CRBG aquifers, and the vertical permeability to represent individual basalt flow interior confining units. Although individual basalt flows and aquifers are not mapped to the level of detail necessary to define aquifers, using thin model layers ensured that shallow aquifers were appropriately connected to local surface-water features, and that deep aquifers were appropriately disconnected. The model grid was supplemented with a limited number of features representing various internal flow boundaries such as discrete barriers to horizontal flow, which generally were correlated to geologic structure, and rivers, streams, and wells.

Upstream Weighting Package

Because the system is being represented as a large number of highly anisotropic layers that may drain at various altitudes, numerical instabilities may occur as model cells go dry or rewet. Historically, groundwater-flow models of the CPRAS have assumed confined conditions for all layers to aid model stability; however, Burns and others (2012a) showed that in order to represent typical long-term declines in CRBG aquifers, it may be necessary to allow the drainage of regions of the model domain. To gain the necessary stability for the mathematical solution of the groundwater-flow equation, the recently developed Upstream Weighting (UPW) Package (Niswonger and others, 2011) was used.

The UPW Package is an internal flow package for MODFLOW-2005 that is intended to be used with the Newton Solver (NWT) Package for problems involving drying and rewetting nonlinearities of the unconfined groundwater-flow equation. The UPW Package treats nonlinearities of cell drying and rewetting by use of a continuous function rather than the discrete approach of drying and rewetting that is used in the Block-Centered Flow (BCF), Layer Property Flow (LPF), and Hydrogeologic-Unit Flow (HUF) Packages (Anderman and Hill, 2000; Harbaugh, 2005). This further enables application of the Newton solution method for unconfined groundwater-flow problems because conductance derivatives required by the Newton solution method are smooth over the full range of head for a model cell. A complete description of the UPW Package is available in Niswonger and others (2011).

Newton Solver

The Newton solution method is commonly used in the Earth sciences to solve nonlinear equations. The method is advantageous because many recently developed MODFLOW packages apply nonlinear boundary conditions. Additionally, the Newton solution method has been particularly beneficial in solving flow equations representing unconfined aquifers. During the course of this study, the Newton solution method provided greater model stability and improved model convergence compared to the solvers used in the standard MODFLOW-2005 code. A complete description of the Newton formulation is available in Niswonger and others (2011).

Layering and Spatial Discretization

MODFLOW-NWT uses data sets that describe internal characteristics and boundary conditions of the groundwater-flow system, and calculates hydraulic heads and flow at discrete points (cell centers) within the model domain. The program requires that the groundwater-flow system be subdivided, vertically and horizontally, into rectilinear blocks called cells. The CPRAS model domain was subdivided into a horizontal grid of 126 rows and 131 columns using a uniform 3-km (9,842.5-ft) grid (fig. 7) that aligns with the 1-km SOWAT model grid (Kahle and others, 2011) allowing straightforward extraction of model boundary conditions (output from nine SOWAT cells were averaged for input to one MODFLOW cell). The large cell size and uniform grid spacing were selected as an appropriate trade-off between computational limitations, the geometry of the flow system, and the areal scale of observed regional head and flow patterns, which typically extend for tens to hundreds of kilometers (Snyder and Haynes, 2010, Burns and others, 2012b).

Vertically, the model domain was subdivided into the six geologic model units of Burns and others (2011): Grande Ronde Basalt, Vantage Interbed, Wanapum Basalt, Mabton Interbed, Saddle Mountains Basalt, and Overburden (table 2). Although individual aquifers are not reliably mapped at the regional scale, each of these basalt model units was discretized vertically into layers that are approximately 100-ft thick for most of the model domain, roughly approximating a typical CRBG lava flow thickness (Burns and others, 2012a). Simulation using 100 ft layers preserved appropriate local-scale connectivity of individual basalt aquifers with hydrologic features. Historical and anecdotal evidence suggests that vertical hydraulic head gradients are orders of magnitude larger than horizontal gradients in basalt aquifers (Vaccaro and others, 2009; Burns and others, 2012a, 2012b), indicating that a relatively fine vertical discretization is appropriate for representing system dynamics.

The groundwater-flow model included 100 model layers, representing up to 17,000 ft (at the thickest part of the active flow system). Although the target thickness of individual basalt layers was 100 ft, model cell thickness ranged from 10 to 200 ft for the Saddle Mountains and Wanapum units and the upper 30 layers of the Grande Ronde unit. Where necessary to represent the Grande Ronde with more than 30 layers (total thickness greater than 3,000 ft), the remaining thickness was equally divided so that the total number of model layers was 100. These thicker cells were limited to very deep parts of the model domain, far below the parts of the system currently being pumped for groundwater. The thickest cells were 365 ft.

The basalt units were assigned to a discrete range of layers (based on total basalt unit thickness); no layer represented more than one CRBG unit, and the sedimentary Overburden and Interbed units were simulated in all remaining layers (table 2). Interbeds may be thin, but they were simulated across the entire extent of the associated basalt unit. Where a CRBG unit is not present, the hydrogeologic unit properties assigned to the model layers assigned to the missing CRBG unit were based on the overlying surface: deposits directly overlain by Wanapum Basalt were defined as Vantage Interbed, deposits directly overlain by Saddle Mountains Basalt were defined as Mabton Interbed, and deposits directly overlain by the land surface were defined as Overburden. The thickness of each interbed and Overburden cell was determined by dividing the total thickness of the respective unit into equal parts. The thinnest model cells occur under the unusual circumstances where Saddle Mountains Basalt overlies Grande Ronde Basalt with no Wanapum Basalt between. Because the overlying basalt is Saddle Mountains, the cells are simulated as Mabton Interbed. These cells occur infrequently (16 locations throughout the model domain), with the thinnest cell being 0.16 ft. The extents and thickness of the Overburden and CRBG units in the model are shown in figures 8*A*–*D*.

When generating the flow simulation model grid for the CRBG, the lowest layer was assumed to be the most extensive (consistent with the general trend of less voluminous lava flows as time progressed over geologic time [Lindholm and Vaccaro, 1988]), and all remaining layers were built upon this lowest layer until the total thickness of the basalt unit was represented. After the total thickness of basalt was assigned to model cells, sedimentary deposits were assigned to remaining overlying cells as described in the previous paragraph. The resulting groundwater-flow model preserved the possibility that low-lying sediments are in hydraulic connection with discontinuous basalt layers in both valley bottoms and at basalt-lava-flow margins, providing a reasonable representation of the interaction between CRBG aquifers and sedimentary units, which is consistent with the approach by Burns and others (2011).

The combination of lateral and vertical discretization resulted in 1,650,000 cells within the model grid, of which 423,394 cells are active. The active cells include an area of almost 33,000 mi^2 and are composed of 32,000 mi^3 of aquifer-system material. Total model domain thickness ranged from 100 to 17,200 ft. Model layers 1–75 were simulated as convertible (confined/unconfined), and layers 76–100 were simulated as confined.

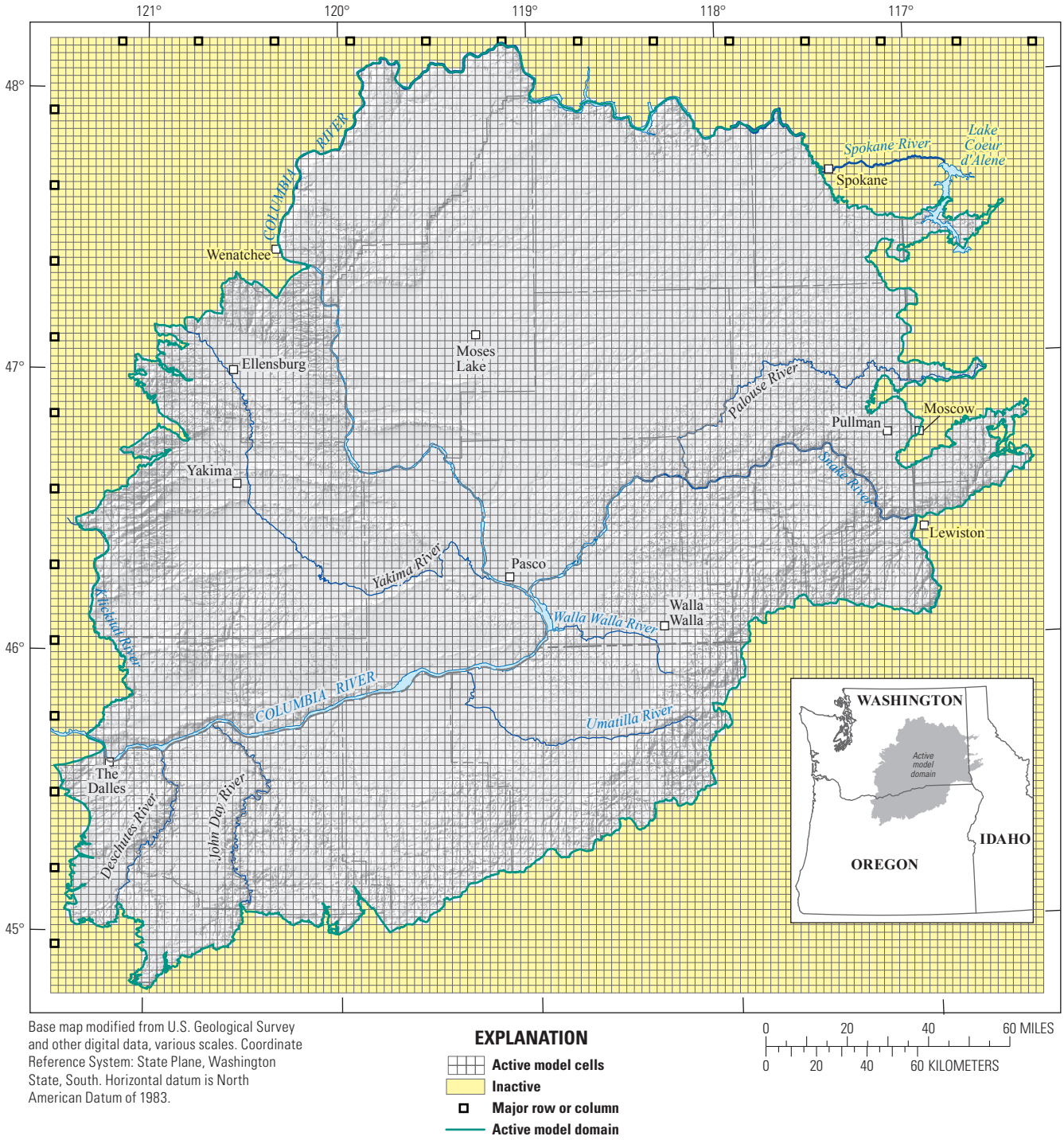

Figure 7. Location and extent of the groundwater-flow model of the Columbia Plateau Regional Aquifer System, Idaho, Oregon, and Washington.

Table 2. Correlation between geologic model units and groundwater-flow model layers of the Columbia Plateau Regional Aquifer System, Idaho, Oregon, and Washington.

[**Geologic model units:** Rock units are Saddle Mountains Basalt, Wanapum Basalt, Grande Ronde Basalt, and Older Bedrock. ft, foot]

Geologic model units (Burns and others, 2011)	Groundwater-flow model layers	Description
Overburden	1–45	Approximately 100 ft model layers between the uppermost rock unit and land surface.
Saddle Mountains Basalt	11–18	Approximately 100 ft layers between the geologic model top of Mabton Interbed and the geologic model top of Saddle Mountains Basalt. Cells are constructed from the bottom up, with the lowest layer being the most laterally extensive.
Mabton Interbed	19–35	Equally spaced layers between the geologic model bottom of Saddle Mountains Basalt and the next rock unit below.
Wanapum Basalt	20–34	Approximately 100 ft layers between the geologic model top of Vantage Interbed and the geologic model top of Wanapum Basalt. Cells are constructed from the bottom up, with the lowest layer being the most laterally extensive.
Vantage Interbed	35	Layer between the geologic model bottom of Wanapum Basalt and the next rock unit below.
Grande Ronde Basalt	36–100	Approximately 100 ft layers between the geologic model top of Older Bedrock and the geologic model top of Grande Ronde Basalt. Cells were constructed from the top down, using a trend surface for top of Grande Ronde Basalt as a guide surface, allowing the representation of river and stream incision exceeding model cell thickness.
Older Bedrock	No flow	

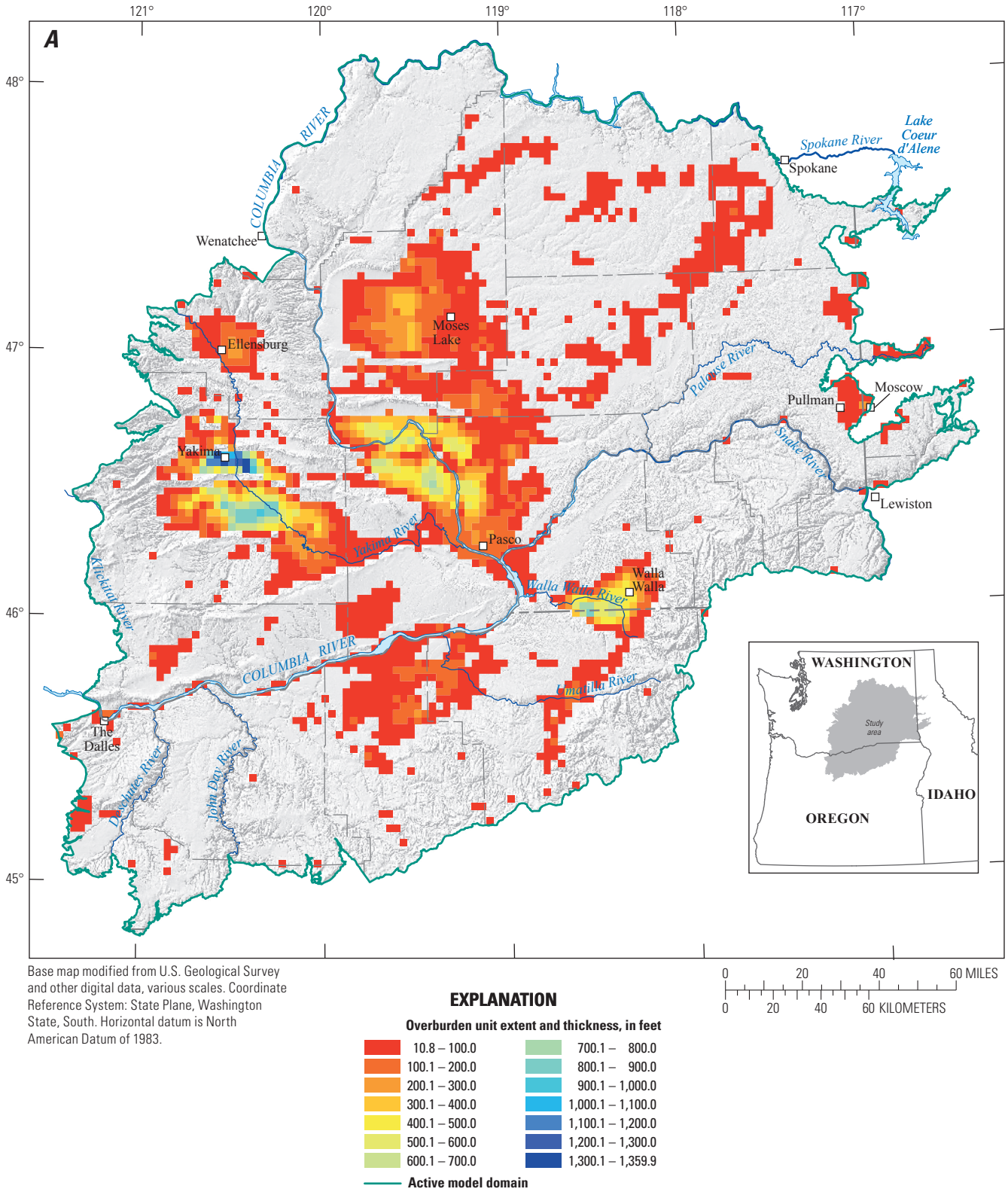

Figure 8. Extent and thickness of the (*A*) Overburden unit, (*B*) combined Saddle Mountains basalt and Mabton interbed unit, (*C*) combined Wanapum basalt and Vantage interbed unit, and (*D*) Grande Ronde basalt unit, Columbia Plateau Regional Aquifer System, Idaho, Oregon, and Washington.

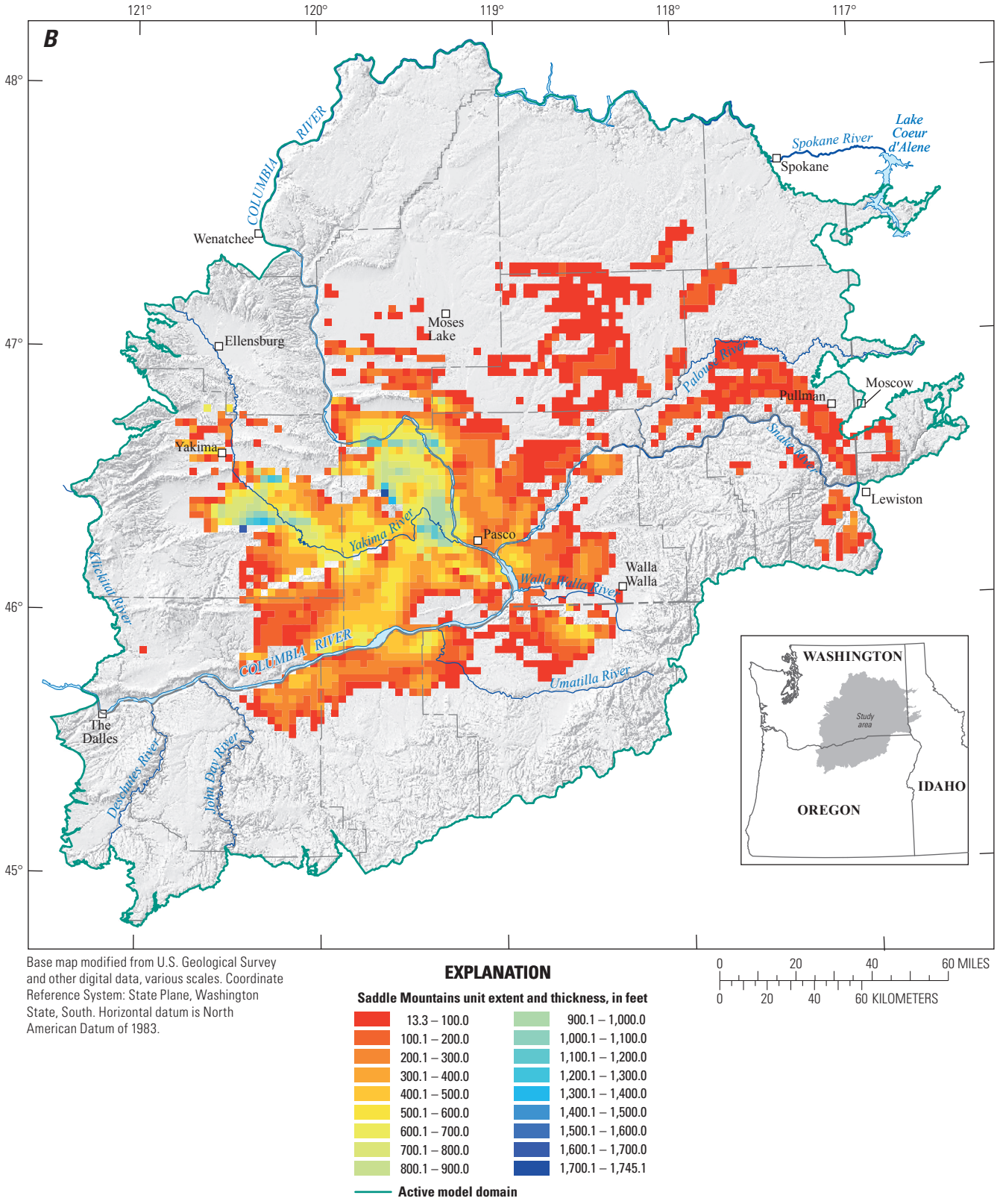

Figure 8.—Continued

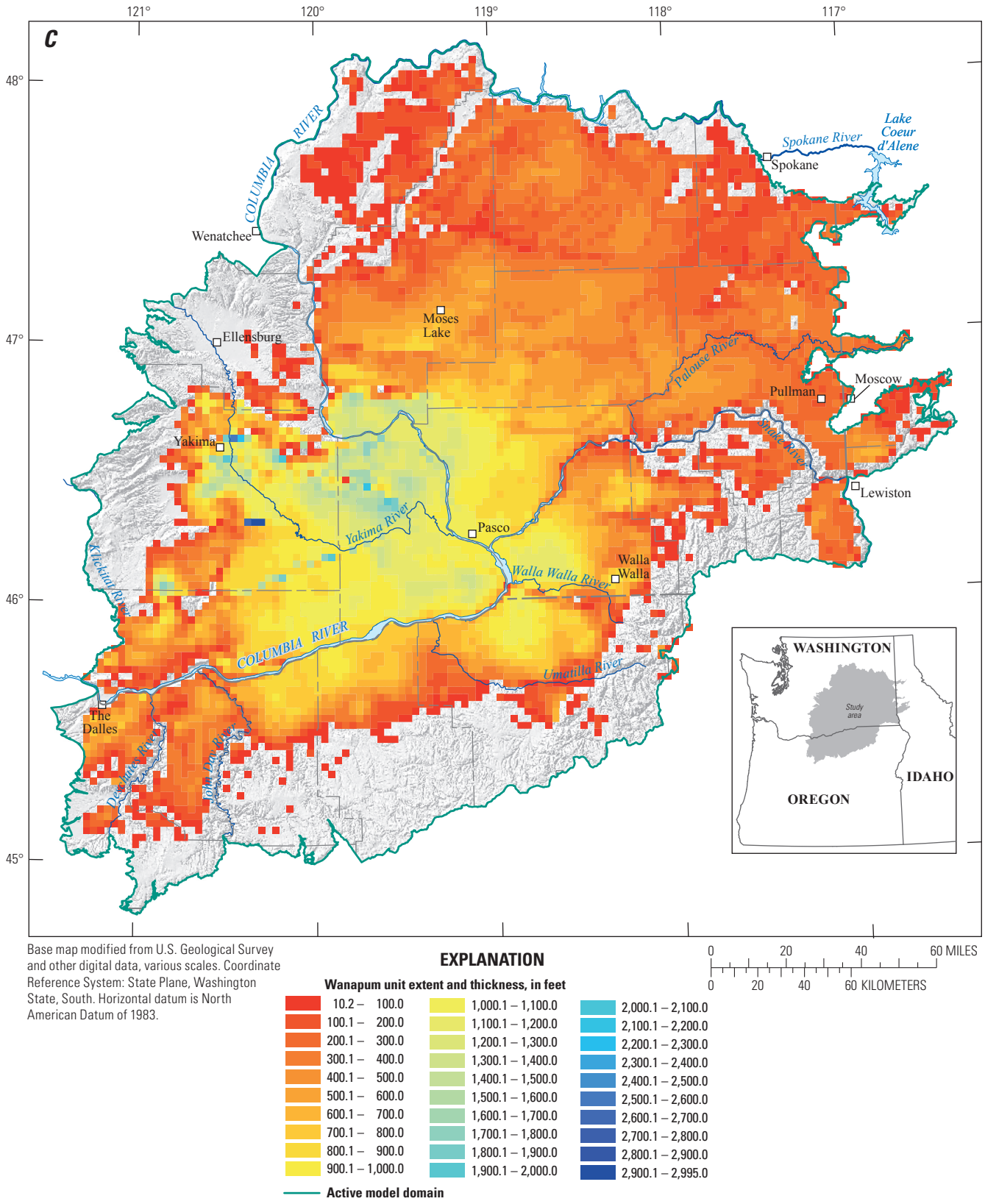

Figure 8.—Continued

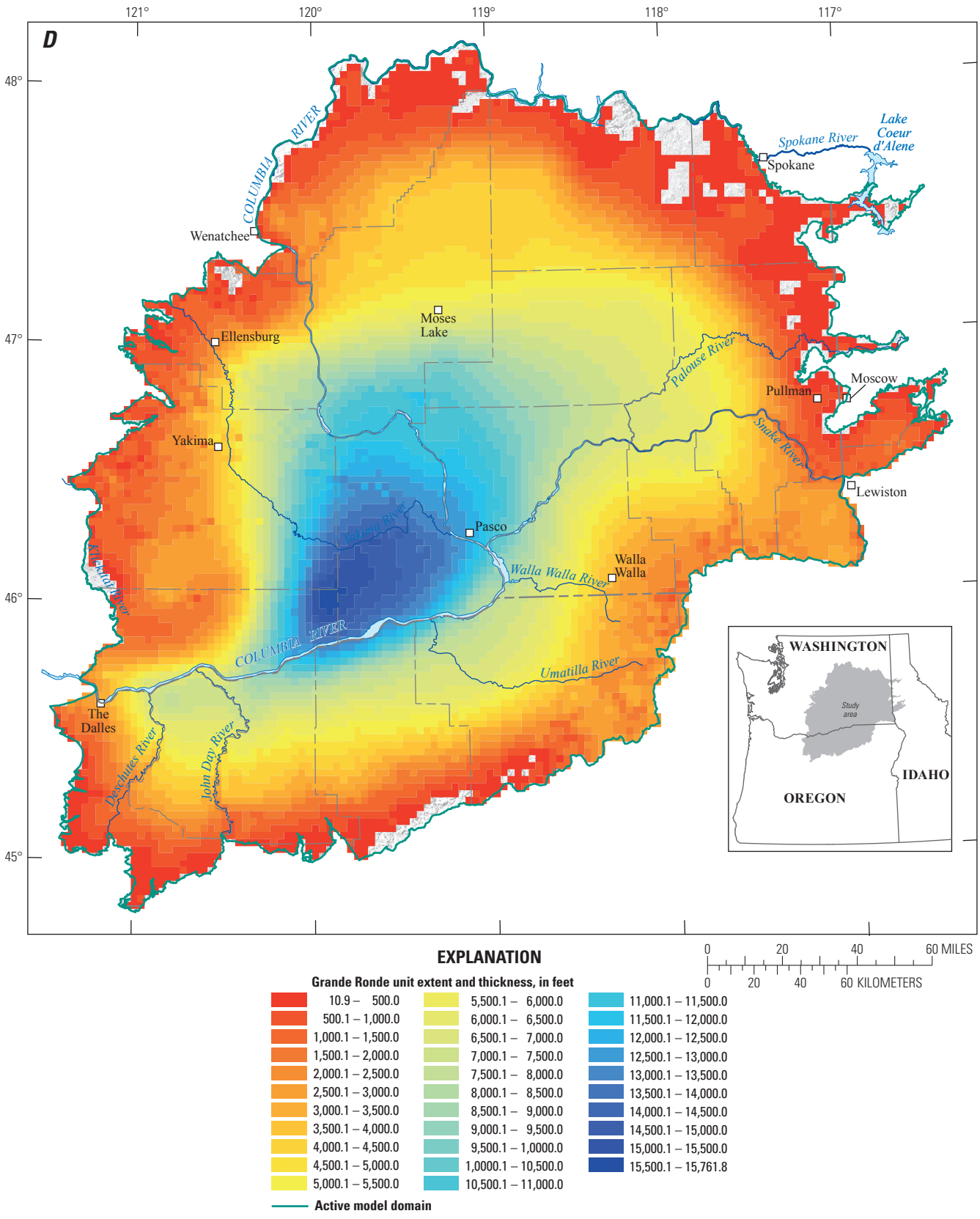

Figure 8.—Continued

Temporal Discretization

Two models were constructed to simulate groundwater flow in the CPRAS: (1) a steady-state predevelopment model representing conditions before large-scale pumping and irrigation altered the system, and (2) a transient simulation representing the period 1900–2007. Agricultural irrigation, from surface-water and groundwater sources, occurred throughout the Columbia Plateau from the late 1800s through early 1900s. However, large-scale groundwater level changes were not recorded until after the 1950s, when large-scale irrigation projects and groundwater development greatly increased. The steady-state predevelopment model was constructed to represent important aspects of the flow system without the complexities of large-scale groundwater withdrawals and aquifer storage properties.

Time discretization in MODFLOW has two levels of division: stress periods and time steps. External stresses, such as pumping rates and recharge, change at the beginning of each stress period. Stress periods, which are commonly monthly, quarterly, or annual in regional models, are divided into time steps. The groundwater flow equation is solved (meaning heads and flows are calculated) for each time step. The first stress period of the MODFLOW simulation represented steady-state predevelopment conditions. The steady-state predevelopment model provided initial conditions for the transient model representing early development (1900–1919), followed by annual stress periods that simulated the groundwater development that occurred throughout most of the 20th century and early 21st century (1920–2007), for a total of 90 stress periods. Recharge, pumping, and cross-connection of aquifers through open well boreholes (hereafter called commingling wells) were estimated for each stress period (see section, "Hydrologic Boundaries").

The long simulation using an annual stress period allowed for a temporal assessment that accounted for large changes in pumping and a range in climatic conditions and, thus, large ranges in simulated groundwater declines. Because the goal of this modeling effort was to understand the decadal-scale trends in water levels and base flow conditions, seasonal effects of pumping, and recharge were not considered with the current model.

Hydraulic Properties

Simulated flow through the model domain is controlled by the hydrologic boundaries (where water enters and leaves the domain) and the hydraulic properties in the flow system (that control the amount of water that may be stored and the ease with which water moves through the system). Each of the geologic units was represented as locally homogeneous and vertically anisotropic with bulk horizontal hydraulic conductivity generally being significantly higher than vertical conductivity. Discrete barriers to groundwater flow (Burns and others, 2012b) were simulated as linear horizontal flow barriers with much lower conductance than surrounding geologic units.

Horizontal Hydraulic Conductivity

Horizontal hydraulic conductivity (Kh) controls the ease with which water moves horizontally through geologic units. For the 100-ft basalt layers, Kh was a bulk conductivity that represents the relatively thin aquifer that typically occupies approximately 10 percent of the total thickness (Burns and others, 2012a). The sedimentary interbeds generally were thin compared to the total basalt thickness at each location; therefore, a single value of Kh for each interbed in each region of the model was appropriate for a regional scale-flow-simulation model. Thick Overburden units were separated horizontally by CRBG unit structural highs (fig. 3), and these units may exhibit significant amounts of heterogeneity horizontally and vertically (Ely and others, 2011). However, there are few large-volume sedimentary basins, and from a regional perspective, these basins are small compared to the regional CRBG aquifer system. Because the primary purpose of this groundwater-flow modeling effort is to understand the flow in the basalt units, the Overburden unit in a basin or region was simulated as locally homogeneous (a single value of Kh), although Kh and other hydraulic properties were allowed to vary between basins during parameter estimation and uncertainty analysis.

Initial values of Kh were assigned based on values tabulated from numerous previous studies and analysis of specific-capacity/aquifer-test data (Kahle and others, 2011, table 3), and on spatial distributions of these hydraulic properties in the calibrated CP-RASA model (Hansen and others, 1994). The initial estimates of Kh for the basalt interflow zones and flow interiors decreased with depth based on Weiss (1982) and Hansen and others (1994). The assumption is that overburden pressure and secondary mineralization have reduced pore space with depth, over time. Hansen and others (1994) decreased the Kh values with depth as a parabolic expression; resulting in a 40-percent decrease of Kh from the surface to a depth of 3,000 ft. The method provided reasonable estimates of Kh for the CP-RASA model (Hansen and others, 1994); therefore, it was used as starting values for the current model. The reduction of Kh with depth has been used by others in modeling groundwater flow in deep systems (for example, the Death Valley regional groundwater-flow system [Faunt and others, 2010] and the California Central Valley [Faunt and others, 2009]). The role of Kh decrease with depth for the CPRAS was examined during model calibration.

Vertical Hydraulic Conductivity

Vertical hydraulic conductivity (Kv) controls the ease with which water moves vertically through geologic units. For the 100-ft basalt layers, Kv is a bulk conductivity that represents the sequential vertical transmission of water through a heterogeneous basalt flow (both interflow and flow interior). Because the flow interior is thick and generally impermeable, basalt Kv is dominated by this part of the basalt flow. Similar to Kh, Kv for the sedimentary interbeds and Overburden was assumed locally homogeneous although variable between basins. Initial values of Kv were assigned based on values tabulated from previous studies and analysis of specific-capacity/aquifer-test data (Kahle and others, 2011, table 4).

Storage Properties

Two storage parameters represent two different storage mechanisms: specific storage (Ss) represents the change in storage associated with compressibility of water and the geologic material in confined aquifers, and specific yield (Sy) represents the water that may be gravity drained from the pore space within the geologic material in unconfined aquifers. In confined aquifers, which are completely filled with water, changes in the amount of water stored are due to compression or expansion of the water and the aquifer framework. Because water and rock are not very compressible, specific storage values typically are quite small (approximately 10^{-4} ft^{-1}). In unconfined aquifers, changes in the amount of water stored are due to actual draining or filling of the open space within the aquifer, so values generally are large (approximately 10^{-1} ft^{-1}). Both confined and unconfined conditions occur in the CPRAS.

Storage properties of the aquifers are highly variable, and a general lack of information makes reliable areal estimates difficult to obtain. A wide range of values for storage terms (Kahle and others, 2011, table 5), which typically reflect Sy when values are greater than 0.1, Ss when values are less than 5.0×10^{-4} ft^{-1}, and a mixed model-estimated calibration storage coefficient when values are between Sy and Ss. When considering estimated storage coefficients, an additional complication is the volume being analyzed. For example, the porosity of a flow interior may be significantly smaller than the porosity of an interflow zone, although each zone may be represented in a single model cell. For the current analysis of the CRBG system, storage coefficients were required that represent the average storage of the entire vertical profile of the basalt flow (both interflow and interior).

Neutron porosity estimates from boreholes on the Hanford Site were used to estimate a bulk specific yield of 0.1 (dimensionless). Values of Ss for basalt were estimated as 2.5×10^{-5} ft^{-1}, which were consistent with the reported values of Kahle and others (2011), and were used as the initial values in the model. Model stability and convergence were not sensitive to Ss and Sy values.

Geologic Structures

The CRBG effective Kh is decreased by several orders of magnitude in areas of intense folding and faulting, especially fault-associated anticlines (Hansen and others, 1994; Packard and others, 1996; Reidel and others, 2002, Ely and others, 2011). Where the distribution of water-level measurements are closely spaced, high Kh regions often can be separated by narrow transition zones (commonly coincident with a fault or fold trace) that are significantly less permeable (Burns and others, 2012b). Low permeability along geologic structures may be due to the offsetting of interflow zones through faulting, which juxtaposes thin basalt aquifers with thick confining units and produces low-conductivity fault breccia and gouge material at that interface (as described by Stearns [1942] and Newcomb [1965, 1969]), and the decreasing pore space through deposition of secondary minerals. Similarly, intense folds accommodate slip along planes of low strength (interflows), grinding and thinning deposits in the slip plane, potentially reducing permeability. Not all folds and faults act as flow barriers and currently, there is no predictive relation between fold and fault type and the extent that the structure forms a barrier to groundwater flow.

Displacement of individual basalt flows along faults, however, locally can enhance vertical movement of water by providing fractured zones across basalt flows that could serve as conduits for vertical groundwater flow. Preferential pathways may be developed locally, but faults commonly tend to act as barriers to flow regionally. Because CRBG flow interiors chemically weather to clays when broken rock (fault gouge) is exposed to moving water, faults are believed to be “self-sealing” on the geologic timescale, which explains why most fault zones across the CPRAS are not vertical conduits for groundwater flow.

The Horizontal-Flow Barrier (HFB) package of Hsieh and Freckleton (1993) was used to simulate low-permeability geologic structures. Additionally, HFBs were used at all high offset faults identified in the geologic model of Burns and others (2011). Flow barriers comprising 34,465 model cells from model layers 10–100 were grouped into 25 hydraulic categories (fig. 9) and initial hydraulic characteristic values of the 25 hydraulic categories ranged from 9.95×10^{-16} to 1.17×10^{-8} 1/d, with the smallest value having the largest control. The hydraulic characteristic of the horizontal-flow barrier for unconfined layers is the barrier hydraulic conductivity divided by the width of the horizontal-flow barrier along the flow path. The hydraulic characteristic of the HFB for confined layers is the barrier transmissivity divided by the barrier width.

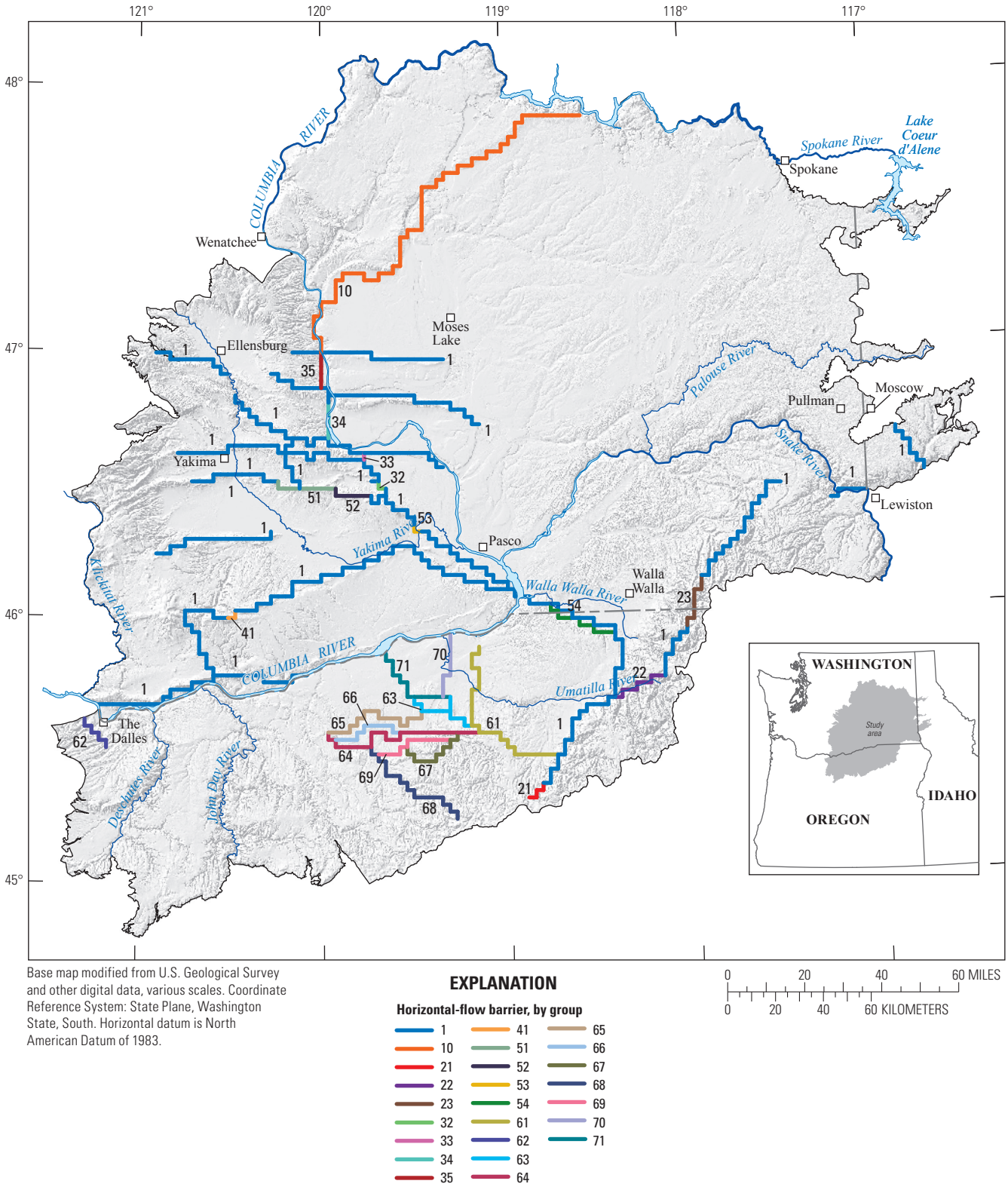

Figure 9. Location and hydraulic characteristic group of the groundwater model structure (horizontal-flow barriers), Columbia Plateau Regional Aquifer System, Idaho, Oregon, and Washington.

Model fit was considered reasonable with no zones of preferential vertical flow associated with faults, which supported the assumption that most vertical preferential flow associated with faulting has sealed over geologic time with respect to the regional groundwater-flow system. However, some vertical flow may be occurring at a local scale. For regions with a high density of mapped geologic folds and faults and steep hydraulic gradients, but where the distribution of water-level measurements was not dense enough to identify the most important structures for controlling flow, a lower Kh was used to represent the effective permeability of the region.

Hydrologic Boundaries

Boundary conditions define the locations and manner in which water enters and exits the active model domain. The specified boundaries of the model coincide as much as possible with natural hydrologic boundaries. Three types of model boundaries were used in the CPRAS model: (1) no-flow boundaries (groundwater divides and basalt unit extents), (2) head-dependent flux boundaries (drains, rivers, and multi-node wells), and (3) specified-flux boundaries (recharge and pumping). Head-dependent and specified-flux boundary conditions were developed for predevelopment conditions and for 1900–2007.

Evapotranspiration (ET) was not simulated using the groundwater-flow model. Instead, net recharge (precipitation plus irrigation minus evapotranspiration minus runoff) was computed using the SOWAT model (Kahle and others, 2011), and used as input to the groundwater-flow model. This approach accounted for most ET, with only a small part of the water budget neglected by ignoring groundwater-fed wetlands.

Hydraulic Conditions Along the Periphery of the Model

All lateral model boundaries were assumed to be no-flow boundaries (fig. 10), with the understanding that some water might be entering the model domain, but the amount likely is small compared with recharge. During model calibration, this assumption was determined to be reasonable, although during transient simulation, some wells along the periphery could not support the desired pumping, indicating that (1) wells were extracting most of their water from beneath the CRBG, (2) local stream capture was occurring, but was not simulated by the model, or (3) some lateral inflow of water exists.

The model domain was selected by identifying hydraulic boundaries with low (ideally zero) groundwater flow across the boundary into or out of the model domain. These hydraulic divides commonly are coincident with major topographic divides associated with mountains and rivers. For example, hydraulic evidence shows that both surface water and groundwater flows away from the crest of the Blue Mountains (fig. 6). To the north, the Columbia River is deeply incised into older pre-Miocene rock, and was represented as a no-flow boundary because of extremely low permeability of pre-Miocene rock. However, incised rivers at no-flow boundaries still may have river and drain cells simulated to allow water to enter or leave the domain. This can allow water to drain from the aquifer system into canyons, if appropriate.

Near the depositional margins of the CRBG, the basalt was deposited as intra-canyon flows, rather than large sheet flows, and lateral inflow of water from adjacent, hydraulically connected deposits might occur more easily in these locations than in areas of unconnected margins. However, recent simulation results for the Yakima River Basin (Ely and others, 2011) indicated that most water that is recharged in the Cascade Range beyond the extent of the CRBG deposits (fig. 1) returns to the stream rather than flowing laterally into the CRBG. This finding was assumed to be applicable to CRBG deposits in the southwestern boundary and in the foothills of western Idaho (fig. 10). The foothills of western Idaho are significantly different from the Cascade Range, but recharge potential also is much smaller in Idaho; therefore, the boundary was selected under the presumption that some water might be entering the CPRAS there.

The two remaining major areas of the CRBG boundary are where the Deschutes River crosses the model boundary in Oregon, and near Lewiston, Idaho (fig. 7). Near Lewiston, a fault offset of several thousand feet was interpreted as a likely barrier to flow. For the Deschutes River, the continued trend of Blue Mountains geologic structures was used to estimate the boundary. River streamgage data and Deschutes River Basin groundwater-flow model results (Gannett and Lite, 2004) support this as a reasonable model boundary.

The base of the CRBG was selected as the lower (no-flow) boundary for the model. Previous studies have used this boundary (Hansen and others, 1994) and the low permeability of the underlying deposits support the location of the no-flow boundary, especially near the center of the study area.

Groundwater Pumpage

The spatial distribution of pumping was estimated on a 1-km grid coincident with the SOWAT grid for 1920–2007. SOWAT-derived estimates of irrigation pumping for 1985–2007 (Kahle and others, 2011) were supplemented with previously published estimates of large-capacity well withdrawals (Cline and Collins, 1992) and new estimates for municipal, industrial, rural, and residential uses.

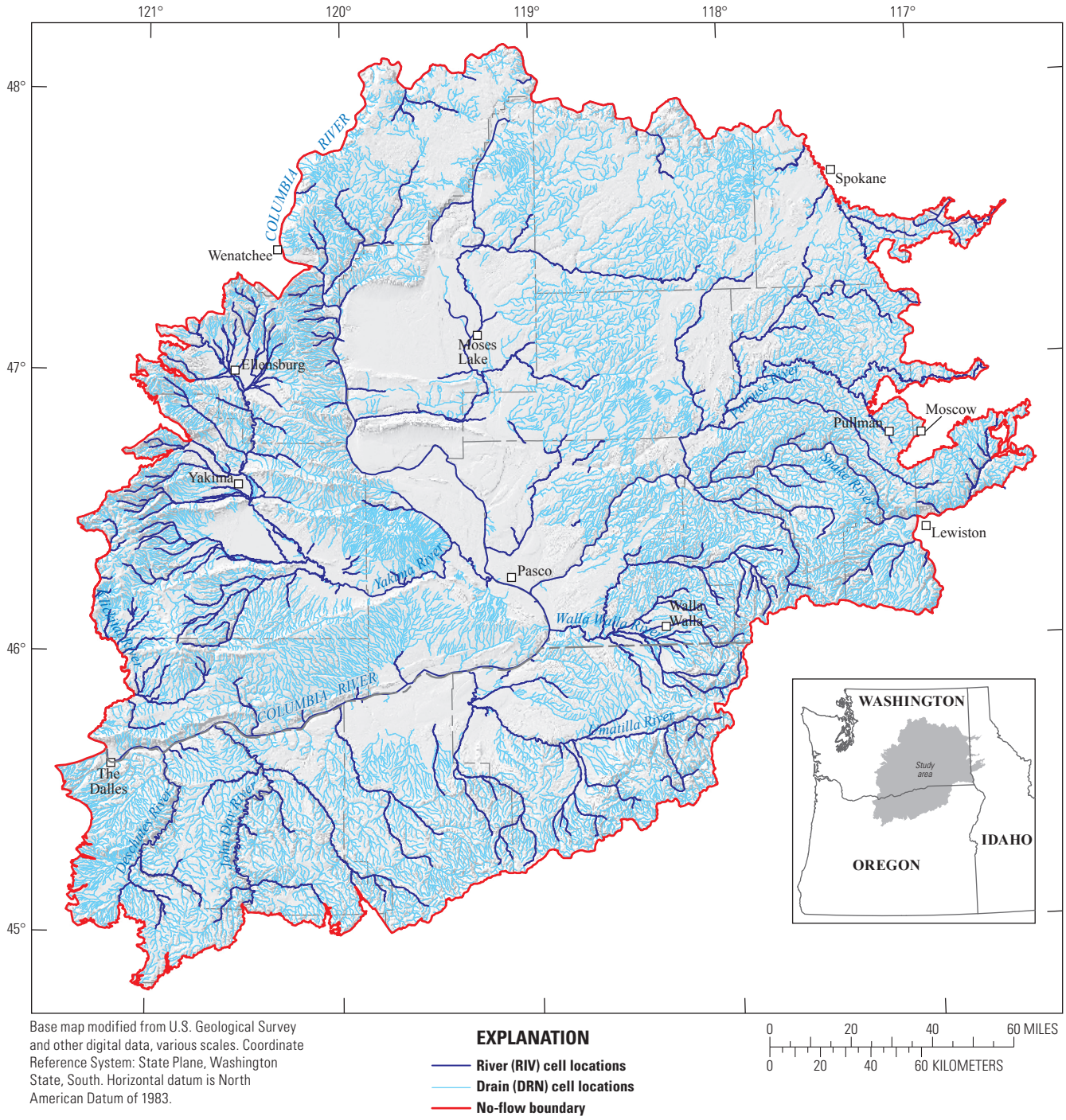

Figure 10. Location of the groundwater-flow model river and drain cells, and the no-flow boundary, Columbia Plateau Regional Aquifer System, Idaho, Oregon, and Washington.

Amounts of historical groundwater pumping in the Columbia Plateau for the period 1945–84 were determined by Cline and Collins (1992) as part of the RASA study of the 1980s. Methods used to estimate well withdrawals are: (1) compiling electrical power consumption records, (2) multiplying irrigated acreage by a water-application rate, and (3) using other methods, such as data from published reports, field visits, population, water-use, water rights, and well construction logs, and information from telephone surveys. The resulting, gridded estimates could be considered the most detailed and accurate estimates of groundwater pumping and were used to hind cast and augment pumpage estimates for 1920–84.

For the period 1985–2007, estimates of total pumpage were made by adding estimates of irrigation pumpage extracted from the 1-km grid-spacing SOWAT model results of Kahle and others (2011) to estimates of pumpage for all other anthropogenic activities (fig. 11). For SOWAT grid cells occupied by irrigated agriculture, the SOWAT model uses estimates of actual evapotranspiration to calculate when irrigation should occur to meet plant needs. When irrigation water is required, SOWAT estimates the amount of water necessary to fill the soil and uses an irrigation inefficiency to estimate the total amount of water applied from each irrigation source. Pumpage was smoothed in the same manner as pumping-associated recharge (see section, "Groundwater Recharge") so that model inflow and outflow estimates were made in a consistent manner. Pumpage also was estimated for each year for public-supply wells, private domestic wells, and other water uses requiring water-rights permits. If the well location was known precisely, pumpage was assigned to the associated SOWAT 1-km grid cell. If water use was assigned to a mapped area, then pumpage was assigned to the 1-km grid proportionally to the fraction of the mapped area intersecting each 1-km grid cell. For example, census blocks were used to estimate rural residential pumpage for census years based on typical per capita water use, and pumpage was distributed equally across the entire census block. Between census years, pumpage was assumed to linearly vary between the years. Pumpage estimates using this method were compared to independent estimates for the Umatilla River Basin (Kahle and others, 2011, fig. 21*B*), the Odessa subarea in east-central Washington (Cline, 1984), and the area of the Yakima River Basin that intersects the CPRAS model domain (Ely and others, 2011). All estimates indicated good agreement.

Pumpage for the period 1920–84 was constructed by hind casting the pumpage estimates for 1985–2007 using the tabulated pumpage estimates of Cline and Collins (1992). The Cline and Collins tabulated pumpage estimates for 1984 were compared to 1985 estimates made using the SOWAT 1-km grid methods to ensure that estimates using these dissimilar methods were consistent. To compare the two methods of

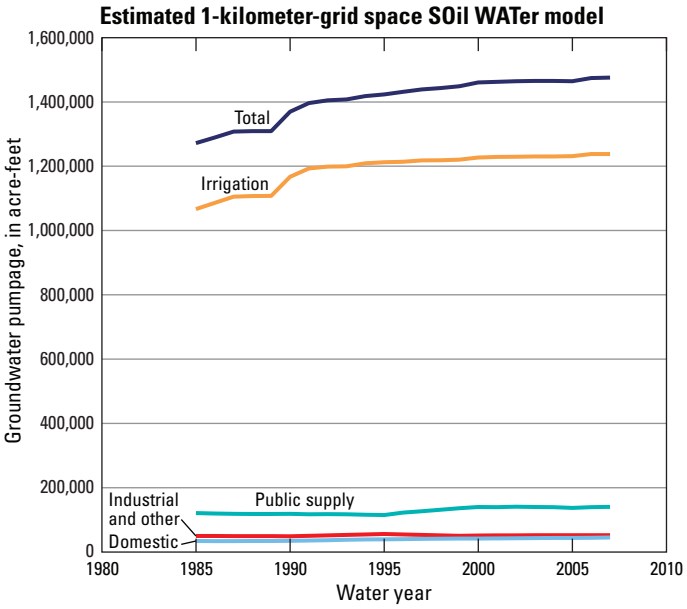

Figure 11. Estimated groundwater pumpage, by category, Columbia Plateau Regional Aquifer System, Idaho, Oregon, and Washington, 1985–2007.

estimation, the 1-km grid was intersected with the quarter-township (9 mi^2) grid of Cline and Collins (1992), and the total intersected pumpage was compared with tabulated values by Cline and Collins. These methods showed good agreement (fig. 12).

Estimating periods of historical pumpage was accomplished differently, depending on whether or not the 1-km grid cell intersected a Cline and Collins (1992) grid cell with appreciable pumpage. If Cline and Collins did not estimate appreciable pumpage, the 1985 pumpage rate at each 1-km cell was tied to an existing nearby deep well (typically within a 3- by 3-km grid centered on the 1-km cell), and simulated pumping began when the presumed well was constructed. For Cline and Collins cells with non-negligible amounts of pumpage, the refined 1-km pattern of 1985 pumping from SOWAT was assumed to be the correct pattern, and the magnitude of pumpage using this pattern was scaled by the estimates of Cline and Collins using linear interpolation for years between estimates, ensuring that both magnitude and distribution of pumpage matched 1985 1-km grid estimates exactly. Pumpage was assumed to be negligible prior to 1920, because pumps with significant hydraulic lift were not common before then (Cline and Collins, 1992). The earliest estimates of pumpage by Cline and Collins were linearly decreased to zero in 1920, even though there are a few records for wells prior to this time.

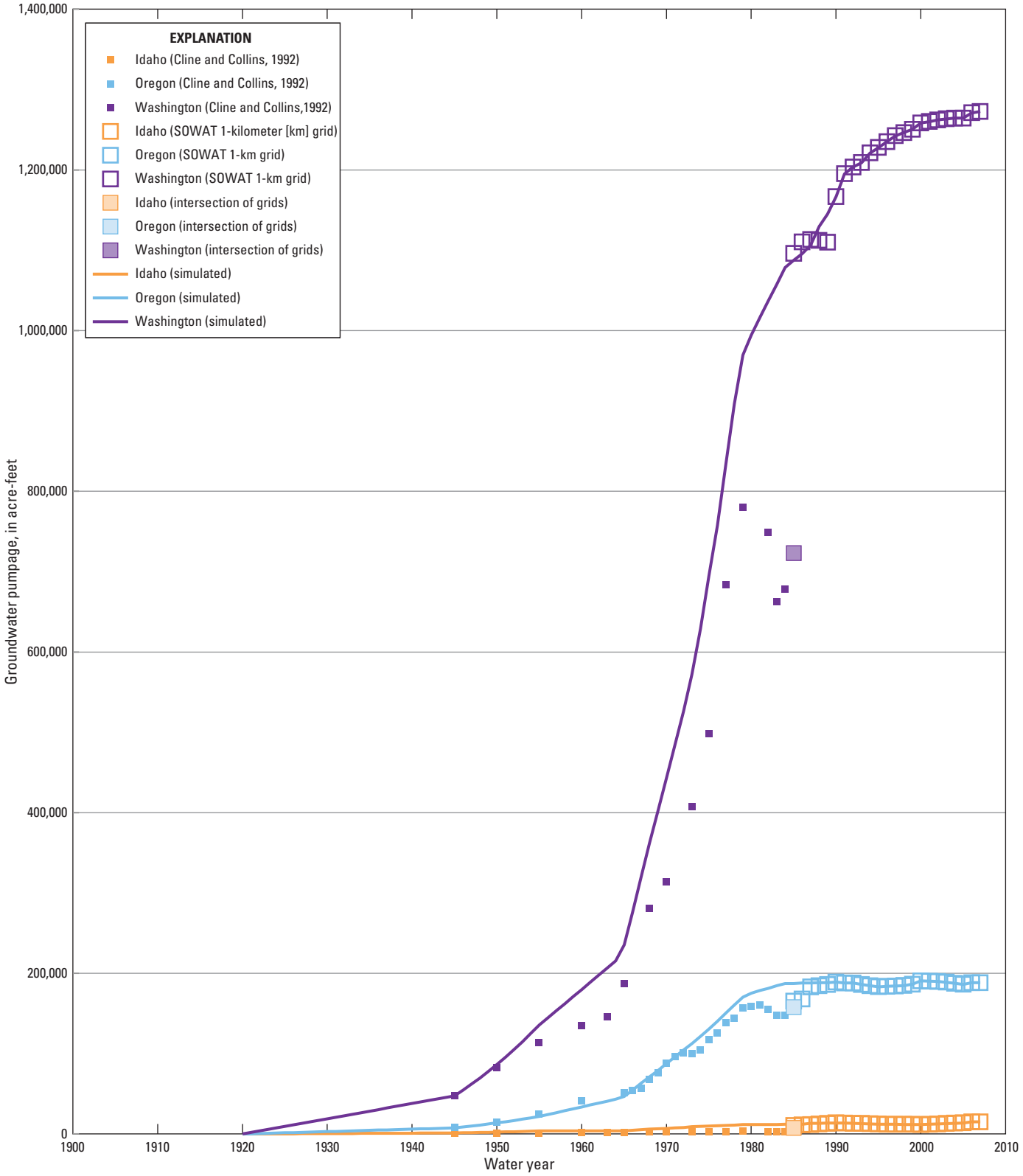

Figure 12. Estimates of groundwater pumpage from Cline and Collins (1992) and SOil WATer (SOWAT) balance (Kahle and others (2011), and simulated groundwater-pumpage, Columbia Plateau Regional Aquifer System, Idaho, Oregon, and Washington.

Groundwater pumping was simulated using the Multi-Node Well (MNW2) Package of MODFLOW-NWT (Konikow and others, 2009). Initially, pumping at each 1-km grid cell was assigned to the deepest nearby well. For 1-km grid cells with pumping estimates derived from Cline and Collins (1992) estimates, the pumping well is the deepest nearby well during the stress period, so pumping moves from shallow wells to deeper wells over time. Because wells in the CRBG typically are open from the base of the Overburden to the bottom of the well, water can be supplied from any open aquifer to meet water demand. If well records indicated full penetration of the CRBG into the deeper pre-Miocene rocks (not simulated), the amount of pumping assigned to these wells was proportional to the fraction of the total length of the borehole that intersects model units, as estimated using the geologic model of Burns and others (2011).

All wells with construction records were simulated in the model if the well either potentially commingles aquifers (the length of the borehole spans multiple model layers) or has pumping assigned to it. Simulation of these wells allows the net pumping and net commingling influence of CPRAS wells to be represented over time. If pumping was indicated by the 1-km grid pumping estimates, but no well record was available within the MODFLOW model cell, pumping with no commingling was simulated from the uppermost aquifer.

Use of the MNW2 Package allowed representation of both pumping and commingling effects. Commingling wells were simulated using the SKIN option in MNW2 where the hydraulic conductivity of a cylindrical region near the borehole is assumed to be less than the hydraulic conductivity of the aquifer system (Konikow and others, 2009). The skin conductivity (Kskin) allows simulation of the imperfect connection between the aquifer system and the borehole that results from geologic and well-construction heterogeneity, and this parameter allows simulation and adjustment of the net effect of commingling. Wells that only intersect a single model layer were simulated using the THIEM option in the MNW2 Package.

Following preliminary transient simulations, it was observed that the desired amount of pumping was not being extracted from the model for current conditions (2000-2007). This occurred because Kskin values that resulted in reasonable time-varying patterns of drawdown were restricting inflow to wells sufficiently that wells were shutting off due to drawdown limits without producing enough water. This apparent contradiction occurred because pumping rates are controlled by the aquifers that are well-connected to wells (aquifers that can supply large amounts of water easily), but commingling between aquifers is limited by aquifers that are less well-connected to wells (reduced flow occurs at restrictions). To split the pumping and commingling processes, pumping was reallocated to vertical strings of single node THIEM wells, and commingling was represented with multi-node wells with a specified Kskin and no associated pumping.

For each vertical string of single node wells, pumping was assigned to each node proportionally to the relative potential for each node to supply water. A node was defined as possibly contributing if a well is contained in the model cell and if simulated hydraulic head in the model cell was above the bottom of the model cell during the stress period. Relative potential to supply water was defined as the product of the hydraulic head above cell bottom (representing flow potential), the cell thickness (representing area available to flow), and an estimate of relative hydraulic conductivity (representing the relative ease of flow). Based on preliminary steady-state model calibration, hydraulic conductivity of Saddle Mountains basalt and Overburden was assumed to be twice the conductivity of the Wanapum basalt, which was twice the conductivity of the Grande Ronde basalt. The resulting distribution of pumping allows water to be removed from upper layers more easily than from lower layers, consistent with the typical history of well construction. Estimation of single node pumping wells required the estimation of hydraulic head; therefore, the transient model was first run allowing commingling, but not allowing pumping. Iterative application of the method allowed reallocation of simulated pumping based on successive improved estimates of head distribution over time.

The methodology to assign pumping and commingling wells resulted in a maximum of 20,752 commingling wells spanning from a minimum of 2 layers to a maximum of 38 layers for a total of 90,938 nodes. Kskin was set to 0.1 ft/d for all commingling well cells. Pumping wells were assigned to 62,446 nodes. Final estimates and the spatial distribution of groundwater pumping for current conditions (2000–2007) are shown in figure 13.

Groundwater Recharge

Over most of the study area, natural recharge occurs only during the wet winters. During the dry summer months, recharge is dominated by irrigation inefficiency and associated irrigation infrastructure (for example, irrigation canals). Irrigated areas have higher antecedent soil moisture at the start of the wet season, increasing the fraction of precipitation that recharges groundwater. Groundwater recharge was estimated using three methods to accommodate three different periods in the simulation: (1) correlation of precipitation to recharge, (2) SOWAT estimates, and (3) hind casting of SOWAT estimates.

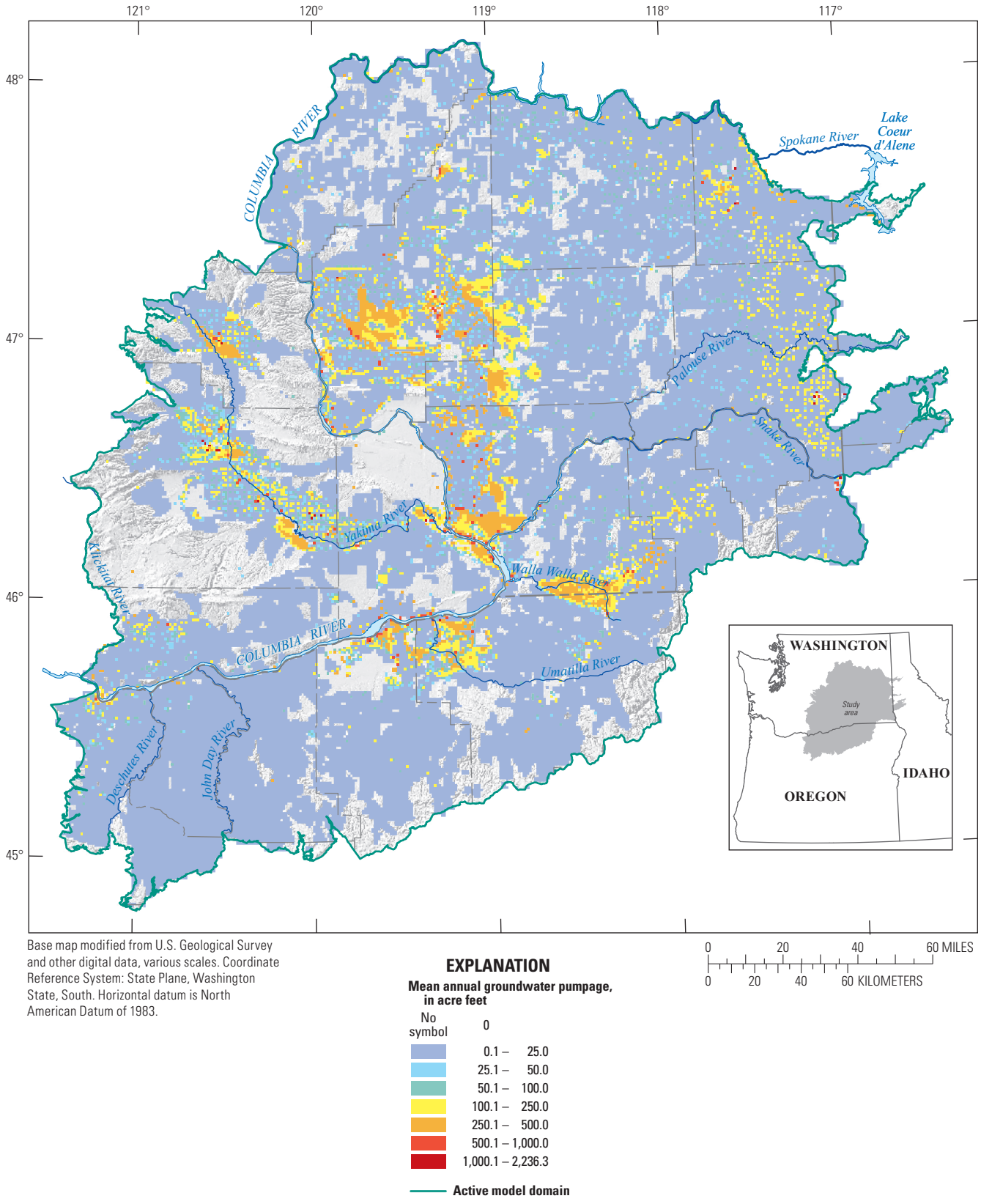

Figure 13. Mean annual groundwater pumpage for current conditions (2000–2007), Columbia Plateau Regional Aquifer System, Idaho, Oregon, and Washington.

Predevelopment groundwater recharge was estimated using the annual 1895–2007 gridded historical estimates of annual precipitation provided by the Parameter-elevation Regressions on Independent Slopes Model (PRISM) (PRISM Climate Group, 2004) and the Bauer-Vaccaro regression equation (Bauer and Vaccaro, 1990) relating annual precipitation to groundwater recharge. Recharge estimates for 1920–84 were derived from the SOWAT recharge estimates combined with the groundwater pumping estimates of Cline and Collins (1992) and a timeline of construction of large-scale surface-water irrigation projects. Recharge estimates for 1920 were used for the period 1900–19. Annual recharge estimates from the SOWAT modeling results of Kahle and others (2011) were limited to the period 1985–2007 because of the availability of evapotranspiration estimates from satellite imagery.

To account for the effect of decadal variations in natural recharge, the SOWAT-estimated recharge was divided into natural recharge and the additional recharge from irrigation. Additional recharge accounts for irrigation inefficiency and high antecedent soil-moisture content, and is computed as the difference between the total SOWAT-estimated recharge and the recharge estimated using the Bauer and Vaccaro regression equation. The additional recharge was divided into surface-water and groundwater sources using the estimates of fraction of irrigated land in each 1-km grid cell supplied by each source used in the SOWAT model.

For the period 1985–2007, recharge estimates were extracted from the 1-km grid SOWAT modeling results of Kahle and others (2011). For grid cells dominated by irrigated agriculture, the SOWAT model used a simplified energy balance and soil reservoir model to estimate net recharge into the groundwater system from irrigation and precipitation. For all other grid cells, net recharge was estimated from annual precipitation using the Bauer and Vaccaro regression equation (Bauer and Vaccaro, 1990). Spatially-distributed annual estimates of precipitation were extracted from historical PRISM simulations (PRISM Climate Group, 2004).

Recharge for 1920–84 was reconstructed by hind casting the 1985–2007 recharge estimates. This method assumed that current irrigation is the most extensive and that irrigation was less extensive in the past. Irrigation from groundwater was related to gridded estimates of pumping (Cline and Collins, 1992), and irrigation from surface water was tied to the history of large-scale irrigation projects.

Predevelopment recharge was smaller than recharge under existing conditions due to the infiltration of irrigation water during delivery and application to croplands. Irrigation projects exist throughout much of the Columbia Plateau, but the largest areas of intense irrigation are in the Yakima and Walla Walla River Basins, Umatilla subarea, and Columbia Basin Irrigation Project (fig. 2). Detailed annual estimates of historical surface-water irrigated acreage do not exist, so irrigation, and therefore recharge from irrigation, was increased linearly from the first year of irrigation water delivery until full irrigation deliveries were in effect.

To replicate the general timing and amount of recharge from large surface-water irrigation projects, recharge was systematically increased to 1985 SOWAT-estimated values using some simple rules: (1) CBIP irrigation was assumed to start in 1950 with irrigation increasing linearly to 100 percent in 1953; (2) Yakima River Basin surface-water irrigation was assumed to start in 1921 with irrigation increasing linearly to 100 percent in 1930; and (3) Umatilla subarea surface-water irrigation was assumed to be 24 percent at the start of the transient simulation (1900), increasing linearly to 34 percent in 1961, to 75 percent in 1975, and to 100 percent by 1984 (M. Ladd, Oregon Water Resources Department, written commun., 2012). Surface-water irrigation outside of the large projects in the Yakima River Basin, Umatilla subarea, and the CBIP are a relatively small fraction of total surface-water irrigation; these irrigated lands were assumed to exist for the entire period of transient simulation. Implementation of the previous assumptions resulted in recharge stresses that are considerably simpler than reality, but provided a reasonable timing of stresses to ensure the timing of changes in recharge correspond to the approximate history of water use on the Columbia Plateau.

The amount of estimated additional recharge from irrigation was examined and two anomalies were noted. First, in areas of sparse irrigation, where 1-km model cells were not dominated by irrigated agriculture, extra recharge was proportionally too high. This was attributed to the fact that the soil-water balance model assumed the entire cell was irrigated, leaving antecedent soil moisture too high for parts of the cell that are not irrigated, overestimating recharge from winter precipitation. Because SOWAT estimates actual ET, the rate of irrigation water applied and recharged from irrigation inefficiency should be correct. The total area occupied by these cells was relatively small compared to the entire model domain, so the error in total estimated recharge was negligible given the model scale. Second, recharge from irrigation varied in an oscillatory manner from year to year by about 20 percent, possibly caused by the method of representing when irrigation occurred. The soil-water balance model assumes a deep soil zone, resulting in infrequent addition of irrigation water (typically 4–5 times a year). Because SOWAT assumes that water is added to the deep soil zone when "maximum allowable soil depletion" is reached, it is possible that irrigation would be simulated on the last day of the simulated irrigation season or that irrigation would have been simulated on the next day, if the end of the season was not simulated, a difference of about 20 to 25 percent (based on events occurring 4–5 times a year) would result. Because the purpose of the groundwater-flow model was to examine long-term signals, the natural component of recharge (Bauer and Vaccaro [1990] regression equation) was subtracted from total SOWAT-estimated recharge, and the irrigation component was smoothed and assumed to increase monotonically due to the increasing area of irrigation until 2007.

The mean annual natural groundwater recharge for the 33,000 mi^2 model domain for 1895–2007 was 3.2 in/yr (5.7 million acre-ft/yr) which was used as the estimate of recharge for the predevelopment steady-state model (fig. 14*A*). During model calibration, large interannual differences in natural recharge estimates caused model instabilities. This was attributed to the fact that the groundwater-flow model does not simulate a vadose zone, which would dampen the highly variable, precipitation-dependent recharge estimated using the Bauer and Vaccaro (1990) method. To add stability while retaining decadal trends in precipitation, annual recharge from precipitation was averaged with the preceding 2 years, resulting in a 3-year rolling average that was applied to the recharge estimates at each 1-km cell. Averaging with preceding years approximated vadose zone lag because high recharge years were damped and spread across several years. By 2007, recharge associated with surface-water irrigation was estimated as 1.0 million acre-ft/yr and recharge associated with groundwater irrigation was estimated as 0.61 million acre-ft/yr. During model calibration, surface-water irrigation efficiency was increased from 50 to 75 percent, similar to assumed groundwater irrigation efficiency. This adjustment reduced recharge due to surface-water irrigation over time. Approximately 21 percent more recharge was entering the aquifer system during 2000–2007 (fig. 14*B*), than during the predevelopment period.

Streams and Surface-Water Features

The exchange of groundwater and surface water is an important hydrologic process in the groundwater-flow system and, to the extent possible for a regional model, the CPRAS model was constructed to simulate this process. Rivers and streams throughout the model domain were simulated with the MODFLOW River (RIV) and Drain (DRN) Packages (Harbaugh, 2005). Surface water was allowed to exchange with groundwater at all mapped surface-water features and where groundwater could seep out from exposed geologic units.

The RIV Package was used to simulate natural stream and river reaches with calculated mean annual flows from the National Hydrography Dataset (NHD; Simley and Carswell, 2009) equal to or greater than 25 ft^3/s throughout the model domain (fig. 10). The DRN Package was used to simulate all other reaches and areas where geologic units that are exposed at land surface can drain into nearby surface waters (fig. 10). To calibrate the model, river and drain fluxes were summed and compared to measured and estimated base flows. River parameters required by the RIV Package include river stage (STAGE), river bottom elevation (RBOT), and river conductance (computed as an adjustable multiplier times the parameter CONDFACT). Drain parameters required by the DRN package include the drain elevation (ELEVATION) and the drain conductance (an adjustable multiplier times the parameter CONDFACT). Initial values of riverbed conductance were based on stream length (determined using a geographic information system), and average depth and width for the river reaches were based on mean annual streamflow from the USGS National Hydrography Dataset (U.S. Geological Survey, 2014) and regression equations determined by Magirl and Olsen (2009). The river and drain conductance parameters that control the effective rate of exchange of surface water with the aquifer system as a function of the head in the aquifer system, were assumed to be proportional to the area through which water can flow, and were adjusted during calibration using a multiplier. In model cells that contain multiple river and (or) drain reaches, those reaches were aggregated and formulated as a single river reach, drain reach, or both. The river and drain conductance parameters were assumed to be proportional to the cumulative area of all features within the cell that act as rivers or drains, respectively.

To estimate the cumulative area associated with all rivers and drains within each model cell, the NHD dataset was intersected with the model grid in plan view, and stream reach lengths and NHD properties were associated with the model grid. For each model row and column, if a reach exceeded the annual flow threshold of 25 ft^3/s, then a RIV cell was simulated at the model layer where the lowest downstream reach elevation existed (plus a 0.1 ft upward offset to ensure no computational problems when rivers and drains have head controlling elevations too close to the NWT dry cell condition). The lowest elevation downstream reach was specified as the value for the RBOT, and STAGE was set to this elevation plus the associated depth of water estimated by Magirl and Olsen (2009) for the NHD. For each stream reach simulated using the RIV Package, area was estimated as the length of the wetted perimeter (computed from NHD estimates of top and bottom width and depth of water) times the length of the reach intersecting the model grid. All of these areas were summed to estimate CONDFACT for the RIV cell. If the maximum mean annual flow from the NHD at any MODFLOW row and column was less than 25 ft^3/s, then the surface-water feature was simulated using the DRN package with CONDFACT computed in the same way and ELEVATION computed as the elevation of the lowest downstream reach plus the associated estimate of depth of water. For all model cells overlying these lowest cells, DRN cells also were simulated with ELEVATION set to the elevation of the top of each model cell. This allowed groundwater to leave the system by draining from the layers that are through-cut by stream incision. Setting the elevation at the cell top improved model stability by limiting dewatering and was consistent with the notion that each layer has an interflow zone. The area estimate for computation of CONDFACT assumed that the drains would be exposed in the canyon walls, and was computed for each reach as the distance from the top of the cell (plus 0.1-ft offset) minus the downstream reach elevation (or the cell bottom, whichever is greater) times the reach length times two (representing the two exposed faces in the canyon cut) times 10 percent (the estimated total thickness occupied by the interflow zone versus the flow interior). This formulation for drain area allowed that drainage was more efficient for stratigraphically high units intersected by more stream reaches, than with low units intersected less frequently.

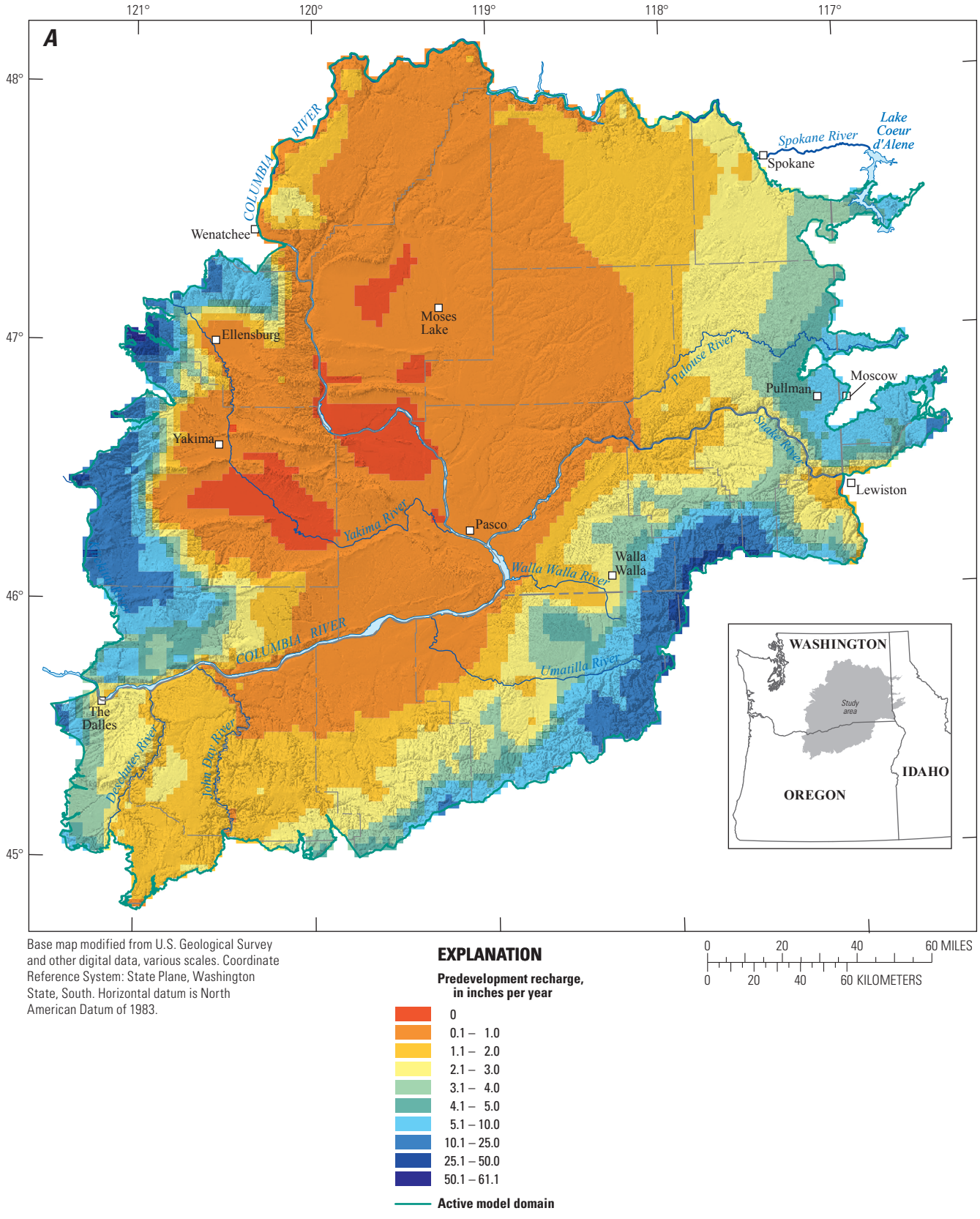

Figure 14. Mean annual groundwater recharge for (*A*) predevelopment and (*B*) current conditions (2000–2007), Columbia Plateau Regional Aquifer System, Idaho, Oregon, and Washington.

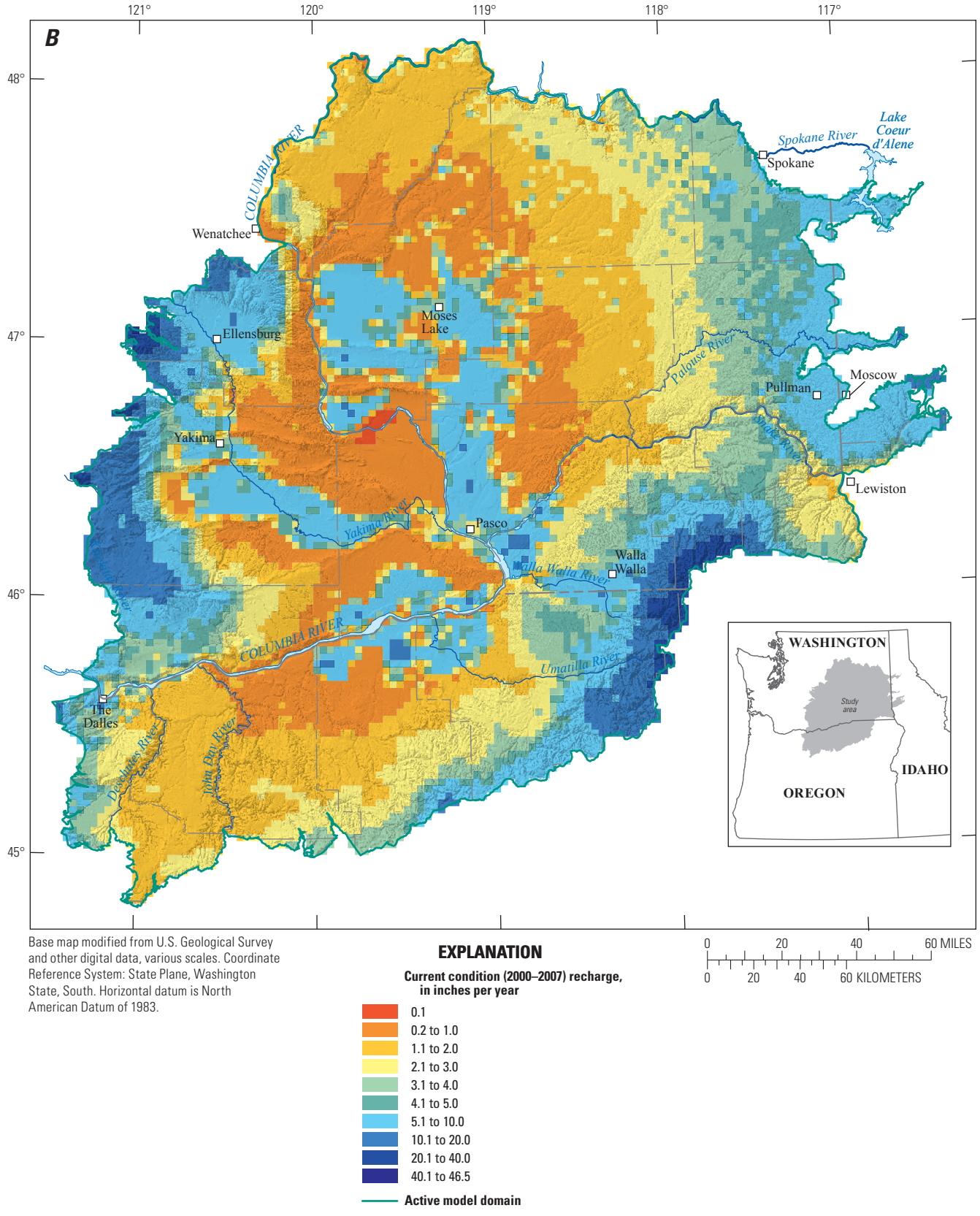

Figure 14.—Continued

The final locations requiring drains were at geologic outcrops controlled by faulting or strong folds combined with erosion and where simulation of horizontal flow barriers along stream valleys might prevent drainage from each side of the valley into the streams. All of these features were represented by the HFB Package (see section, "Geologic Structures"), so during model construction, both sides of each HFB were checked to determine if a stratigraphic layer was exposed in outcrop on one side of the HFB. If this condition occurred, a DRN cell was simulated with ELEVATION set to the elevation of the top of the model cell and CONDFACT equal to the thickness of the model cell times the effective length of the outcrop times the fraction of the thickness contributing to the flow (for erosional cuts, this was assumed to be 10 percent). The product of the effective length times the thickness fraction was selected by iteration with an early version of the model, and a value of 5,000 ft provided robust and stable solutions that prevented anomalous hydraulic heads near fault scarps. Uncertainty was not evaluated, but the probability that drainage occurs from the broken uplifted side of a fault is consistent with the conceptual model of flow through CRBG units.

This approach added numerical stability to the model in areas far from regions of greatest interest and accounted for the generally gaining stream reaches. The drain hydraulic conductance is a function of the surrounding hydrogeologic material and the drain geometry. Information necessary to calculate a drain conductance, such as the distribution and hydraulic conductivity of material near the drain, were not available. Commonly, drain conductance is a lumped parameter that is adjusted during calibration to match measured flows. The CPRAS model included 43,311 drain cells assigned from model layers 1–64 and 1,727 river cells assigned to model layers 2–60.

Model Calibration and Sensitivity

Model calibration is the process in which model parameters, model structure, and boundary conditions are adjusted to obtain a reasonable fit between simulated heads and fluxes and measured data. The final CPRAS model used the principle of parsimony, where the simplest model that provides a good fit between observed data and simulated equivalents is retained. If the model fit is determined to be "good enough" by the modeler, taking into account the purpose of the model, limitations imposed by the modeling assumptions, and quality and distribution of the data supporting estimation of model parameters then the model is considered to be adequately calibrated. Initially, a simple distribution of parameters was used, followed by addition of a large number of parameters that allowed testing of the role of geologic structure on groundwater flow, followed by a process of simplifying the model by grouping parameters. Highly parameterized models require a different approach to model calibration and uncertainty, such as regularized inversion (Doherty and Hunt, 2010).

The model was calibrated using the iterative parameter estimation (PEST) software package (Doherty, 2010). PEST uses a nonlinear least-squares regression to find the set of parameter values that minimizes a weighted sum-of-squared-errors objective function. Throughout the calibration process, no adjustments were made that conflicted with the general understanding of the aquifer system and previously documented information.

Although the results of the predevelopment steady-state and long-term transient models are presented here in logical order, in reality, the models were calibrated iteratively. Model run times associated with the transient (1900–2007) simulation period and the complexities added by the MNW2 Package, increased recharge from irrigation, and addition of storage properties, made automated calibration of the transient model impractical. Parameter-estimated values and hydraulic heads from the predevelopment model were used as starting parameter values and initial conditions in the transient model runs. After the transient model was evaluated, changes were made to the steady-state model (for example, locations of RIV, DRN, and HFB cells) and the automated calibration of the steady-state model was repeated. In this way, the utility of automated parameter estimation and the computational efficiency of trial-and-error calibration were used to create well-constrained models.

Observations Used in Model Calibration

Water-Level Altitudes, Water-Level Altitude Changes, and Associated Errors

The winter median groundwater levels described by Burns and others (2012b) were used for model calibration. For purposes of this study, the winter median level is defined as the median value of all water-level measurements collected during the first 3 months of each calendar year. These measurements were selected because they are not strongly affected by seasonal pumping and provide a record of longer-scale hydraulic response to system stresses.

Because most of the water-level measurements were taken in or near commingling wells (Burns and others, 2012b), the standard approach of defining error-based observation weights (Hill, 1998) was not appropriate because the larger part of the error in much of the model domain is due to bias in the measurement resulting from commingling. Burns and others (2012b) identified measurement noise (attributed to commingling and geologic complexity) of about ±200 ft over much of the Palouse Slope. The large range in water levels from relatively similar locations and stratigraphic positions are shown in figure 15 (well groups are explained in section, "Transient Model Fit and Model Error—Comparison of Simulated and Measured Hydraulic Heads"). Discontinuous

interflow zones, differing times of well construction, and thus commingling, and different screen intervals in the completed wells further complicated information that could be obtained from the water level. Most correctly, for the CPRAS each water-level measurement should be considered a complex flow-weighted average of hydraulic heads in all aquifers intersected by the well or neighboring wells. This complex interpretation of each hydraulic-head measurement explains why water-level measurements in nearby, similarly constructed wells can be hundreds of feet different (fig. 15; Burns and others, 2012b). Given this complexity in interpreting individual hydrographs, it was assumed that each observation had a similar amount of error, and the error increased over time as commingling became more prevalent.

For calibration of the steady-state model, well screen information was not available, so the earliest water-level measurement at each well was used with the value of the observation being assigned to the model layer with the top closest to the well bottom altitude. This assumes that most aquifers are associated with interflow zones, and that the driller stopped at an altitude where a productive aquifer was detected. In areas of significant upward hydraulic gradient, the simulated head likely would be higher than the measured commingled head, and conversely in areas of downward gradient. The total number of head observations used for the steady-state and transient model calibrations were 10,525 and 46,460, respectively.

Examination of well hydrographs (Burns and others, 2012b) indicated that the first widespread water-level changes was in response to large-scale surface-water irrigation projects about 1950. Next, about 1970, many areas across the CPRAS started to exhibit strong declines associated with rapid development of the groundwater resource. Because the earliest observation at a well was possibly during the period of transient hydraulic response, the uncertainty associated with using late-time observations to calibrate the steady-state groundwater model was represented by selecting lumped weights based on response periods identified in the data. Observation weights reduce the influence of observations that are less accurate and increase the influence of observations that are more accurate (Hill, 1998). A weight of 1.0 was assigned for pre-1950 measurements, 0.01 for pre-1970 measurements, and 0.0001 for post-1970 measurements. This weighting strategy ensured that the earliest-time data in each area of the model domain would have the most influence on parameter estimates.

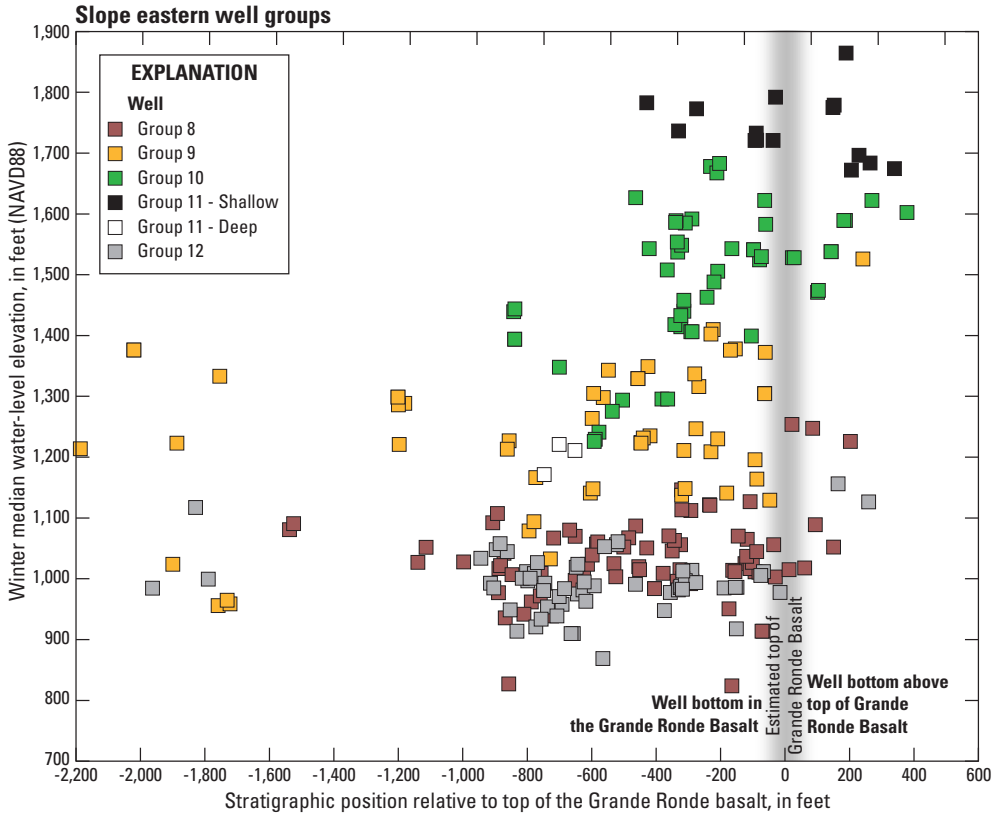

Figure 15. Distance of the well bottom from the estimated top of Grande Ronde Basalt compared with water levels measured in wells for the Palouse Slope eastern well groups, Washington. From Burns and others (2012b, fig. 20*E*).

Following steady-state model calibration, a transient model was developed for the period 1900–2007. An initial 1900–1919 transient stress period was simulated using pre-1920 commingling wells with pumping rates increased from zero starting in 1920. Predevelopment steady-state model heads were used as initial conditions for the transient model. Using the transient 1900–1919 stress period provided a better match of simulated to measured water levels than using a steady-state 1920s condition model. Use of a steady-state stress period for 1920 resulted in significant head declines due to pumping in structurally complex basins, especially those with strong upward hydraulic gradients such as the Yakima and Walla Walla River Basins. Because pre-1920 pumps had poor lift characteristics (Cline and Collins, 1992), the historical use of artesian aquifers in these basins is consistent with the conceptual model and the drilling records.

After reasonably good steady-state model fit was achieved using lumped weights, preliminary transient simulations were completed, and computed post-2000 drawdowns were used to adjust steady-state model calibration weights. If large transient simulated drawdowns were detected (usually in the most heavily anthropogenically influenced areas), then the observation target was determined to be less useful for steady-state calibration; therefore, the steady-state observation weight was reduced. An exponential decay function was used to decrease observation weight such that for every 50 ft of computed drawdown (magnitude), observation weight was reduced by an order of magnitude (fig. 16). The iterative process for the steady-state and transient model calibration improved confidence that higher weight measurements likely were closer to predevelopment conditions.

Several limitations of the steady-state model calibration are implied:

- Few, if any of the water-level measurements were taken during true predevelopment conditions, but they might still represent predevelopment, or near predevelopment conditions.
- Assignment of the measured hydraulic head to the deepest model layer is not strictly correct for a commingled measurement.
- Predevelopment vertical gradients are poorly reflected in the measured data because most observations represent some degree of commingling, commonly with an apparently random distribution of high and low measured values in many areas (Burns and others, 2012b). Because few if any data constrain high vertical gradients, the calibrated predevelopment model will have the tendency to overestimate Kv, matching measured heads on average in many regions.

Subject to these limitations, the steady-state model calibration is best at providing good general estimates of model parameters for use with the transient model, and adjustments in model parameters that improve transient model fit should take precedence over steady-state model-calibration parameter estimates. The transient model incorporated the addition of stresses that provided information about aquifer properties that could not be explored in a non-stressed system and used more recent, and presumably more accurate, records of stresses (pumping and recharge) and responses (water levels).

Use of the water-level measurements to calibrate the transient model is subject to the same limitations regarding measuring water levels in commingling wells, but the limitations associated with the fact that few observations truly represent predevelopment conditions is removed. To address the commingling problem, Burns and others (2012b) showed that locally, hydraulic gradients were frequently much more variable vertically than horizontally. This indicates that simulated heads spanning many layers of a row and column should produce a range of heads that, when averaged by layer, can reasonably produce the range of heads observed. Because this method of using the observation data to evaluate model performance is complex, because transient model run times were long, and because further tightening of Kv of CRBG units resulted in model instability, manual calibration and automated parameter estimation, was accomplished for the transient model. However, the spatial patterns of differences between simulated and measured water levels for selected periods were examined (under the assumption that measured head represented head at the altitude of the well bottom). Ideally, multi-layer observations would have been used to constrain the transient model calibration. However, attempting to simulate open screen intervals in the appropriate aquifer units would have introduced an unknown and unquantified level of uncertainty.

Streamflow Observations and Associated Errors

The emphasis of the CPRAS model is the groundwater system, and streamflow observations are important to augment the water-level information and further constrain the parameter estimation about groundwater-surface-water interaction. Correctly simulating stream base flow (the groundwater discharge component of streamflow) is an important way of ensuring the correct amount of water is moving through the system. The modeling effort did not attempt to simulate the heavily regulated and managed surface-water features of the study area, such as reservoir releases or diversions and returns. Estimated or measured base flows were compared to simulated groundwater discharge to selected stream reaches.

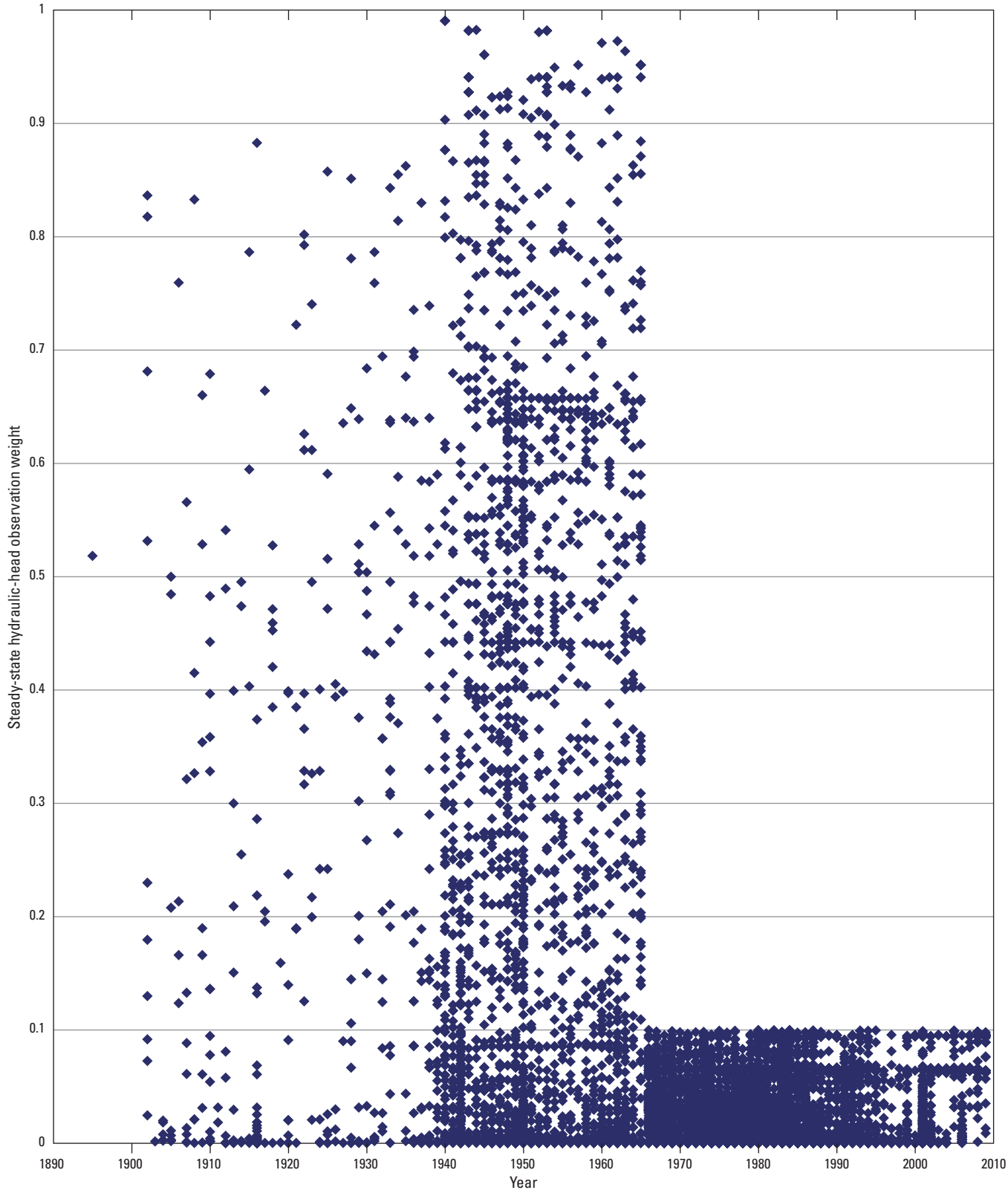

Figure 16. Hydraulic-head observation weights used in the steady-state model, Columbia Plateau Regional Aquifer System, Idaho, Oregon, and Washington.

Two methods were used to estimate base flows at 50 locations (fig. 17; table 3). The most reliable estimates of base flow were computed from an automated hydrograph separation technique (HYSEP; Sloto and Crouse, 1996) used to evaluate the groundwater contribution to total streamflow (base flow) at active and inactive USGS streamflow-gaging stations in Washington State (applied by Sinclair and Pitz, 1999). The estimates by Sinclair and Pitz (1999) are basin-scale averages for the period of record; therefore, the estimates were considered appropriate observations for model calibration.

For streamflow-gaging stations not included in Sinclair and Pitz (1999), base flow was estimated as 62 percent of annual median streamflow. This approach was based on the findings by Sinclair and Pitz (1999) that groundwater discharge in eastern Washington averaged about 62 percent of total annual median streamflow. All estimates by this method were checked to ensure the estimate was greater than the minimum monthly streamflow.

Base-flow estimates by the two methods (62 percent of annual median streamflow and methods of Sinclair and Pitz [1999]) provided a general idea of groundwater contributions to streamflow, but were not appropriate to use as a specific model observation because of the variability of recharge and effects of human activities on streamflow. Therefore, an upper and lower bound around the base-flow estimate were used to calibrate the model. For estimates based on the hydrograph method of Sinclair and Pitz (1999), the bounds were an order of magnitude greater than and less than the base-flow estimate. For estimates based on 62 percent of annual median streamflow, the upper bound was the median annual flow and the lower bound was the minimum monthly flow. If the simulated streamflow gain was within the upper and lower bounds, the observation did not contribute to the objective function and no penalty was assessed during automated calibration of the steady-state model.

Model Evaluation

Parameterization and Regularization

To test the effect of geologic variability on groundwater flow, the model domain was divided into zones of similar geologic character. The division of units created the possibility of 24 plan-view model parameter zones (fig. 18) and 8 vertical zones (5 geologic units plus 3 confining units), but not all of the vertical zones existed in each of the 24 plan-view zones. Within each parameter zone, Kh and Kv, and river and drain conductance multipliers were selected as independent parameters.

The model then was parameterized to test the importance of geologic features that had been simulated in the CP-RASA model (Hansen and others, 1994). The following parameter zones were created for testing:

- *Plan-view zones*: Burns and others (2012b) observed that in areas where data were too sparse to resolve individual horizontal flow barriers, the net effect of increasing geologic structure was a corresponding decrease in Kh. Zones were created by dividing the model domain into model cell zones with similar observable patterns of structure (fig. 18). To prevent the possibility of an ill-posed parameter estimation problem, Tikhonov Regularization (Doherty, 2010) was used to relate zones of similar structural patterns, indicating that properties in these zones are likely to have similar parameter values.
- *Vertical (geologic unit) zones*: Within each plan-view zone, it was postulated that each of the geologic units of Burns and others (2011) could have markedly different hydraulic characteristics because of changes in deposition. Tikhonov Regularization was used to inform the parameter estimation process that, unless observations support otherwise, each of the three basalt units should have similar hydraulic properties and each of the sedimentary units (Overburden and two interbeds) should have similar hydraulic properties. This parameterization allowed testing of the postulated reduction in hydraulic conductivity with increasing depth and testing of the role of depositional style on hydraulic conductivity.
- *Zones with larger vertical conductance (basalt units only):* Basalt flow interiors were postulated to be confining units even though jointing patterns frequently crosscut most of the dense flow interior. Although tight sealing of joints is expected where overlying rock compresses flow interiors, it was postulated that in the absence of large amounts of overlying rock, joints could provide enhanced vertical conductivity, enhancing areal recharge and discharge in river valleys. This mechanism could explain the pattern of enhanced vertical permeability estimated near major rivers in the work of Davies-Smith and others (1988) and Hansen and others (1994). To test this mechanism, the uppermost two basalt model layers (about 200 ft in thickness) were allowed to have a different Kv than the underlying units. Tikhonov Regularization was used to inform the parameter estimation process that unless the observation data indicated otherwise, the Kv of each cell should be similar to the deeper parts of the same geologic unit.

In addition to the spatial parameter zones, 25 discrete HFB categories were parameterized, generally based on mapped geologic structure. The adjustable parameter, barrier conductance, was assumed to be constant along the fault and with depth. Tikhonov Regularization was used to inform the parameter estimation process that fault conductance in a region should have similar values unless data support differences.

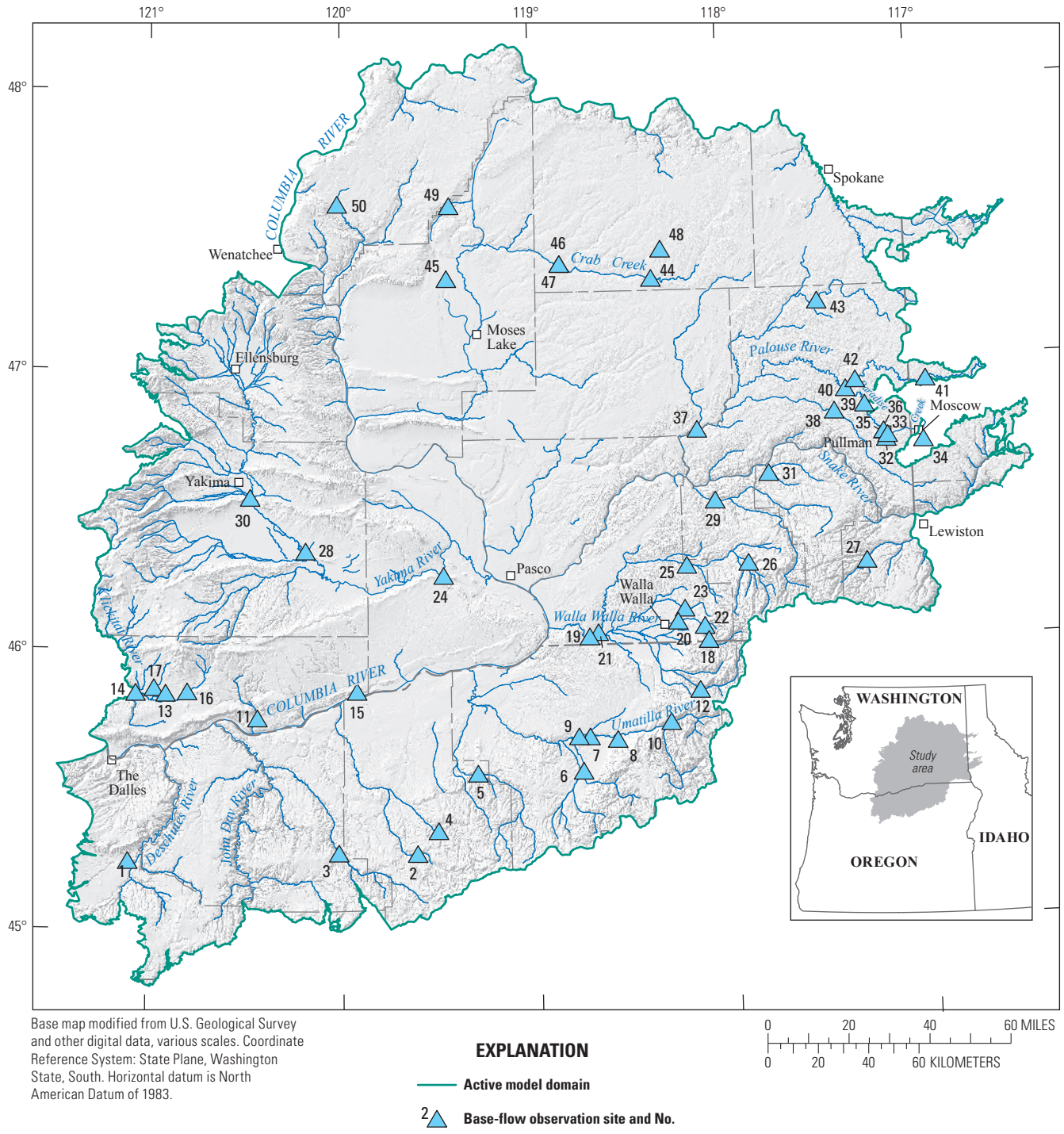

Figure 17. Locations of base-flow observation sites used to calibrate the steady-state and transient models of the Columbia Plateau Regional Aquifer System, Idaho, Oregon, and Washington.

Table 3. Mean annual base-flow estimates, and upper and lower bounds used to calibrate the steady-state and transient models of the Columbia Plateau Regional Aquifer System, Idaho, Oregon, and Washington.

[Site locations are shown in figure 17. **Station name:** OR, Oregon; WA, Washington; ID, Idaho; NR, near; R, river, W, west; abv, above; BNDY, boundary; CR or C, creek; SO, south, FK, fork. ft^3/s, cubic foot per second]

Base-flow observation site	Station name	Base-flow estimate (ft^3/s)	Lower bound (ft^3/s)	Upper bound (ft^3/s)	Weight	Source
1	WHITE RIVER BELOW TYGH VALLEY, OR	234.70	118.9	378.6	10	62 percent of annual median streamflow
2	RHEA CREEK NEAR HEPPNER, OR	16.09	4.0	26.0	10	62 percent of annual median streamflow
3	ROCK CREEK AB WHYTE PARK NR CONDON, OR	42.28	2.0	68.2	10	62 percent of annual median streamflow
4	WILLOW CREEK ABV WILLOW CR LAKE, NR HEPPNER, OR	11.66	1.2	18.1	10	62 percent of annual median streamflow
5	BUTTER CREEK NEAR PINE CITY, OR	22.89	5.2	36.9	10	62 percent of annual median streamflow
6	MCKAY CREEK NEAR PILOT ROCK, OR	71.21	1.4	114.9	10	62 percent of annual median streamflow
7	UMATILLA R AT W RESERVATION BNDY NR PENDLETON, OR	322.51	41.5	520.2	10	62 percent of annual median streamflow
8	MOONSHINE CREEK NEAR MISSION, OR	1.77	0.1	2.9	10	62 percent of annual median streamflow
9	UMATILLA RIVER AT PENDLETON, OR	299.91	45.6	483.7	10	62 percent of annual median streamflow
10	UMATILLA RIVER ABOVE MEACHAM CREEK, NR GIBBON, OR	138.40	44.1	223.2	10	62 percent of annual median streamflow
11	ROCK CREEK NEAR ROOSEVELT, WA	17.00	1.7	170.0	1	Sinclair and Pitz, 1999
12	SOUTH FORK WALLA WALLA RIVER NEAR MILTON, OR	104.38	102.2	168.4	10	62 percent of annual median streamflow
13	SPRING CREEK NEAR BLOCKHOUSE, WA	14.00	1.4	140.0	1	Sinclair and Pitz, 1999
14	LITTLE KLICKITAT R NR WAHKIACUS, WA	103.00	10.3	1,030.0	1	Sinclair and Pitz, 1999
15	ALDER CR AT ALDERDALE, WA	3.00	0.3	30.0	1	Sinclair and Pitz, 1999
16	LITTLE KLICKITAT R NR GOLDENDALE, WA	35.00	3.5	350.0	1	Sinclair and Pitz, 1999
17	MILL CREEK NEAR BLOCKHOUSE, WA	14.00	1.4	140.0	1	Sinclair and Pitz, 1999
18	MILL CREEK NEAR WALLA WALLA, WA	69.00	6.9	690.0	1	Sinclair and Pitz, 1999
19	WALLA WALLA RIVER NEAR TOUCHET, WA	346.03	18.4	558.1	10	62 percent of annual median streamflow
20	BLUE CREEK NEAR WALLA WALLA, WA	10.00	1.0	100.0	1	Sinclair and Pitz, 1999
21	TOUCHET R NR TOUCHET, WA	148.00	14.8	1,480.0	1	62 percent of annual median streamflow
22	MILL CREEK NEAR WALLA WALLA, WA	47.99	1.1	77.4	10	62 percent of annual median streamflow
23	DRY CREEK NEAR WALLA WALLA, WA	13.00	1.3	130.0	1	Sinclair and Pitz, 1999
24	YAKIMA RIVER AT KIONA, WA	1,977.48	1,489.4	3,189.5	10	62 percent of annual median streamflow
25	TOUCHET RIVER AT BOLLES, WA	145.00	14.5	1450.0	1	Sinclair and Pitz, 1999
26	EAST FK TOUCHET R NR DAYTON, WA	95.00	9.5	950.0	1	Sinclair and Pitz, 1999
27	ASOTIN CREEK BELOW CONFLUENCE NEAR ASOTIN, WA	30.20	23.9	48.7	10	62 percent of annual median streamflow
28	GRANGER DRAIN AT GRANGER, WA	21.61	19.5	34.9	10	62 percent of annual median streamflow
29	TUCANNON RIVER NEAR STARBUCK, WA	127.00	12.7	1,270.0	1	Sinclair and Pitz, 1999
30	AHTANUM CREEK AT UNION GAP, WA	42.41	15.4	68.4	10	62 percent of annual median streamflow
31	MEADOW CREEK NR CENTRAL FERRY, WA	1.90	0.2	19.0	1	Sinclair and Pitz, 1999
32	SO FK PALOUSE R ABV PARADISE C NR PULLMAN, WA	7.20	0.7	72.0	1	Sinclair and Pitz, 1999
33	PARADISE CR NR PULLMAN, WA	5.10	0.5	51.0	1	Sinclair and Pitz, 1999
34	PARADISE CR AT UNIVERSITY OF IDAHO AT MOSCOW, ID	4.33	0.8	7.0	10	62 percent of annual median streamflow
35	SOUTH FORK PALOUSE RIVER AT PULLMAN, WA	18.13	3.8	29.2	10	62 percent of annual median streamflow

Table 3. Mean annual base-flow estimates, and upper and lower bounds used to calibrate the steady-state and transient models of the Columbia Plateau Regional Aquifer System, Idaho, Oregon, and Washington.—Continued

[Site locations are shown in figure 17. **Station name:** OR, Oregon; WA, Washington; ID, Idaho; NR, near; R, river, W, west; abv, above; BNDY, boundary; CR or C, creek; SO, south, FK, fork. ft^3/s, cubic foot per second]

Base-flow observation site	Station name	Base-flow estimate (ft^3/s)	Lower bound (ft^3/s)	Upper bound (ft^3/s)	Weight	Source
36	MISSOURI FLAT CREEK AT PULLMAN, WA	3.80	0.4	38.0	1	Sinclair and Pitz, 1999
37	PALOUSE RIVER AT HOOPER, WA	333.53	37.9	538.0	10	62 percent of annual median streamflow
38	UNION FLAT CREEK NEAR COLFAX, WA	18.00	1.8	180.0	1	Sinclair and Pitz, 1999
39	FOURMILE CR AT SHAWNEE, WA	4.80	0.5	48.0	1	Sinclair and Pitz, 1999
40	PALOUSE RIVER BELOW SOUTH FORK AT COLFAX, WA	211.63	21.9	341.3	10	62 percent of annual median streamflow
41	PALOUSE RIVER NR POTLATCH, ID	152.88	11.2	246.6	10	62 percent of annual median streamflow
42	PALOUSE RIVER NEAR COLFAX, WA	175.00	17.5	1,750.0	1	Sinclair and Pitz, 1999
43	PINE CREEK AT PINE CITY, WA	20.00	2.0	200.0	1	Sinclair and Pitz, 1999
44	CRAB CREEK AT ROCKY FORD ROAD NEAR RITZVILLE, WA	22.09	11.9	35.6	10	62 percent of annual median streamflow
45	ROCKY FORD CREEK NEAR EPHRATA, WA	69.00	6.9	690.0	1	Sinclair and Pitz, 1999
46	CRAB CREEK AT IRBY, WA	20.82	4.9	33.6	10	62 percent of annual median streamflow
47	CRAB CREEK AT IRBY, WA	29.00	2.9	290.0	1	Sinclair and Pitz, 1999
48	COAL CREEK AT MOHLER, WA	1.20	0.1	12.0	1	Sinclair and Pitz, 1999
49	PARK CREEK BLW PARK LAKE NR COULEE CITY, WA	9.50	1.0	95.0	1	Sinclair and Pitz, 1999
50	DOUGLAS CREEK NEAR ALSTOWN, WA	0.92	0.1	9.2	1	Sinclair and Pitz, 1999

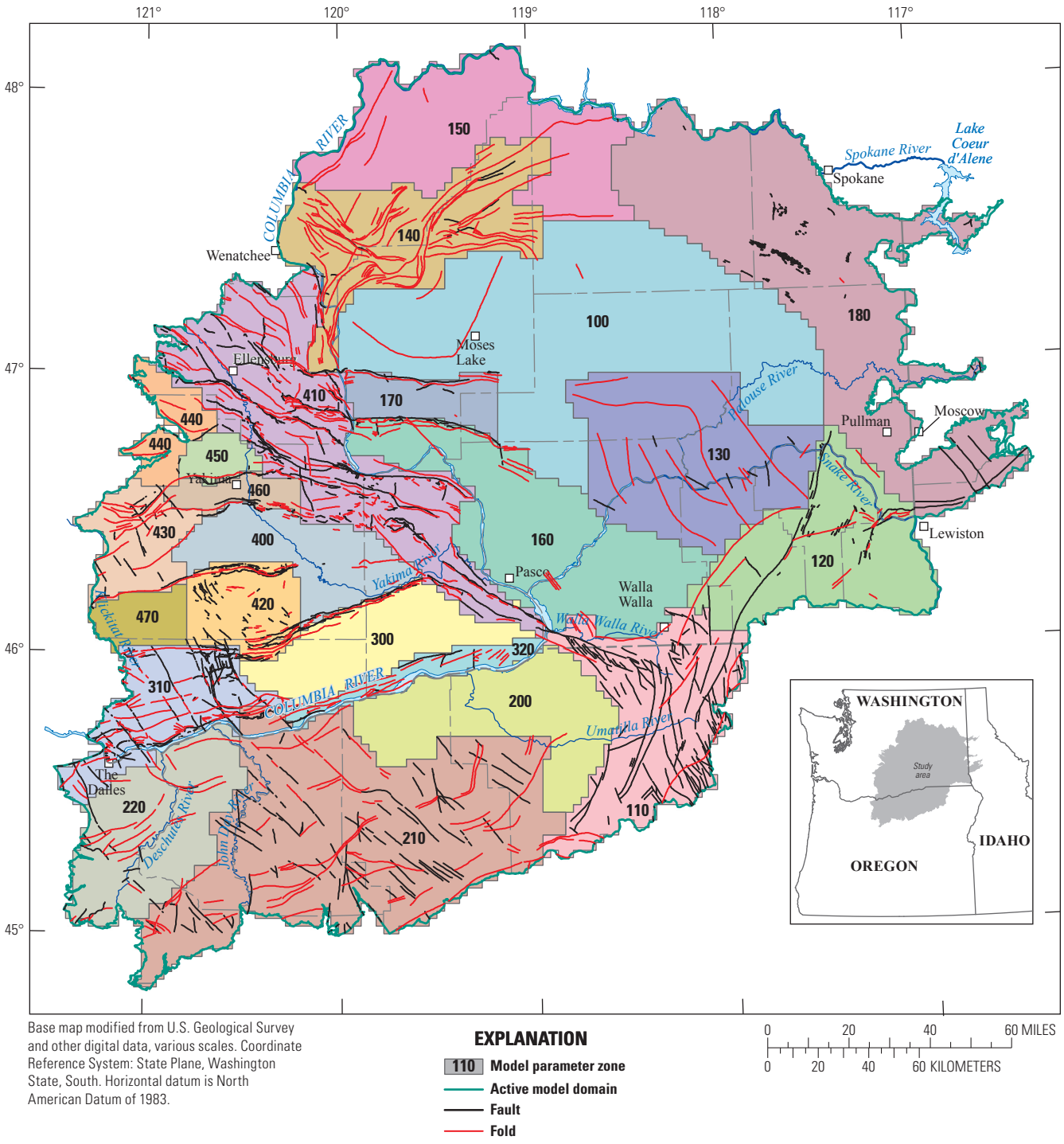

Figure 18. Initial model parameter zones and geologic structure for the Columbia Plateau Regional Aquifer System, Idaho, Oregon, and Washington.

Optimal Parameter Estimates

Parameter estimation was iterative with 684 parameters being the most parameters estimated at one time for the predevelopment steady-state model. Results of these highly-parameterized PEST runs were used to evaluate the mechanisms identified in section, "Parameterization and Regularization."

The 24 plan-view parameter zones (fig. 18) were incrementally combined manually into larger zones with constant horizontal conductivity until 4 distinct Overburden zones (fig. 19*A*) and 3 CRBG zones (fig. 19*B*) remained. Zones were combined when calibrated Kh was sufficiently close to the same value such that use of a single value caused only a minor increase in the weighted least-squares objective function. Final calibrated parameter values are presented in table 4.

Basalt Kh was highest near the center of the CPRAS where flows are the thickest and are less folded and faulted. At the margins of the lava flows, Kh of the relatively undeformed basalt units decreased slightly. As lavas continue to thin and are increasingly cross-cut by geologic structure on the flanks of the Cascades Range and the Blue Mountains, effective Kh of the basalts decreased greatly. From a regional perspective, the Overburden unit could be simulated even more simply than the basalt units. All Overburden in the Yakima River Basin could have a single homogeneous value (Kh = 99.81 ft/d) and all other Overburden values could range from 0.35 ft/d (zone 1) to 100 ft/d (zone 3). The Mabton and Vantage Interbeds proved to be negligibly thin so they were lumped with the overlying basalt unit in each case. The distribution of Kv was even simpler, with a uniform value of 5.24×10^{-3} ft/d used for the upper 200 ft of the CRBG units and 1.00×10^{-4} ft/d for the rest of the CRBG (table 4). Overburden Kv was tied to the Kh at a fixed ratio of 100 times less than Kh. This relatively simple model of the Overburden unit conductivity was used to simulate the net effect of the relatively sparse overburden on the CRBG aquifers, and little effort was placed on refining and improving model fit through modifications of the overburden aquifer parameters.

Parameter estimation was performed for storage properties, but the model proved to be relatively insensitive to changes in those parameters. Trial and error manual calibration and values from previous studies were evaluated to provide initial parameter values for the transient calibration. Throughout the calibration process, the storage parameters occasionally were reassessed and changed to improve model results. Final values for specific yield for the Overburden and CRBG units were 1.0×10^{-1} and 2.5×10^{-2}, respectively. Final values for specific storage for the Overburden and CRBG units were 2.50×10^{-5} ft^{-1} and 2.50×10^{-6} ft^{-1}, respectively (table 4).

When all 684 parameters were estimated independently, there was no clear pattern of Kh with depth between CRBG units. Even though prior information was used to inform the automated parameter estimation process that CRBG units have similar hydraulic properties to other nearby CRBG units, some plan-view zones showed decreasing Kh with depth, whereas others displayed the opposite behavior. This was attributed to tradeoffs between river and drain parameters and Kh resulting in small improvements to model fit at the expense of highly irregular estimates of river and drain conductance. Based on preliminary calibration, river and drain conductance multipliers were combined into three major zones for much of the calibration: all Overburden, Yakima River Basin CRBG units, and all other CRBG units. Generally, the resulting multipliers were of similar magnitude, especially when comparing similar rock types, indicating that scaling the conductance to stream geometry factors worked well. Combining river and drain parameters into these three groups allowed the CRBG units to be combined into four groups with similar Kh, after which drain multipliers were allowed to vary by zone to fine tune the model fit. Lastly, the Overburden river conductance was adjusted to fine-tune river exchange in the deep sedimentary valleys.

When evaluating the initial estimates of Kv for the parameter zones "*zones with larger vertical conductance (basalt units only)*" with 684 independent parameters, automated parameter estimation frequently tended to make these units less permeable (lower Kv) than corresponding underlying layers, which contradicted the expected behavior. Following the grouping of similar zones, however, the calibrated Kv value for the upper 200 ft of basalt was approximately 1.5 orders of magnitude greater than the underlying basalts. Other than the upper 200 ft and unlike the previous CP-RASA model (Hansen and others, 1994), the final model parameter distribution had no vertical trend in hydraulic conductivity in the underlying CRBG units. This lack of vertical trend is likely because the current model was connected to surface-water features only where thin model layers intersected the land surface. The CP-RASA model used five thick layers, requiring that Kh partially account for the lack of connection between deep parts of CPRAS and surface-water features. In the new model, the Kv controlled this lack of connectivity.

During parameter estimation, the river and drain conductances were varied as a function of geology, similar to Burns and others (2012a). For each model cell, the length of a stream depends on the path across the cell, and conductance is linearly dependent on the path length. The adjustable multipliers to determine final river and drain conductances are presented in table 4.

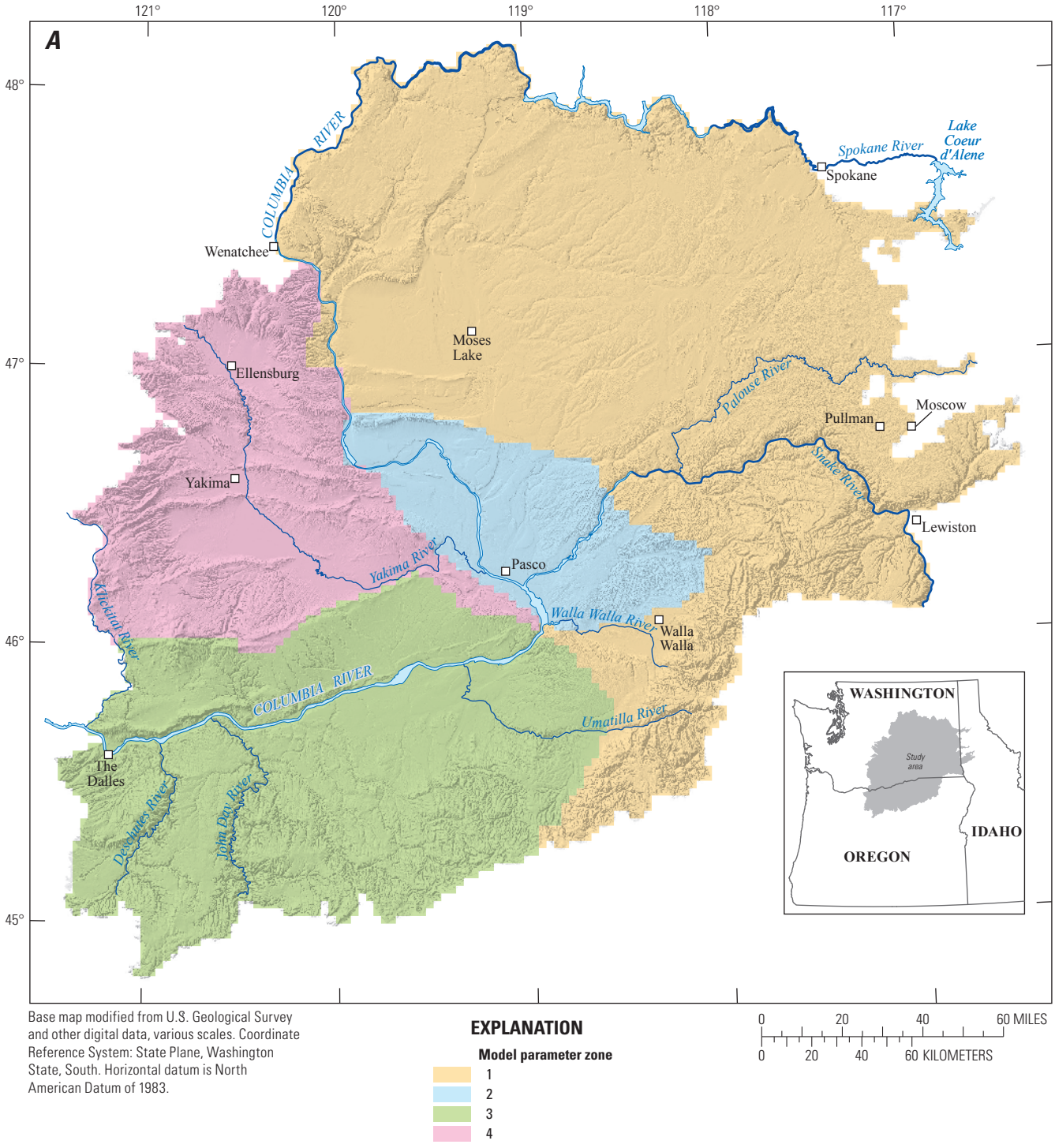

Figure 19. Simplified final model parameter zones for the (*A*) Overburden unit and (*B*) Columbia River Basalt Group, Columbia Plateau Regional Aquifer System, Idaho, Oregon, and Washington.

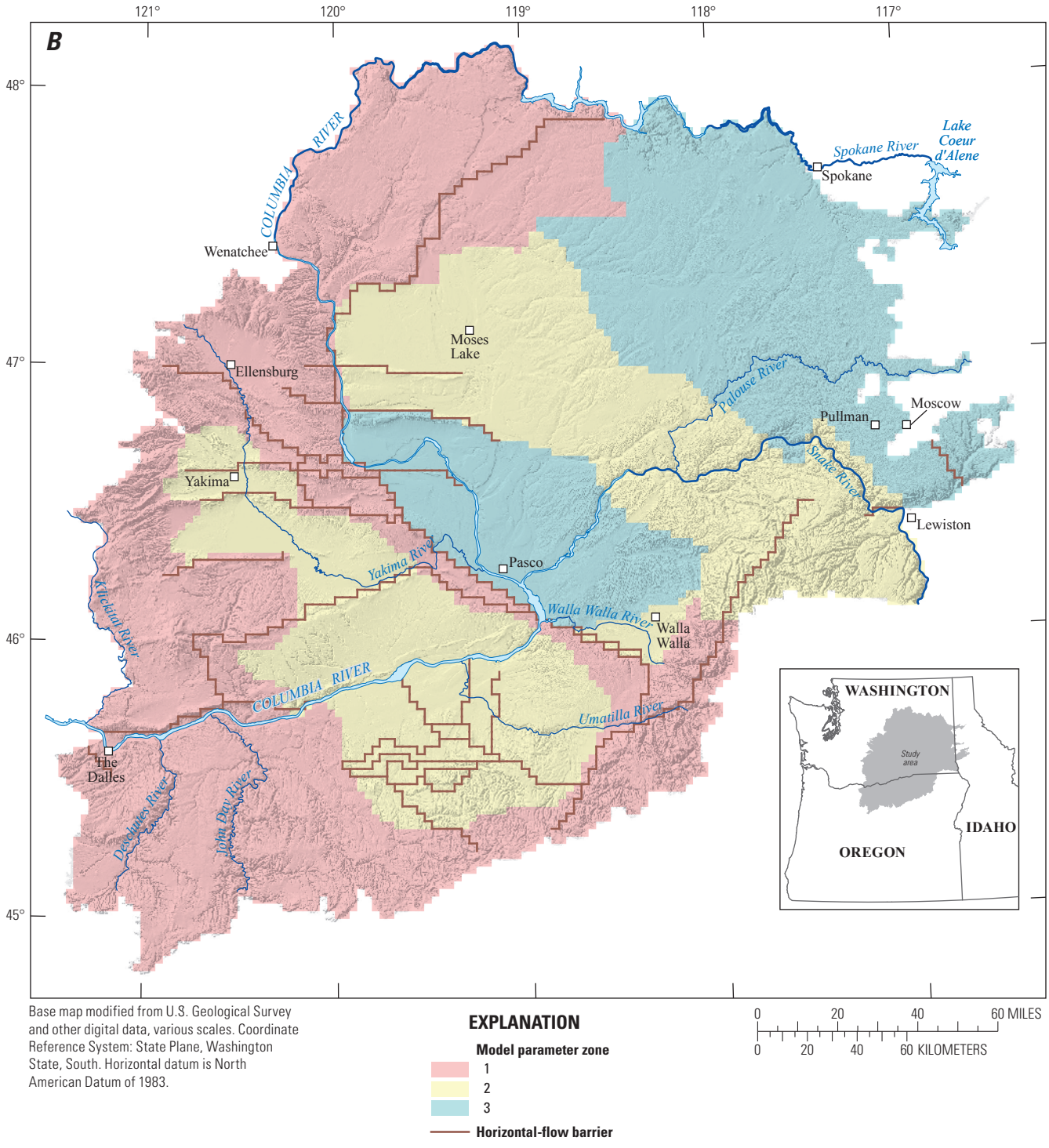

Figure 19.—Continued

Table 4. Final calibrated model parameters for the Columbia Plateau Regional Aquifer System, Idaho, Oregon, and Washington.

[**Unit:** OB, Overburden unit; CRBG, Columbia River Basalt Group. **Complex parameter zones** are shown in figure 18. **Simplified parameter zones** are shown in figure 19*A* (OB) and figure 19*B* (CRBG). **HFB groups** are shown in figure 9. **Abbreviations:** HFB, horizontal-flow barrier; ft, foot; ft^{-1}, per foot; ft/d, foot per day; ft^2/d, foot squared per day; (ft/d)/ft, foot per day per foot]

Unit	Horizontal hydraulic conductivity (ft/d)			Complex parameter zone	Simplified parameter zone
	Minimum allowable value	Parameter value	Maximum allowable value		
OB	1.00E-04	3.05	1.00E+03	100, 110, 120, 130, 140, 150, 170, 180	OB 1
OB	1.00E-04	30.15	1.00E+03	160	OB 2
OB	1.00E-04	200	1.00E+02	200, 210, 220, 300, 310, 320	OB 3
OB	1.00E-04	150.81	1.00E+03	400, 410, 420, 430, 440, 450, 460, 470	OB 4
CRBG	1.00E-04	1.07	1.00E+06	110, 140, 150, 210, 220, 310, 410, 420, 430, 440, 470	CRBG 1
CRBG	1.00E-04	8.16	1.00E+06	120, 130, 170, 180, 200, 300, 320, 400, 450, 460	CRBG 2
CRBG	1.00E-04	27.90	1.00E+06	100, 160	CRBG 3

Unit	Vertical hydraulic conductivity (ft/d)			Complex parameter zone	Simplified parameter zone
	Minimum allowable value	Parameter value	Maximum allowable value		
OB	1.00E-07	3.05E-02	1.00E+02	100, 110, 120, 130, 140, 150, 170, 180	OB 1
OB	1.00E-07	3.01E-01	1.00E+02	160	OB 2
OB	1.00E-07	2.00	1.00E+02	200, 210, 220, 300, 310, 320	OB 3
OB	1.00E-07	1.51	1.00E+02	400, 410, 420, 430, 440, 450, 460, 470	OB 4
CRBG–above 200 ft	5.00E-05	5.24E-03	1.00E+02	All zones	All
CRBG–below 200 ft	1.00E-10	1.00E-04	1.00E-03	All zones	All

Unit	Specific yield (dimensionless)
	Parameter value
OB	0.10
CRBG	0.025

Unit	Specific storage (ft^{-1})
	Parameter value
OB	2.50E-05
CRBG	2.50E-06

Unit	Drain conductance (ft^2/d)		
	Minimum value	Mean value	Maximum value
OB	1.00	84.20	125.00
CRBG	0.20	92.50	200.00

Unit	River conductivity (ft/d)	
	Minimum value	Maximum value
OB	0.01	0.57
CRBG	0.01	0.01

Table 4. Final calibrated model parameters for the Columbia Plateau Regional Aquifer System, Idaho, Oregon, and Washington.—Cont.

[**Unit:** OB, Overburden unit; CRBG, Columbia River Basalt Group. **Complex parameter zones** are shown in figure 18. **Simplified parameter zones** are shown in figure 19*A* (OB) and figure 19*B* (CRBG). **HFB groups** are shown in figure 9. **Abbreviations:** HFB, horizontal-flow barrier; ft^{-1}, per foot; ft/d, foot per day; ft^2/d, foot squared per day; (ft/d)/ft, foot per day per foot]

Unit	HFB hydraulic characteristic (1/d)			HFB group
	Minimum allowable value	Parameter value	Maximum allowable value	
CRBG	1.00E-16	1.00E-15	1.00E+03	1
CRBG	1.00E-16	2.11E-09	1.00E+03	10
CRBG	1.00E-16	1.20E-14	1.00E+03	21
CRBG	1.00E-16	8.67E-08	1.00E+03	22
CRBG	1.00E-16	1.16E-05	1.00E+03	23
CRBG	1.00E-16	4.53E-06	1.00E+03	32
CRBG	1.00E-16	1.94E-05	1.00E+03	33
CRBG	1.00E-16	1.20E-10	1.00E+03	34
CRBG	1.00E-16	2.30E-11	1.00E+03	35
CRBG	1.00E-16	5.96E-11	1.00E+03	41
CRBG	1.00E-16	1.93E-14	1.00E+03	51
CRBG	1.00E-16	3.88E-05	1.00E+03	52
CRBG	1.00E-16	4.26E-15	1.00E+03	53
CRBG	1.00E-16	8.82E-11	1.00E+03	54
CRBG	1.00E-16	6.53E-14	1.00E+03	61
CRBG	1.00E-16	4.94E-11	1.00E+03	62
CRBG	1.00E-16	6.12E-11	1.00E+03	63
CRBG	1.00E-16	1.17E-11	1.00E+03	64
CRBG	1.00E-16	5.19E-15	1.00E+03	65
CRBG	1.00E-16	1.44E-13	1.00E+03	66
CRBG	1.00E-16	1.15E-13	1.00E+03	67
CRBG	1.00E-16	7.31E-11	1.00E+03	68
CRBG	1.00E-16	1.05E-08	1.00E+03	69
CRBG	1.00E-16	8.94E-13	1.00E+03	70
CRBG	1.00E-16	2.80E-12	1.00E+03	71

Examination of groundwater-level residuals revealed a few water levels measured in river valleys that would have been more closely matched by simulated water levels if Kv was significantly higher. However, upon closer examination of the measured hydraulic head in the valleys, the head was determined to be typically at the same approximate altitude as the trace of the axis of an anticline that crosses the river at a downgradient location. Because the geologic model of Burns and others (2011) did not capture all mapped folds (a result of low data density in some areas), the geologic model (and therefore the layers of the flow model) was frequently smoother than the mapped geology, indicating that deeper geologic strata may be exposed along the river than was being simulated in the groundwater-flow model. This indicated that the flow model included layers (and associated Kv) that did not exist at certain locations, and explained why higher values of Kv would improve the simulated fit to observed values. To improve simulation of hydraulic head in areas where an anticline is eroded, possibly exposing deeper interflow zones, DRN cells were added to the deeper model layers. Because the new drains were associated with river reaches, ELEVATION and CONDFACT for these new DRN cells were computed in the same way as described in section, "Streams and Surface-Water Features."

Horizontal-flow barrier hydraulic characteristic was highly variable with a range of 1.0×10^{-15} to 3.88×10^{-5} (fig. 9; table 4). Early in the calibration process, results were not sensitive to the hydraulic characteristic assigned to the large offset faults at flow divides, so these values were fixed at a low value of 1.0×10^{-15}.

Statistical Measures of Model Fit

The measure of model fit can be represented with many statistical and graphical methods. One measure of model fit is based on the difference between simulated and measured heads and flows, or residuals. The overall magnitude of the residuals was considered, but the distribution of those residuals, both statistically and spatially, could be equally important. The magnitude of residuals could initially point to gross errors in the model, the data (measured quantity), or how the measured quantity is simulated (Hill, 1998). A complete discussion of the statistical measures discussed in this section is available in Hill (1998).

Steady-State Model Fit and Model Error

The calibrated predevelopment steady-state model was a parsimonious model in which model simplification was made with relatively minor degradation to model fit. The distribution of Kh and Kv was considerably simpler than the distribution used in previous models (Davies-Smith and others, 1988; Hansen and others, 1994; Ely and others, 2011). This is attributed to two features of the new model: (1) the use of the HFB package precluded the need to simulate very narrow regions of low Kh (for example, see the permeability distributions of Hansen and others [1994]), and (2) the use of many thin layers to represent the CRBG units ensured proper local connectivity with hydraulic features, excluding the need to create complex Kh and Kv zones to explain local head anomalies that were the result of attempting to simulate fine scale hydraulic features with a coarse model grid.

A relatively good fit of the steady-state predevelopment model was achieved with a wide range of parameters. Many thin layers were used in model construction and a detailed geologic model ensured that the head-controlling hydraulic features (for example, surface-water features) were well represented. Continued automated calibration was determined to further minimize the calibration objective function, but deviate from the conceptual understanding of the flow system. This occurred because of calibration data bias, in particular:

- Most water-level measurements were made in commingling or commingling affected-wells, which resulted in highly variable head observations assigned to most of the constructed depth interval of wells. This indicated that the average vertical gradient is small, even though the high variability of measurements likely is caused by commingling of wells in heterogeneous geology (Burns and others, 2012b). Predevelopment vertical gradients were seldom, if ever, represented by the data. Because automated calibration will seek to match most of the data on average, Kv will be erroneously increased.

- In areas with simulated strong upward gradients, measured commingled heads would be persistently less than simulated head at the well bottom (where the head observation is assigned). Conversely, in areas of strong downward gradients, measured commingled heads would be persistently higher than simulated head at the well bottom. Use of the simulated value of head at the well bottom would cause regional bias in residuals that automated parameter estimation will seek to remove. Because commingled heads depend on aquifer heterogeneity and the combination of wells constructed in an area, there is no a-priori way to select the model layer to assign reliably to the measurement.

- Little of the data represented true predevelopment conditions. Weights were developed to minimize the effect of observations that likely are compromised by anthropogenic activities, but the large number of late-time data and the uneven coverage of data representing true predevelopment conditions will result in calibrated parameters that fit the biased measurements.

A modified automated calibration was used to ensure that the final parameters resulting from the predevelopment steady-state calibration were appropriate for use with the transient simulation. In particular, Kv of the CRBG units was decreased to approximately fit the few locations where vertical gradients were supported by the data. Predevelopment and transient simulations were run using progressively lower values of Kv, and the final selected value (1.00×10^{-4} ft/d) was the lowest value above which model convergence issues began to occur for the transient simulation; actual Kv may be somewhat lower. Nevertheless, this value of Kv provided reasonable model fit to the few data documenting high vertical gradients, and allowed testing of the transient model. Final steady-state model calibration was achieved by fixing CRBG Kv at this value, finding reasonable values of CRBG Kh, and allowing PEST to adjust HFB conductances to obtain estimates of model parameters for transient model testing.

Comparison of Simulated and Measured Hydraulic Heads

Unweighted hydraulic-head residuals (fig. 20) and a comparison between unweighted and weighted residuals (fig. 21) for the steady-state, predevelopment model indicates that most large-error simulated values occur at locations with lower observation weights. Low weights are used for observations that likely do not represent true predevelopment conditions (see figure 16 and the summary of the weighting strategy in section, "Water-Level Altitudes, Water-Level Altitude Changes, and Associated Error"). Observations with low weights are still valuable in the model calibration, and therefore are not removed. In areas with data ranging from high to low quality (for example, water levels likely affected by groundwater development), high-quality data will dominate the calibration. However, some areas of the model contain only low-quality data, and their removal from the calibration would leave the parameter estimation process completely unconstrained.

Following transient model calibration, the steady-state calibration was rechecked by comparing the magnitude and direction of the unweighted residuals to simulated drawdowns. Because the anticipated high-error low-weight residuals potentially represent late-time conditions, the unweighted steady-state residuals should be similar in magnitude and direction to the late-time drawdowns (2000–2007). For example, the Saddle Mountains Basalt unweighted residuals were similar in magnitude and direction when compared with the late-time simulated drawdown maps (fig. 22), indicating that the weighting scheme was appropriate and that the magnitude of declines was approximately correct. This comparison is not always straightforward (especially for thick sequences of hydrogeologic unit) because the computed drawdown maps show average values across many cells vertically, and because the measurements are affected by commingling. However, this method of comparison shows that unweighted residuals generally compare favorably with drawdown maps, indicating that the steady-state calibration method provided robust results. The generally good agreement between the location and magnitude of the residuals compared to simulated drawdown shows that steady-state calibration error can be because many measurements do not represent predevelopment conditions.

Comparison of Simulated and Measured Streamflow

The CPRAS model simulated streamflow for 1,727 river and 43,311 drain cells. The simulation of streamflow included only streamflow gains (river and drain cells) and losses (river cells only) and did not account for diversions and returns or any other aspects of the regulated system. This approach is valid for the predevelopment steady-state model presented here, but would not have accurately reproduced streamflow in the transient simulation. A comparison of simulated and estimated base flow at selected sites in the study area provided additional information on the reliability of the CPRAS model. Streamflow gains and losses also are important components of the simulated flow-system water budget, especially related to the total water mass balance.

Simulated annual base flows for predevelopment conditions generally were within the upper and lower bounds of estimated observations (table 5; fig. 17). Of the 50 base flow sites, 14 (28 percent) were not within the observations bounds, but the errors (simulated base flow minus lower/upper bound) generally were small. The largest error, Yakima River at Kiona, Washington (site 24), has a large amount of uncertainty associated with the base-flow estimate. The Yakima River and its major tributaries originate outside the model domain and some attempt was made to subtract that amount of inflow from the base-flow estimate. However, deriving annual groundwater contributions to streamflows downstream of the headwaters for predevelopment conditions introduced errors.

The method of constraining the parameter estimation with upper and lower bounds allowed for a wide margin of error in some cases. Therefore, this method was considered appropriate for the regional nature of the model, the lack of predevelopment and annual base-flow estimates, and the simplistic approach toward simulating a heavily regulated surface-water system.

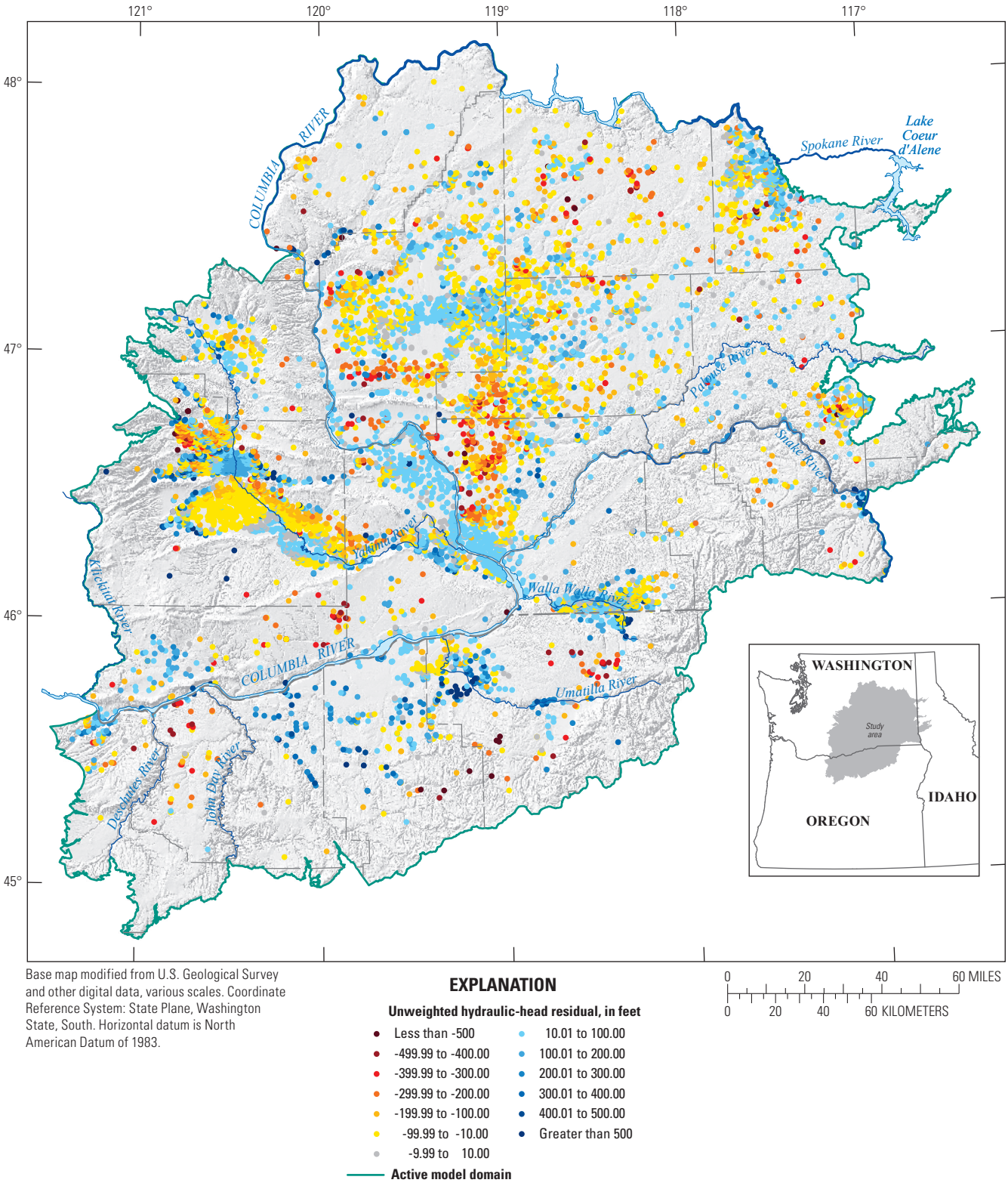

Figure 20. Unweighted hydraulic-head residuals (simulated minus measured) from the steady-state model, Columbia Plateau Regional Aquifer System, Idaho, Oregon, and Washington.

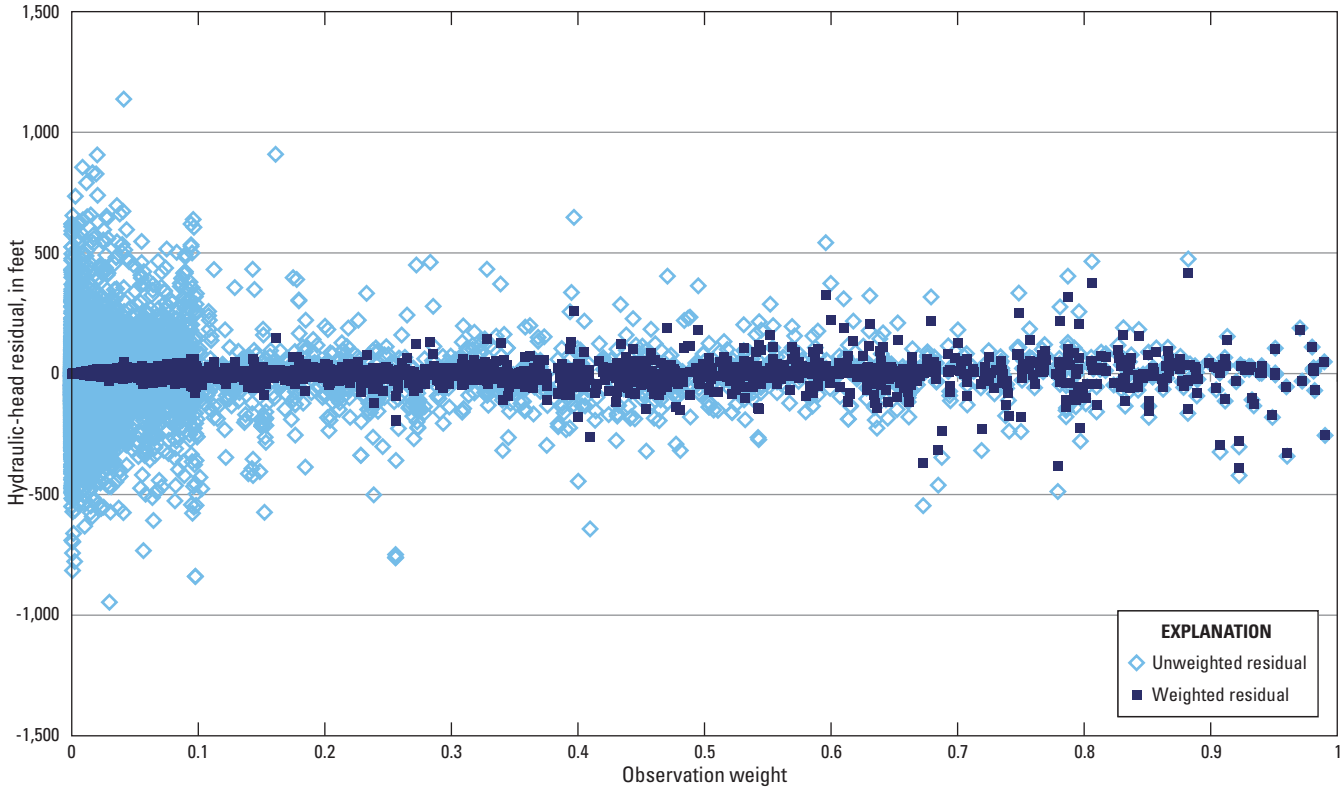

Figure 21. Comparison of unweighted and weighted hydraulic-head residuals with weight, Columbia Plateau Regional Aquifer System, Idaho, Oregon, and Washington.

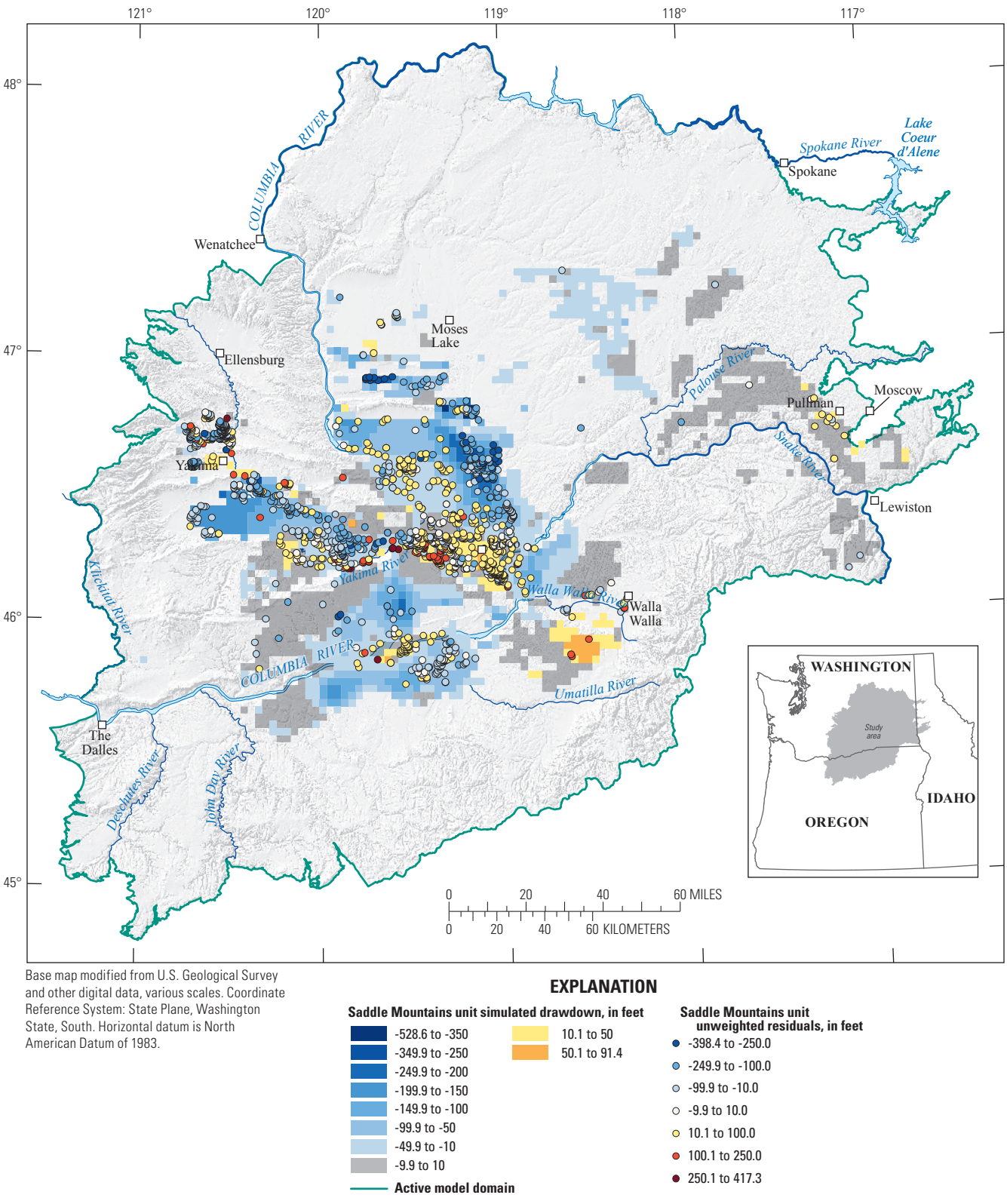

Figure 22. Comparison of the unweighted residuals with simulated current conditions (2000–2007) average drawdown for the Saddle Mountains unit, Columbia Plateau Regional Aquifer System, Idaho, Oregon, and Washington.

Table 5. Simulated steady-state base flow and errors, Columbia Plateau Regional Aquifer System, Idaho, Oregon, and Washington.

[Site locations are shown in figure 17. All values are in cubic feet per second. **Station name:** OR, Oregon; WA, Washington; ID, Idaho; NR, near; R, river, W, west; abv, above; BNDY, boundary; CR or C, creek; SO, south, FK, fork. **Error:** Calculated as simulated base flow minus lower/upper bound. If simulated base flow is within the lower and upper bounds, error is 0]

Base flow observation site	Station name	Simulated base flow	Lower bound	Upper bound	Error
1	WHITE RIVER BELOW TYGH VALLEY, OR	26.0	118.9	378.6	-92.9
2	RHEA CREEK NEAR HEPPNER, OR	11.5	4.0	26.0	0.0
3	ROCK CREEK AB WHYTE PARK NR CONDON, OR	28.0	2.0	68.2	0.0
4	WILLOW CREEK ABV WILLOW CR LAKE, NR HEPPNER, OR	11.2	1.2	18.1	0.0
5	BUTTER CREEK NEAR PINE CITY, OR	51.9	5.2	36.9	15.0
6	MCKAY CREEK NEAR PILOT ROCK, OR	118.0	1.4	114.9	3.1
7	UMATILLA R AT W RESERVATION BNDY NR PENDLETON, OR	391.5	41.5	520.2	0.0
8	MOONSHINE CREEK NEAR MISSION, OR	4.8	0.1	2.9	1.9
9	UMATILLA RIVER AT PENDLETON, OR	438.9	45.6	483.7	0.0
10	UMATILLA RIVER ABOVE MEACHAM CREEK, NR GIBBON, OR	163.2	44.1	223.2	0.0
11	ROCK CREEK NEAR ROOSEVELT, WA	58.7	1.7	170.0	0.0
12	SOUTH FORK WALLA WALLA RIVER NEAR MILTON, OR	137.1	102.2	168.4	0.0
13	SPRING CREEK NEAR BLOCKHOUSE, WA	3.4	1.4	140.0	0.0
14	LITTLE KLICKITAT R NR WAHKIACUS, WA	117.5	10.3	1,030.0	0.0
15	ALDER CR AT ALDERDALE, WA	2.5	0.3	30.0	0.0
16	LITTLE KLICKITAT R NR GOLDENDALE, WA	29.3	3.5	350.0	0.0
17	MILL CREEK NEAR BLOCKHOUSE, WA	12.3	1.4	140.0	0.0
18	MILL CREEK NEAR WALLA WALLA, WA	74.0	6.9	690.0	0.0
19	WALLA WALLA RIVER NEAR TOUCHET, WA	784.7	18.4	558.1	226.6
20	BLUE CREEK NEAR WALLA WALLA, WA	6.9	1.0	100.0	0.0
21	TOUCHET R NR TOUCHET, WA	281.0	14.8	1,480.0	0.0
22	MILL CREEK NEAR WALLA WALLA, WA	87.1	1.1	77.4	9.7
23	DRY CREEK NEAR WALLA WALLA, WA	17.6	1.3	130.0	0.0
24	YAKIMA RIVER AT KIONA, WA	1,003.8	1,489.4	3,189.5	-485.6
25	TOUCHET RIVER AT BOLLES, WA	250.7	14.5	1,450.0	0.0
26	EAST FK TOUCHET R NR DAYTON, WA	119.9	9.5	950.0	0.0
27	ASOTIN CREEK BELOW CONFLUENCE NEAR ASOTIN, WA	13.2	23.9	48.7	-10.7
28	GRANGER DRAIN AT GRANGER, WA	0.0	19.5	34.9	-19.5
29	TUCANNON RIVER NEAR STARBUCK, WA	222.2	12.7	1,270.0	0.0
30	AHTANUM CREEK AT UNION GAP, WA	78.4	15.4	68.4	10.0
31	MEADOW CREEK NR CENTRAL FERRY, WA	22.1	0.2	19.0	3.1
32	SO FK PALOUSE R ABV PARADISE C NR PULLMAN, WA	11.0	0.7	72.0	0.0
33	PARADISE CR NR PULLMAN, WA	7.2	0.5	51.0	0.0
34	PARADISE CR AT UNIVERSITY OF IDAHO AT MOSCOW, ID	1.8	0.8	7.0	0.0
35	SOUTH FORK PALOUSE RIVER AT PULLMAN, WA	20.1	3.8	29.2	0.0
36	MISSOURI FLAT CREEK AT PULLMAN, WA	1.6	0.4	38.0	0.0
37	PALOUSE RIVER AT HOOPER, WA	471.0	37.9	538.0	0.0
38	UNION FLAT CREEK NEAR COLFAX, WA	36.4	1.8	180.0	0.0
39	FOURMILE CR AT SHAWNEE, WA	0.8	0.5	48.0	0.0
40	PALOUSE RIVER BELOW SOUTH FORK AT COLFAX, WA	93.6	21.9	341.3	0.0
41	PALOUSE RIVER NR POTLATCH, ID	25.6	11.2	246.6	0.0
42	PALOUSE RIVER NEAR COLFAX, WA	63.3	17.5	1,750.0	0.0
43	PINE CREEK AT PINE CITY, WA	53.4	2.0	200.0	0.0
44	CRAB CREEK AT ROCKY FORD ROAD NEAR RITZVILLE, WA	16.9	11.9	35.6	0.0
45	ROCKY FORD CREEK NEAR EPHRATA, WA	2.4	6.9	690.0	-4.5
46	CRAB CREEK AT IRBY, WA	53.7	4.9	33.6	20.1
47	CRAB CREEK AT IRBY, WA	57.9	2.9	290.0	0.0
48	COAL CREEK AT MOHLER, WA	1.5	0.1	12.0	0.0
49	PARK CREEK BLW PARK LAKE NR COULEE CITY, WA	11.8	1.0	95.0	0.0
50	DOUGLAS CREEK NEAR ALSTOWN, WA	13.0	0.1	9.2	3.8

Transient Model Fit and Model Error

Comparison of Simulated and Measured Hydraulic Heads

A traditional and intuitive assessment of model calibration is a simple plot of measured hydraulic heads as a function of simulated hydraulic heads (fig. 23). For 46,460 water-level measurement points, the mean and median difference between simulated minus measured hydraulic heads is -10 and 4 ft, respectively. The residuals for the transient simulation period show that 52 percent of the simulated heads exceeded measured heads with a median residual value of 43 ft, and 48 percent were less than measured heads with a median residual value of -76 ft. The residuals should be normally distributed along a line with a 1:1 line (slope equal to 1.0 and a y-intercept of zero), if no model bias exists. The weighted measurements compared with weighted simulated values generally are along a straight line with a slope of 1.03 and a y-intercept of -18.0 ft.

The root-mean-square (RMS) error of the difference between simulated and measured hydraulic heads in the observation wells, divided by the total difference in measured hydraulic heads in the groundwater system (Anderson and Woessner, 1992, p. 241), should be less than 10 percent to be acceptable (Drost and others, 1999). The calibrated transient model produced an RMS error of 167, which divided by the total difference in water levels (5,648 ft), was 2.9 percent.

The residuals for overburden and basalt units indicated a reasonable fit (66 percent of the residuals were within ±100 ft); however, the spatial distribution of the residuals less than -100 ft or greater than 100 ft showed definite patterns of bias (fig. 24). For example, 67 percent of simulated heads in the GWMA were less than measured heads, in 187 instances at 24 locations, by greater than 500 ft. Most of the largest GWMA residuals were on the margins of the GWMA boundary or in the northern part of the region.

Simulated heads generally were larger than measured heads in the Yakima River Basin and Umatilla subarea, 63 and 67 percent of the time, respectively. There also was a bias toward residuals of greater than 500 ft in areas of the Yakima River Basin and Umatilla subarea.

The pattern of underprediction in the GWMA and overprediction in the Yakima River Basin and Umatilla subarea was somewhat expected. In areas of significant upward hydraulic gradient, the simulated head likely would be higher than the measured commingled head, and conversely, in areas of downward gradient. The Yakima River Basin and Umatilla subarea have areas of upward gradients, and the GWMA has areas of downward gradients for approximately the upper 1,000 ft, although this pattern varies by position.

Model observations were assigned to one layer represented by the well depth reported on drillers' logs. Many, if not most, of the wells used for this analysis are open to multiple transmissive interflow zones; therefore, the measured water level is a composite hydraulic head from across the open well interval, so water-level residuals (simulated minus measured) can be misleading. Burns and others (2012b) determined that in some areas of the Palouse Slope, hydraulic heads measured in wells open to the same formations at similar altitudes were highly variable (differing by hundreds of feet). The variability was attributed to strong vertical hydraulic gradients and geologic or well-construction variability causing different amounts of commingling, with heads in well-connected and more transmissive aquifers dominating individual boreholes. Evaluation of residuals shows bias associated with the use of commingled wells as observations. A more detailed analysis of residuals indicates that model fit likely would be better if all measurements were from wells constructed only in single aquifers.

Another way to assess the ability of the CPRAS model to represent groundwater flow and trends is to examine the vertical distribution of hydraulic heads in the Umatilla subarea and Palouse Slope well groups identified in Burns and others (2012b). The model layers containing simulated heads selected for plotting were identified as potentially commingled by using well construction records.

A total of 4,235 measured water levels from 286 wells in the Umatilla River Basin in the CRBG aquifers were divided into clustered groups of wells with similar water levels and trends (fig. 25). The method and justification for well zonation is described in Burns and others (2012b). Zones of low permeability may separate the groups of wells with similar water levels and trends. These zones represent leaky barriers to groundwater flow and compartmentalize the CRBG aquifer system. The degree of compartmentalization is variable, but it occurs in both the vertical and horizontal directions in the Umatilla area. Within each well group in the Umatilla River Basin, hydraulic heads can be correlated over tens of miles in the horizontal direction.

The transient simulation results showed a reasonably good match to measured water levels in the Umatilla area (fig. 26). The presence of large vertical gradients within groups can explain the large range of data values within many of the groups. For example, for Umatilla well group 2, simulated heads in layers 32–41 span the range of measured water levels. The timing of simulated declines agreed with measured water-level trends, with steeper declines occurring during the mid-1970s. Head differences between groups were preserved, ensuring that regional flow patterns were adequately simulated.

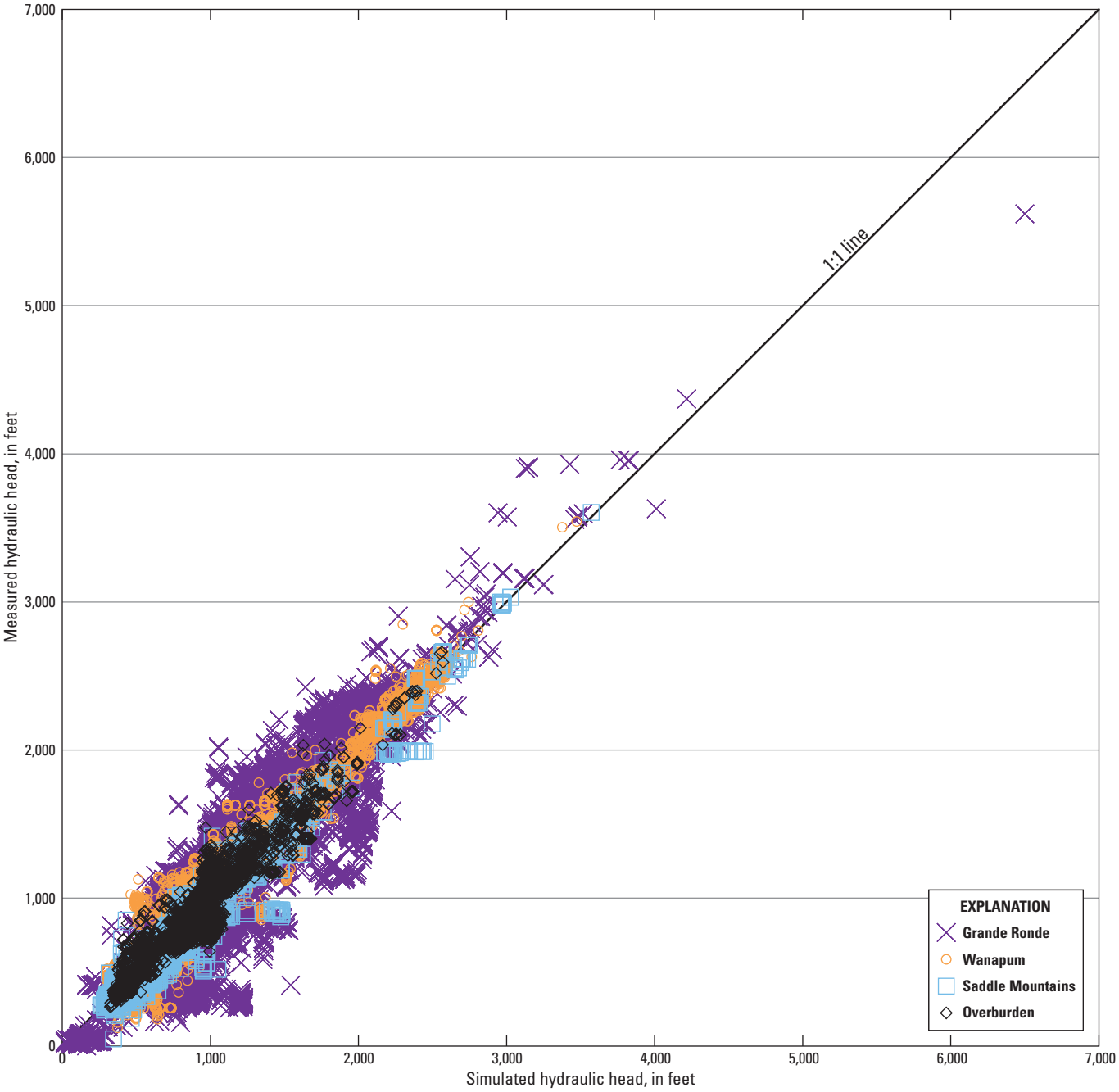

Figure 23. Measured hydraulic heads as a function of simulated heads, Columbia Plateau Regional Aquifer System, Idaho, Oregon, and Washington.

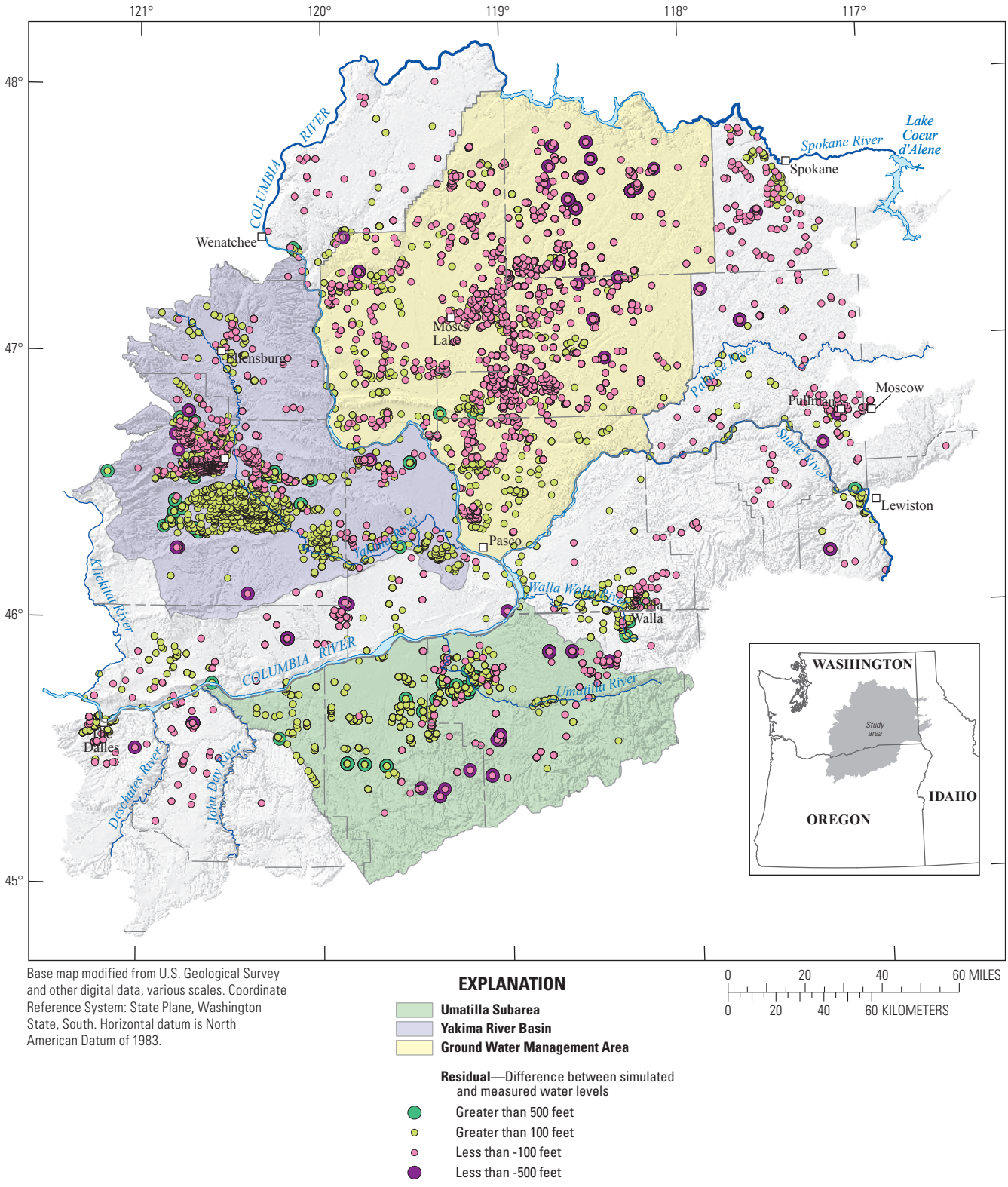

Figure 24. Differences between simulated and measured water levels (residuals), Columbia Plateau Regional Aquifer System, Idaho, Oregon, and Washington. The spatial distribution of residuals less than -100 feet or greater than 100 feet showed definite patterns of bias.

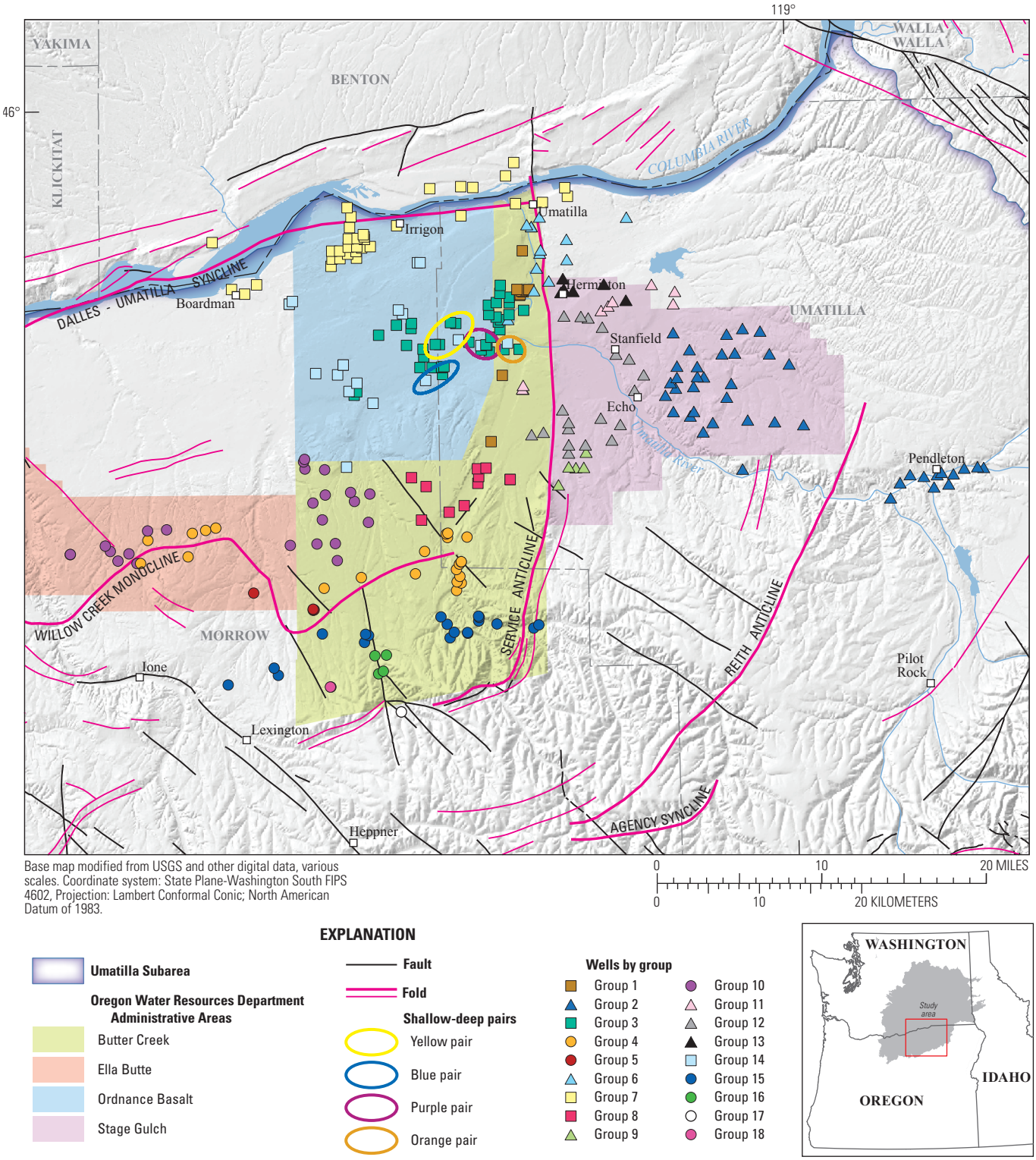

Figure 25. Well groups with similar hydraulic response within the Umatilla subarea, Oregon. Wells are grouped to show a general North–South transect (circles and squares) and a general East–West transect (triangles and squares). From Burns and others (2012b).

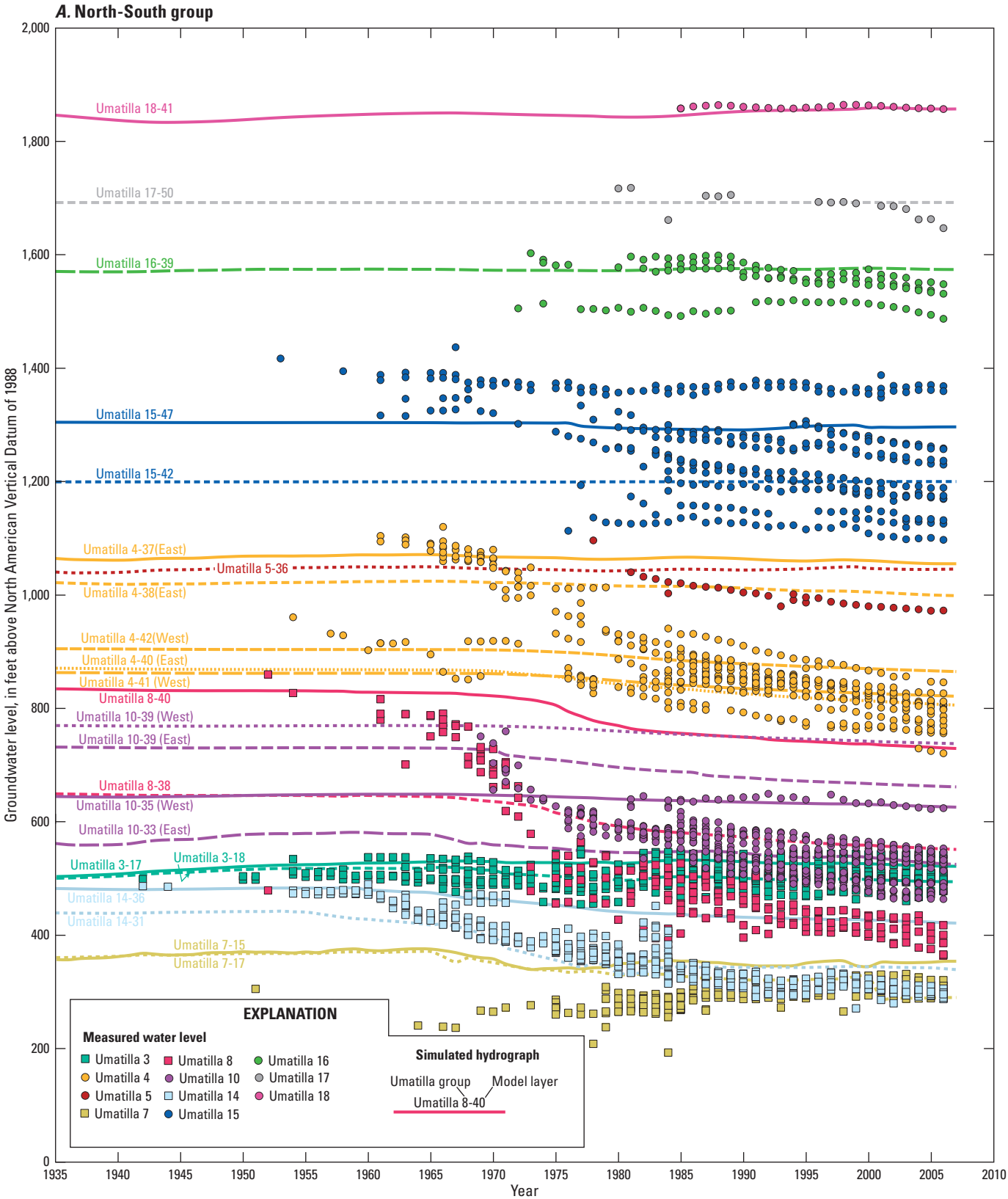

Figure 26. Simulated water levels for the (*A*) North-South; and (*B*) East-West well groups near the Oregon Water Resources Department administrative areas in the Umatilla subarea, Oregon. Measured water levels depict the winter median water level for individual wells within each well group. Locations of wells are shown in figure 25. The numbered lines corresponding to each data series show transient simulated water levels from layers intersected by nearby potentially commingling wells.

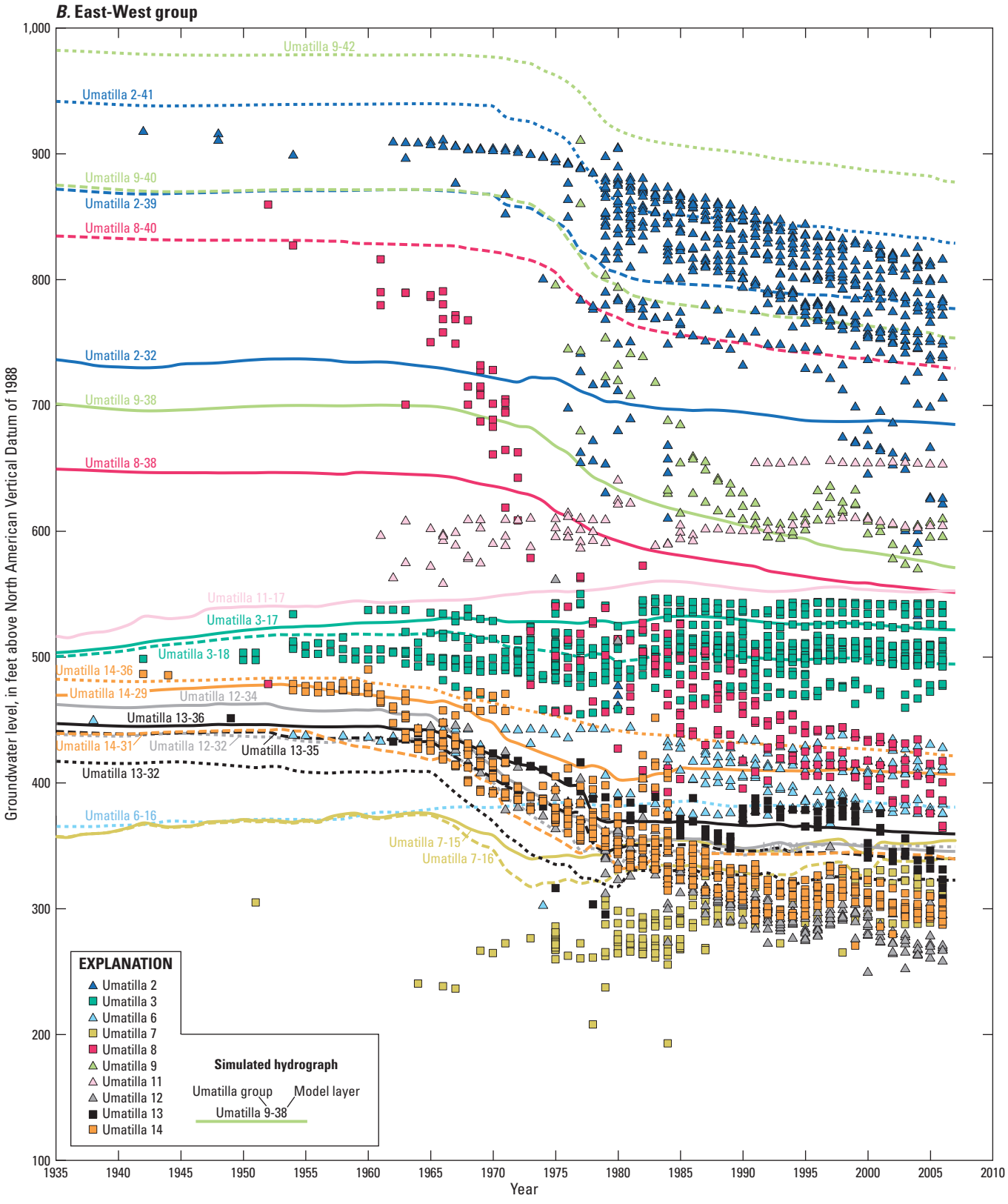

Figure 26.—Continued

During model calibration, it was determined that wells near groups 4, 8, and 10 had steeper water-level declines than simulated declines, so modifications to the model were made to better match the observations. Two mechanisms were identified as possible causes: (1) flow barriers that exist in shallow CRBG units were not present in deep units, allowing commingling to drain water away through the deeper aquifer system, or (2) aquifer storage is much lower in some mid-slope areas, causing much steeper water-level declines in response to the relatively modest amount of simulated pumping. To evaluate the efficacy of the first mechanism, the final model was calibrated by removing horizontal-flow barrier segments 61, 63, and 65 below model layer 40 and horizontal-flow barrier segments 70 and 71 from all CRBG units except Saddle Mountains (fig. 9). This mechanism was deemed the more likely cause of the observations, because (1) the final heads in several different groups apparently were trending toward the same final head value and (2) storage parameter adjustments had a negligible effect. Mechanistically, the flow barriers in the shallower units are attributed to depositional variability that occurred as the younger lava flows onlapped the anticline that was contemporaneously forming the Blue Mountains.

The GWMA encompasses much of the Palouse Slope and the eastern part of the Yakima Fold Belt, which forms a transition area between the two physiographic provinces (fig. 1). Burns and others (2012b) examined 8,622 measured water levels from 1,202 wells within the Palouse Slope and eastern Yakima Fold Belt in the CRBG aquifers and divided them into groups of wells exhibiting similar changes in hydraulic head over time (fig. 27).

Similar to the analysis of the Umatilla subarea well groups, a comparison of measured and simulated heads by group was performed for the Palouse Slope. Unlike the Umatilla subarea, discrete horizontal-flow barriers were much less influential in the Palouse Slope area, consistent with the lower degree of structural deformation in this gently folded area. The lack of horizontal-flow barriers explains the significant overlap of measured heads between groups, with the large range in measured heads attributed to using commingling water levels in an area with large vertical gradients (fig. 28).

The magnitude, timing, and range of simulated heads were in good general agreement with measured water levels. Comparison between the groups of wells representing different flow paths (figs. 28*A*–*D*), indicated that the simulated regional flow field matched the measured flow field, including the reversal of groundwater-flow direction in the shallow aquifers that accompanied application of large quantities of CBIP irrigation water (Burns and others, 2012b).

Comparison of Simulated and Measured Streamflow

Average long-term base-flow estimates of streamflow were helpful in calibrating the steady-state model during automated calibration, but uncertainties in those estimates made them insufficient to fully evaluate the transient model. The addition of large-scale agricultural irrigation and groundwater pumping has had competing effects on streamflow in the CPRAS. Surface-water irrigation, and to a lesser degree groundwater irrigation added large amounts of water to shallow groundwater storage throughout the period of development. This additional water has increased streamflow in areas of irrigation, even resulting in groundwater flooding and landslides. However, in areas away from major surface-water irrigation, pumping has reduced groundwater in storage, lowering water levels and streamflows. These patterns and trends were largely reproduced by the transient model, as shown by the change in base flows from predevelopment to current conditions (2000–2007; fig. 29). The Yakima River Basin and the Columbia River along the eastern boundary of the Yakima River Basin consistently showed an increase in base flow compared to predevelopment conditions. Groundwater pumping has captured and thereby reduced annual streamflow in the Yakima River system by about 200 ft^3/s (Ely and others, 2011), but that reduction is small compared to increases from irrigation, so there is a net gain in flow. Surface-water irrigation in the Yakima River Basin has been extensive, but simulating the Yakima River headwaters and the basin-wide regulation (reservoirs, diversions, and returns) was beyond the scope of this study.

The vast majority of stream reaches in the CPRAS model area have decreased simulated base flows compared to predevelopment conditions (fig. 29). This decrease is caused by two factors. First, predevelopment recharge from precipitation is greater than current condition recharge from precipitation. Second, groundwater pumping has reduced water levels and captured streamflow. One area of interest is Crab Creek (sites 44, 46, and 47, fig. 17). Base flow along the upper reaches of Crab Creek has decreased over recent time, whereas the model simulated modest increases. The model did simulate the decreased flow in the lower reaches of Crab Creek. This inconsistency shows the difficulty of simulating site-specific stresses in a regional model with coarse horizontal discretization.

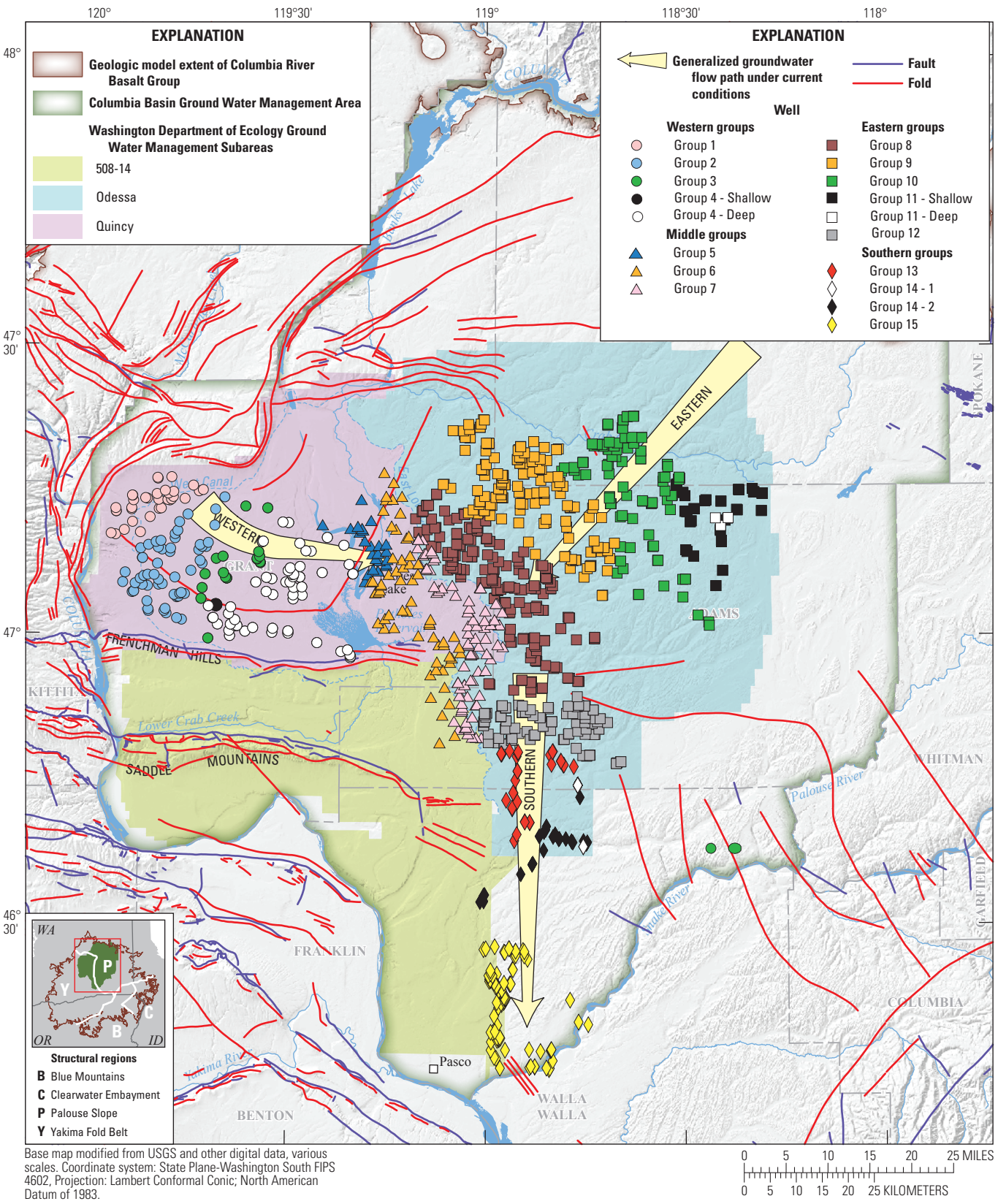

Figure 27. Well groups with similar hydrologic responses and generalized groundwater-flow paths under 2000–10 conditions near the Washington State Department of Ecology administrative areas in parts of the Palouse Slope/eastern Yakima Fold Belt and the Columbia Basin Ground Water Management Area, Washington. From Burns and others (2012b).

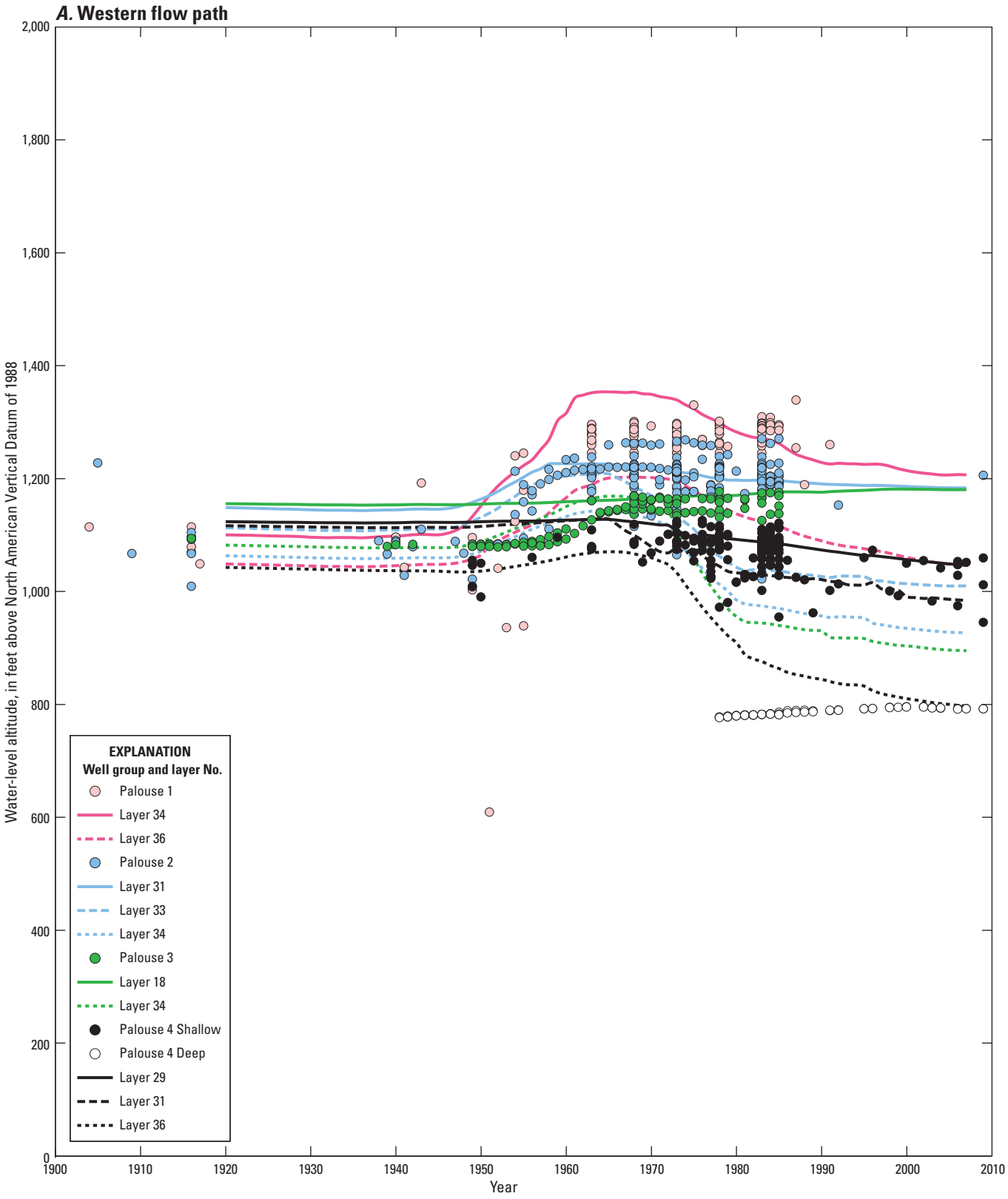

Figure 28. Simulated water levels for the (*A*) western flow path; (*B*) eastern flow path; (*C*) middle flow path; and (*D*) southern flow path well groups near the Washington State Department of Ecology administrative areas in parts of the Palouse Slope/eastern Yakima Fold Belt and the Columbia Basin Ground Water Management Area, Washington. Locations of wells are shown in figure 27. The lines under each well group show corresponding transient model simulation results from layers intersected by nearby potentially commingling wells.

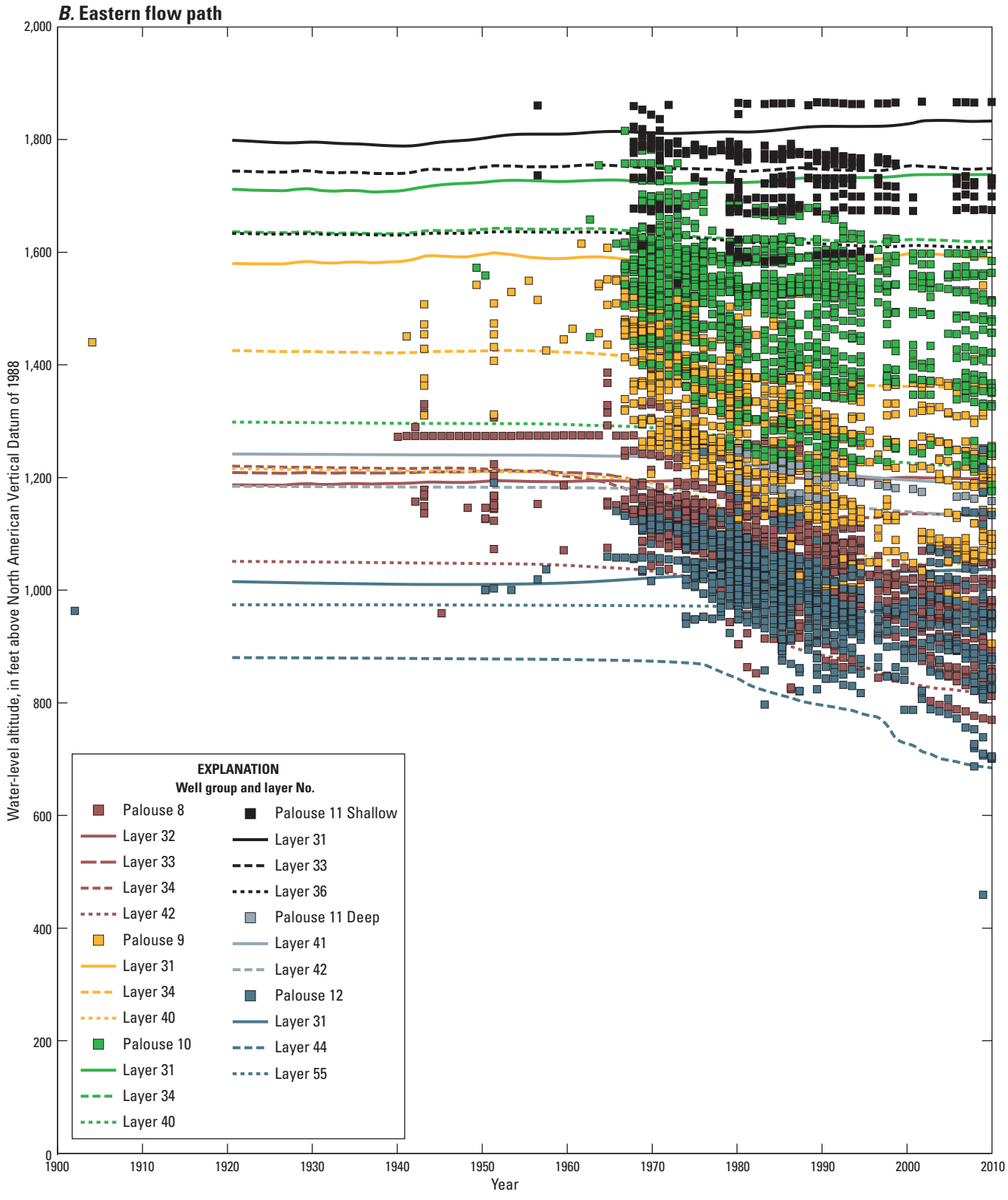

Figure 28.—Continued

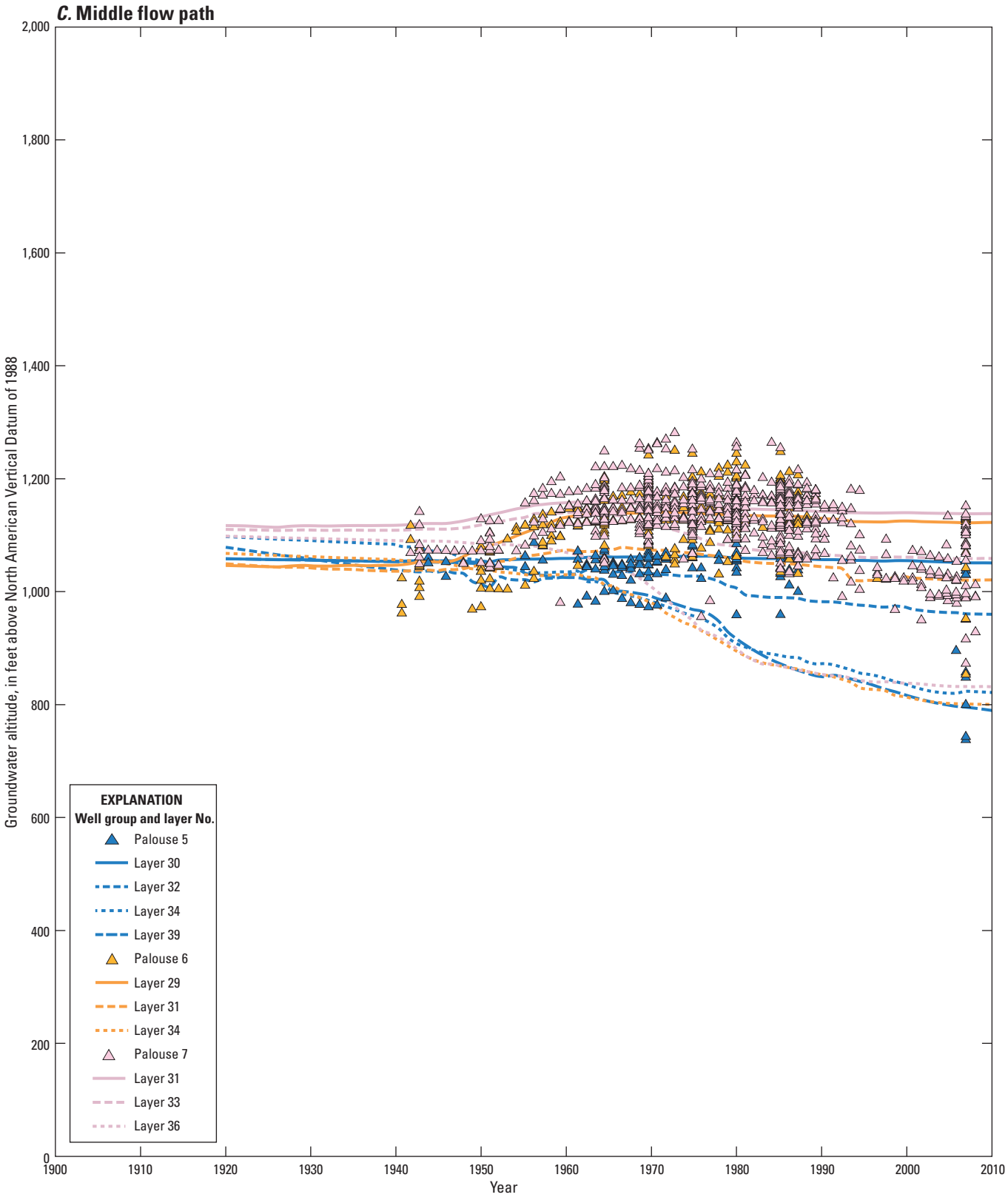

Figure 28.—Continued

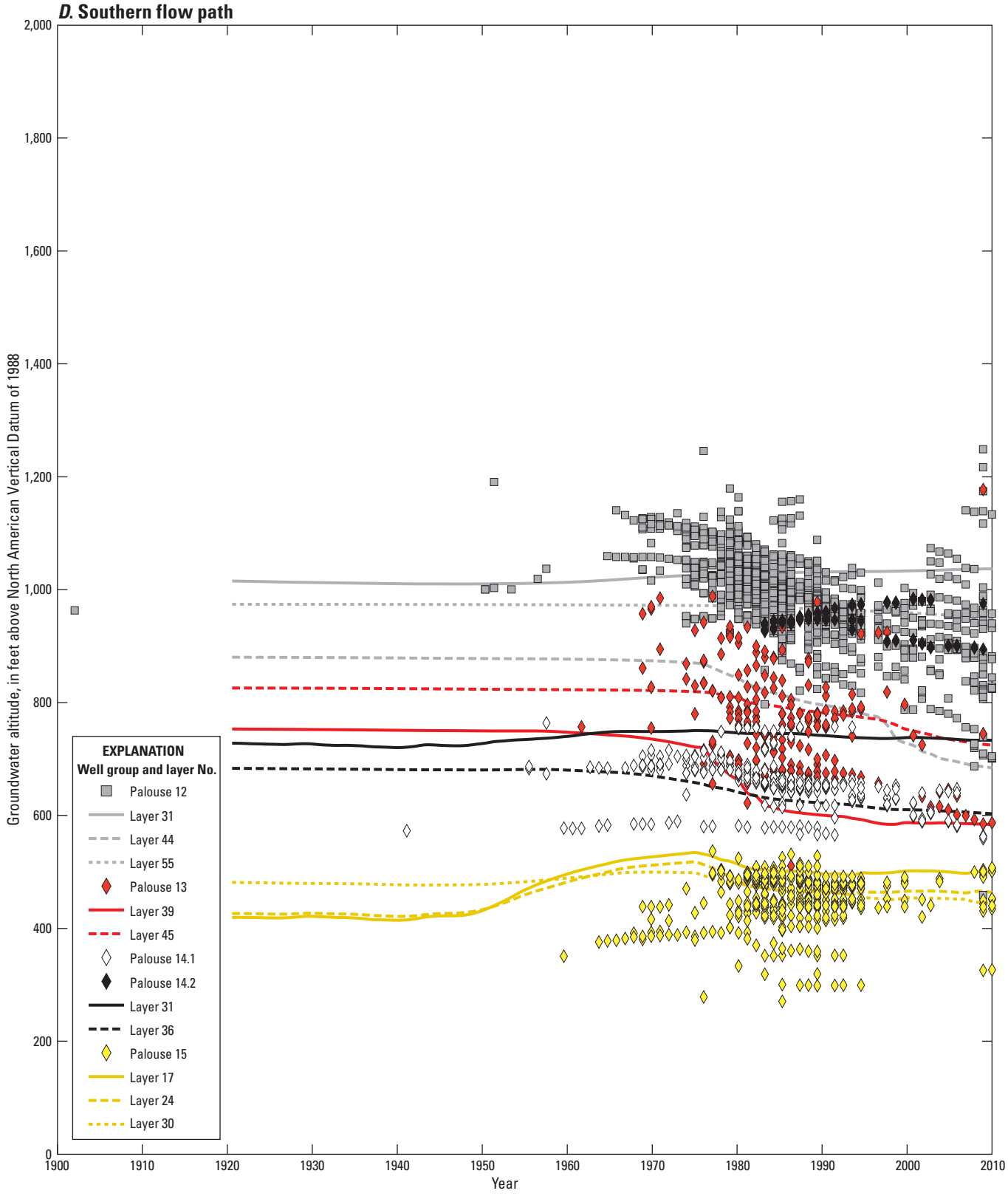

Figure 28.—Continued

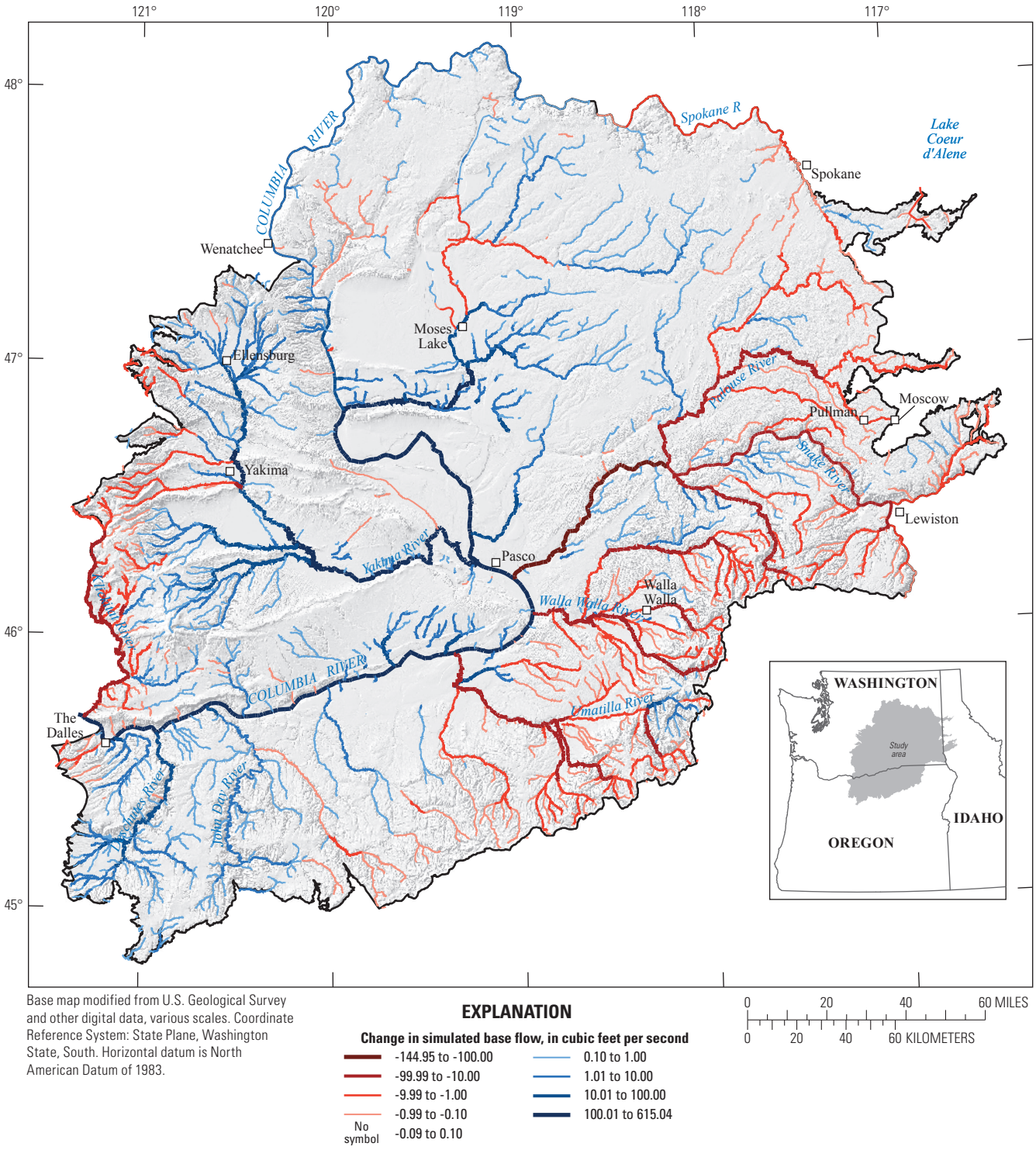

Figure 29. Change in simulated base flow from predevelopment (pre-1900) to current conditions (2000–2007) for the Columbia Plateau Regional Aquifer System, Idaho, Oregon, and Washington. Red indicates current condition base flow is less than predevelopment base flow. Blue indicates current condition base flow is greater than predevelopment base flow.

Simulated Potentiometric Surfaces

Each layer of the model can be conceptually viewed as a (potential) aquifer. The presence of an actual aquifer is controlled by the presence of sufficient local porosity and permeability, which varies as a function of geologic deposition. Previous modeling studies simulated significantly fewer model layers. To allow comparison with previous studies and create summary maps of conditions, composite head and drawdowns were computed (figs. 30 and 31, respectively) for the Overburden, Saddle Mountains, and Wanapum units, and the upper 10 model layers of Grande Ronde Basalt (as much as 2,000 ft near the center of the study area). Composite heads were computed as the thickness-weighted average of heads in the layers being averaged. Dry cells (simulated head below the cell bottom) were not used in the computation. Composite drawdown was computed as predevelopment composite head minus the late-time (2000–2007) average of the composite heads for each year. In all cases where cells were dry for only a few of the years, the bottom elevation of the lowest model layer used in the average was used for the dry years. If all cells were dry for all years, the final drawdown value was 0.

Model Uncertainty and Limitations

The CPRAS model is a set of mathematical equations designed to represent an extremely complex natural system. Furthermore, this natural system has been perturbed by human activities in ways only generally understood and not fully quantified. Intrinsic to the model is the error and uncertainty associated with the approximations, assumptions, and simplifications that must be made. In addition to those intrinsic errors, hydrologic modeling errors typically are the consequence of a combination of errors in the (1) input data, (2) representation of the physical processes by the algorithms of the model, and (3) parameter estimation during the calibration procedure (Troutman, 1985). These three types of model errors limit application of the CPRAS model as follows:

- Data on extents and thicknesses of mapped hydrogeologic units, location and nature of structural features, water levels, pumpage, recharge, and hydraulic properties were taken from Kahle and others (2009), Burns and others (2011, 2012b), and other previous investigations. Most of the data were concentrated along major river valleys and populated areas. This means that for some of the study area, information was not available to calibrate the model, especially for the areas lacking water-level data. Additionally, the methods used to estimate important stresses of the flow system, such as groundwater pumping and recharge, were limited to recent years. Reconstructing model stresses for the first half of the model simulation period likely led to larger error and uncertainty.
- A numerical model cannot completely represent all physical processes within a flow system. Determining if a weakness in a simulation is attributable simply to input data error or to shortcomings in how the model represents the governing physical processes is often not possible. The model inevitably relies on simplifying assumptions and generalizations that affect the results of the simulation in complex ways. The CPRAS model was not designed to represent some details of the hydrologic processes. For example, the extensive network of surface-water diversions, canals, wasteways, and drains were not directly simulated. Model drain cells were placed in any model cell that might have streamflow based on the NHD (Simley and Carswell, 2009). Reservoirs and reservoir releases on the Columbia River and its tributaries were not included in the CPRAS model. Furthermore, model-discretization errors resulted from (1) the effects of averaging altitude information over the model cell size, (2) the time averaging of observed values inherent in an annual simulation stress period, and (3) the inaccuracies in translating mapped hydrogeologic units into orthogonal model cells.
- Errors in parameter estimates occur when improper values are selected during the calibration process. Various combinations of parameter values can result in low residual error, yet improperly represent the natural system. An acceptable degree of agreement between simulated and measured values does not guarantee that the estimated model parameter values uniquely and reasonably represent the actual parameter values. The use of automated parameter estimation techniques and associated statistics, such as composite scaled sensitivities and correlation coefficients, removes (or allows consideration of) some of the effects of non-uniqueness, but certainly does not eliminate the problem entirely. Ensuring that calibrated values are comparable to a reasonable range of independently-derived or literature values also can reduce error caused by parameter estimation. Limitations of the model observations used in this study include errors in simulated heads for multilayer wells, uncertainty in the model hydrogeologic unit designations and depths, and streamflow observations based on base-flow estimates from different sources and methods.

If the coarse horizontal discretization, annual stress periods, and estimated stresses are considered, the effects of the simplifications and other potential errors can be limited. If the model is used for simulations beyond which it was designed, however, the generalizations and assumptions used could significantly affect the results.

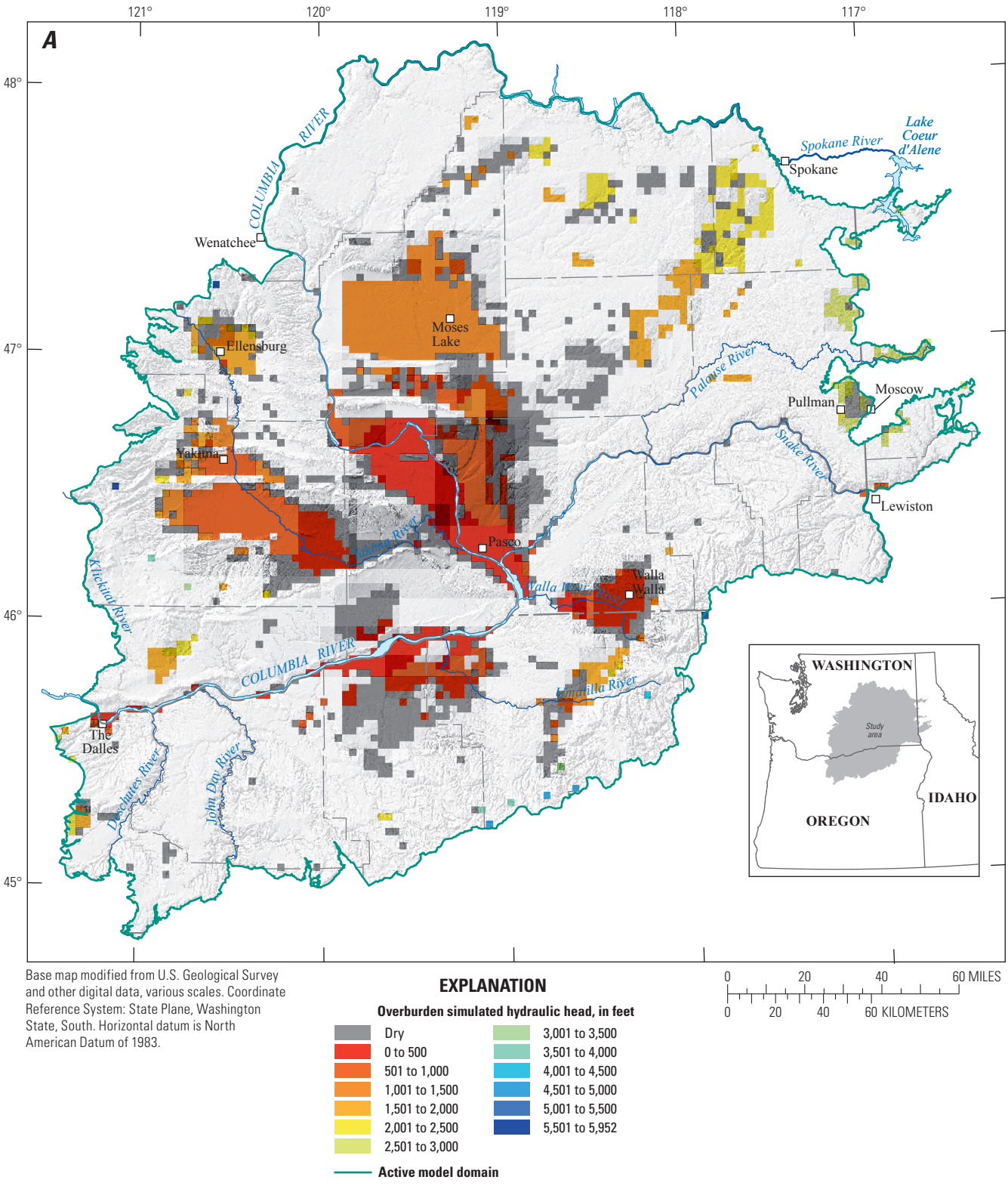

Figure 30. Simulated composite hydraulic head for (*A*) Overburden unit, (*B*) Saddle Mountains unit, (*C*) Wanapum unit, and (*D*) upper Grande Ronde unit for the Columbia Plateau Regional Aquifer System, Idaho, Oregon, and Washington.

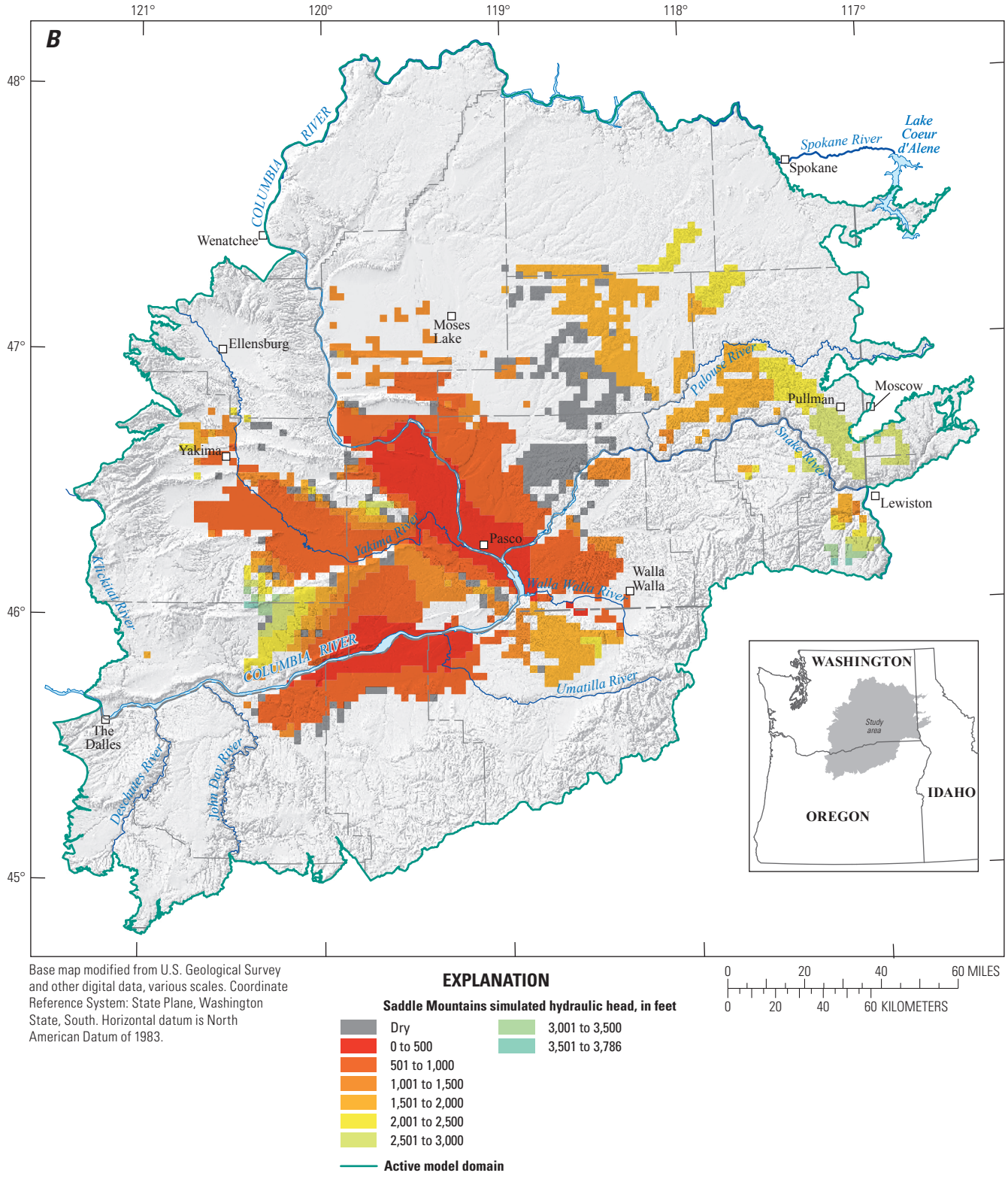

Figure 30.—Continued

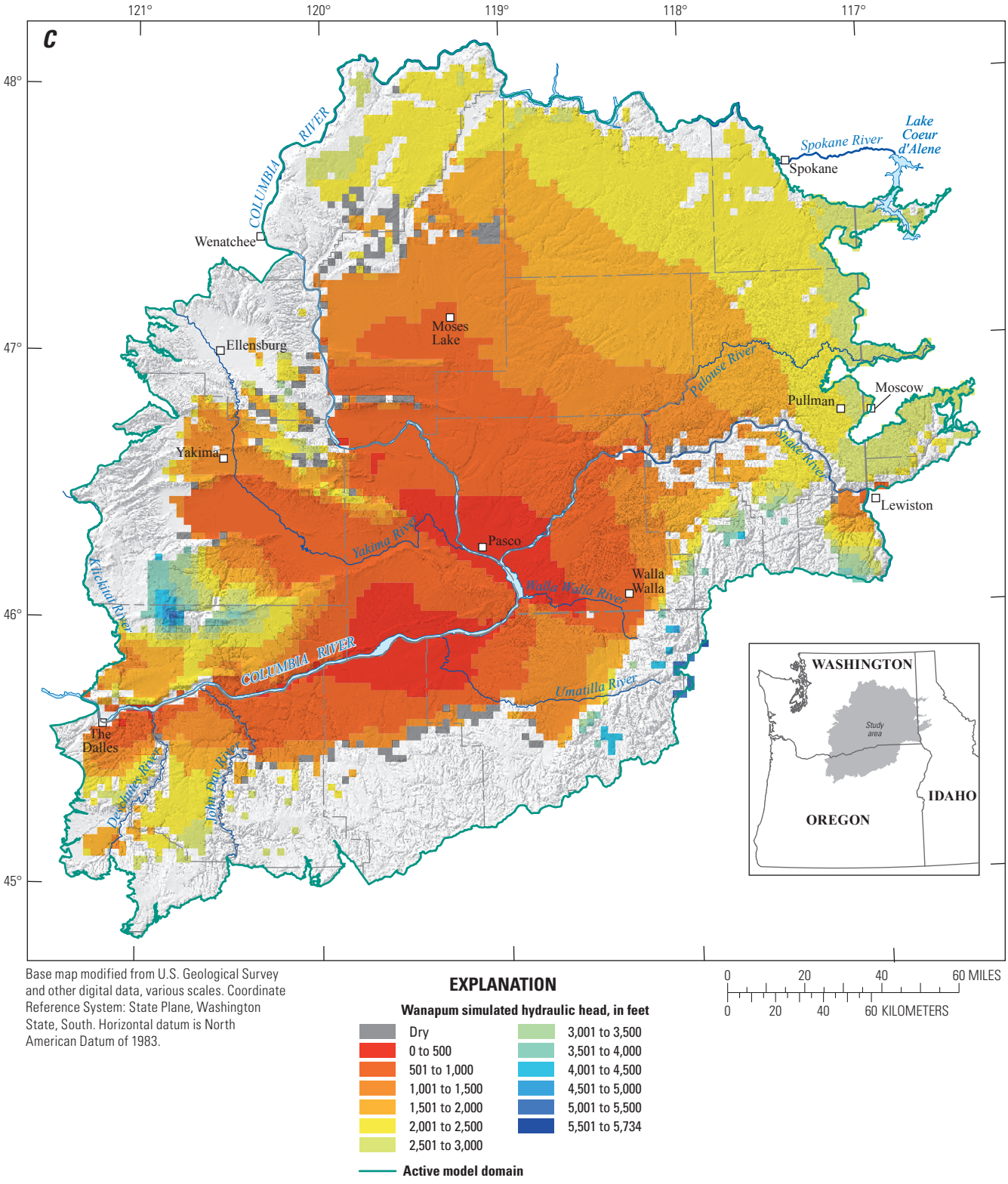

Figure 30.—Continued

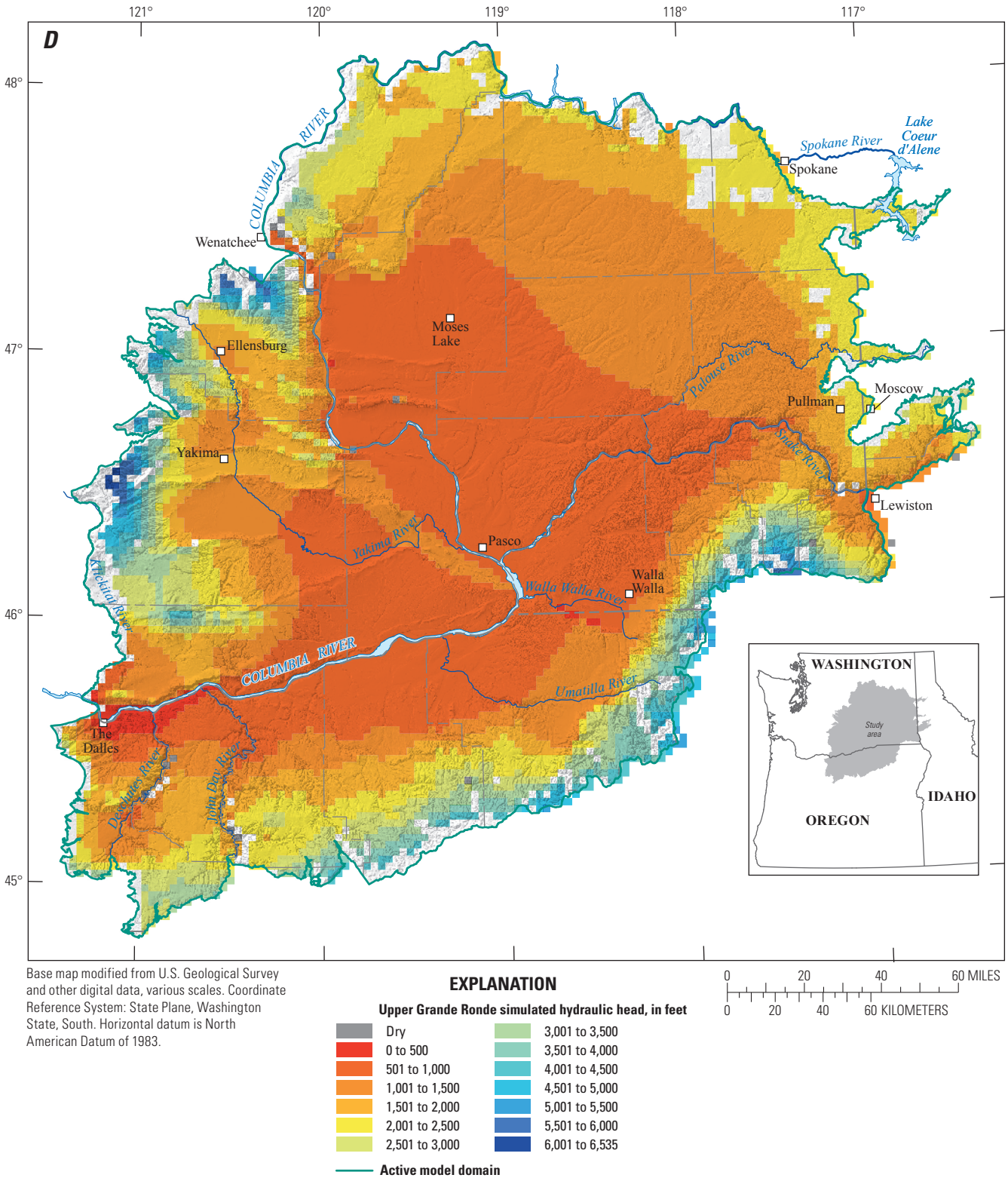

Figure 30.—Continued

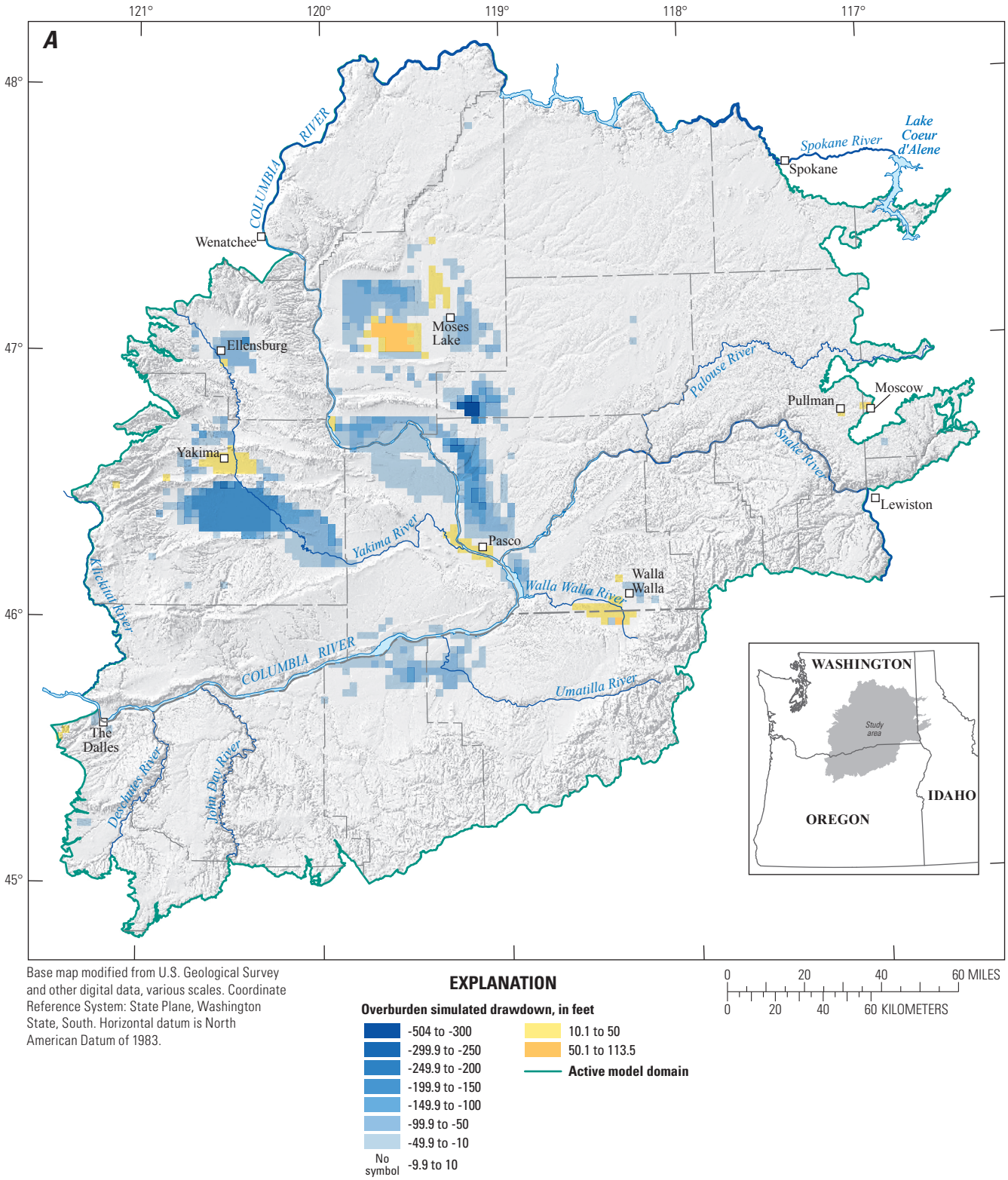

Figure 31. Simulated composite drawdowns from predevelopment to current conditions (2000–2007) for (*A*) Overburden unit, (*B*) Saddle Mountains unit, (*C*) Wanapum unit, and (*D*) upper Grande Ronde unit for the Columbia Plateau Regional Aquifer System, Idaho, Oregon, and Washington.

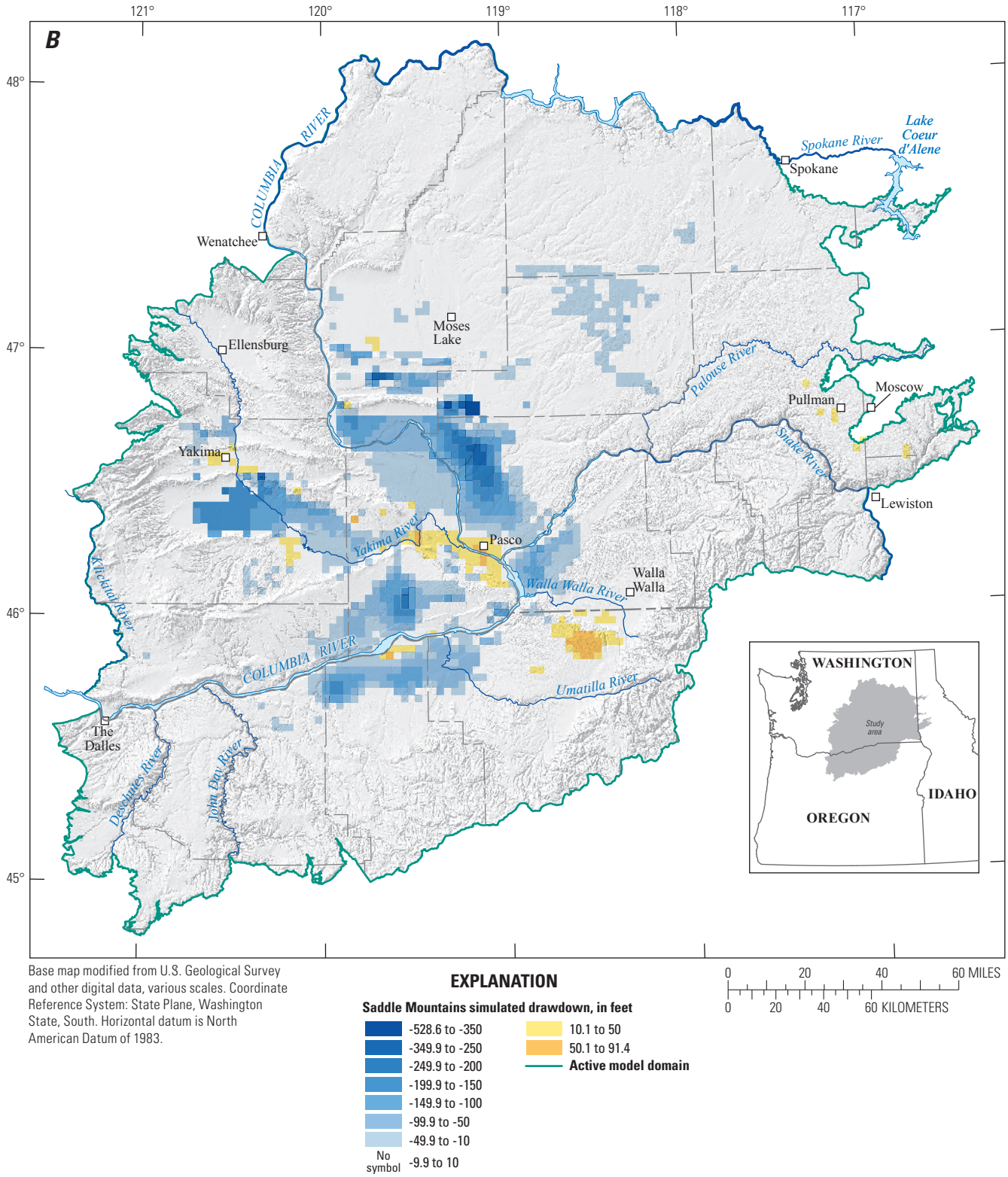

Figure 31.—Continued

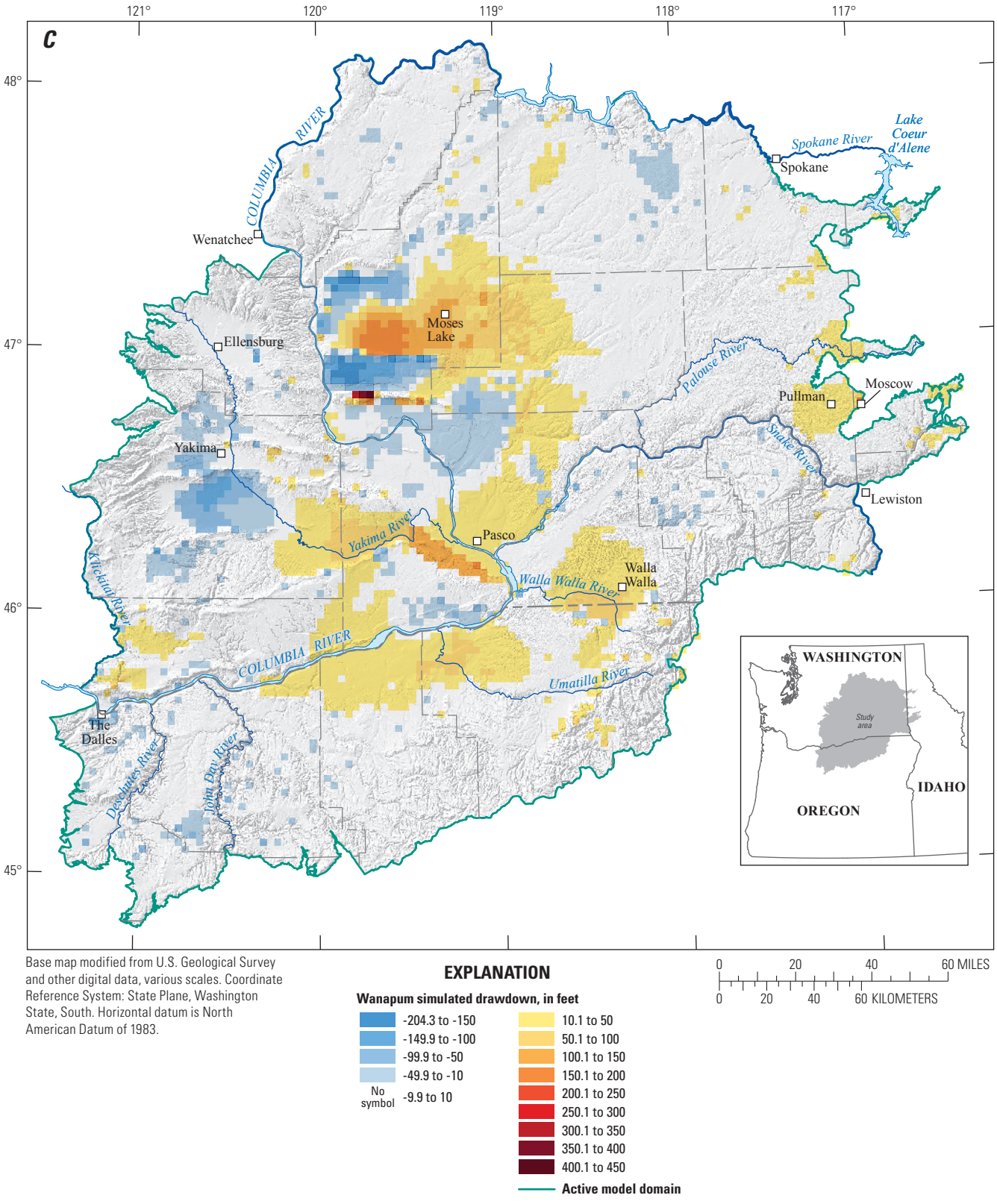

Figure 31.—Continued

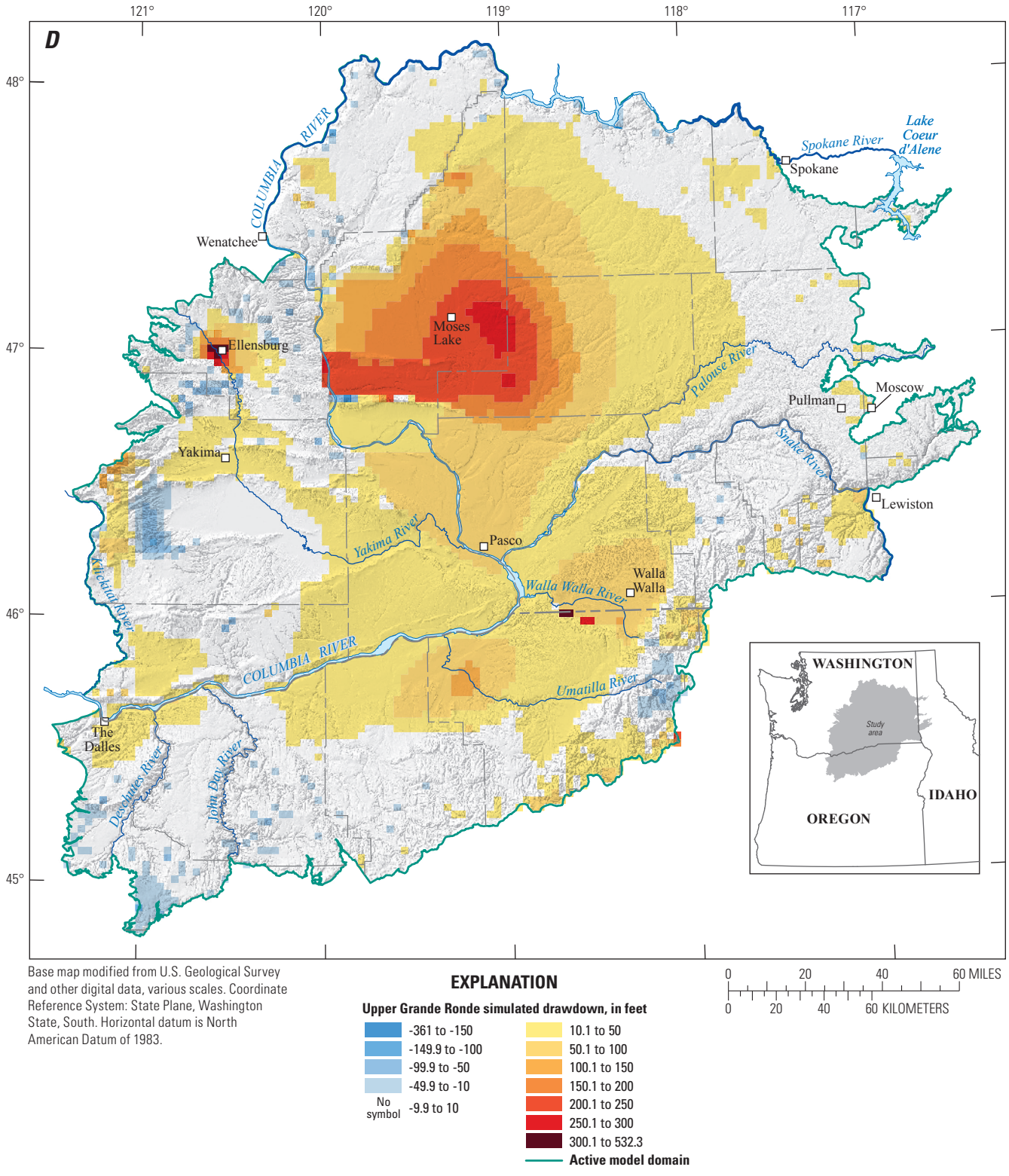

Figure 31.—Continued

Model Application

The CPRAS model was constructed to simulate regional-scale groundwater flow and it can be used to help answer questions regarding groundwater-flow issues at that scale. For example, the interactions of stresses, such as recharge and groundwater pumping, on the groundwater or surface-water system can be evaluated for major basins or subbasins, such as the Yakima and Umatilla River Basins or the Palouse Slope. The CPRAS model includes some localized features and site-specific data, where available, but it is not meant to evaluate issues or hydrologic processes at local scales.

The CPRAS model also can be used to evaluate alternative conceptualizations of the flow system that are likely to have a regional effect. These might include the effects of climate, different interpretations of geologic structures, or the role of commingling wells on hydraulic heads.

Many aspects of the CPRAS affect the groundwater-flow system, including groundwater pumping, irrigation application, geologic structure (faults and folds), and the complex, heterogeneous hydraulic properties of the CRBG and Overburden unit. Throughout some of the study area, data are limited and the CPRAS model has been the appropriate tool to understand the role of these aspects of the system over time.

The annual stress period used in the model was selected to provide adequate temporal resolution for analyses of variations in pumping and recharge rates corresponding to annual changes in precipitation, pumping, and irrigation. Effects of management decisions on time scales less than multi-year are unlikely to be adequately simulated with the CPRAS model; however, the model can be used appropriately to analyze long-term changes in water-use practices or potential future climate.

The basic structure of the calibrated model allows for alternative uses of the model. Sensitivities of stresses on the flow system can provide information for directing additional data analyses and (or) data collection. Cause and effect also can be assessed. For example, assessing the dual effects of increased irrigation recharge and groundwater development on the water levels would be an appropriate use of the model.

The model can be used to examine the effects of continued or increased pumping on the regional groundwater-flow system to evaluate the efficacy of various groundwater resources management alternatives. For increased pumping, the model should not be used for assessing the effects of one or two new wells on the flow system, but could be used for such applications as estimating the quantity of pumpage in an area that leads to specified water-level declines and (or) streamflow capture. With increasing demand for water throughout the Columbia Plateau, the CPRAS model could be further developed to test optimization strategies for the conjunctive use of surface water and groundwater given specified constraints.

Groundwater Budget

The CPRAS model was used to derive components of the groundwater budget for the simulation period of predevelopment to 2007. During this period, the distribution and amount of pumpage changed and recharge varied, and a cumulative or mean annual water budget would not highlight these variations. Thus, simulated annual water budgets are presented for predevelopment to 2007 (fig. 32).

Water-budget components are presented as the difference between inflows and outflows to the groundwater system. Inflows are fluxes into the aquifer system. Outflows are fluxes out of the aquifer system. For example, recharge is considered an inflow and net well withdrawals are considered an outflow. Discharge from the groundwater system to streamflow (rivers and drains) is presented as an outflow. Storage is shown so negative numbers represent outflows from the groundwater system into storage, so a net gain in storage is represented by negative numbers.

The annual groundwater budgets show several trends over the simulation period (fig. 32). Groundwater pumping was negligible until the 1950s and began to increase significantly during the 1970s and 1980s. Recharge was highly variable due to the interannual variability of precipitation, but began to increase in the late 1940s because of the increase in irrigation projects. Streamflow gains and net storage followed recharge closely, but a loss of groundwater in storage increased and streamflow decreased as groundwater pumping increased.

Included in the simulation period were examples of a wet (1997), average (2000), and dry (2001) year (fig. 33).

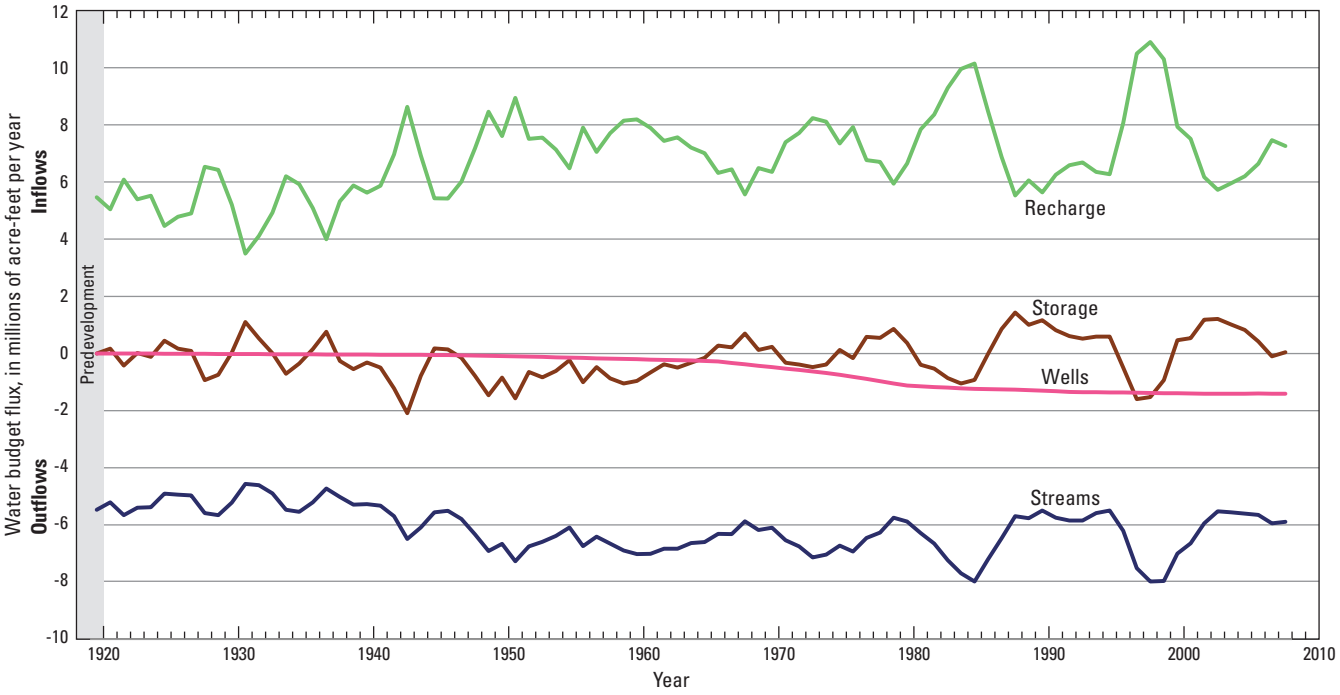

Figure 32. Simulated annual water-budget flux for predevelopment to 2007 for the Columbia Plateau Regional Aquifer System, Idaho, Oregon, and Washington.

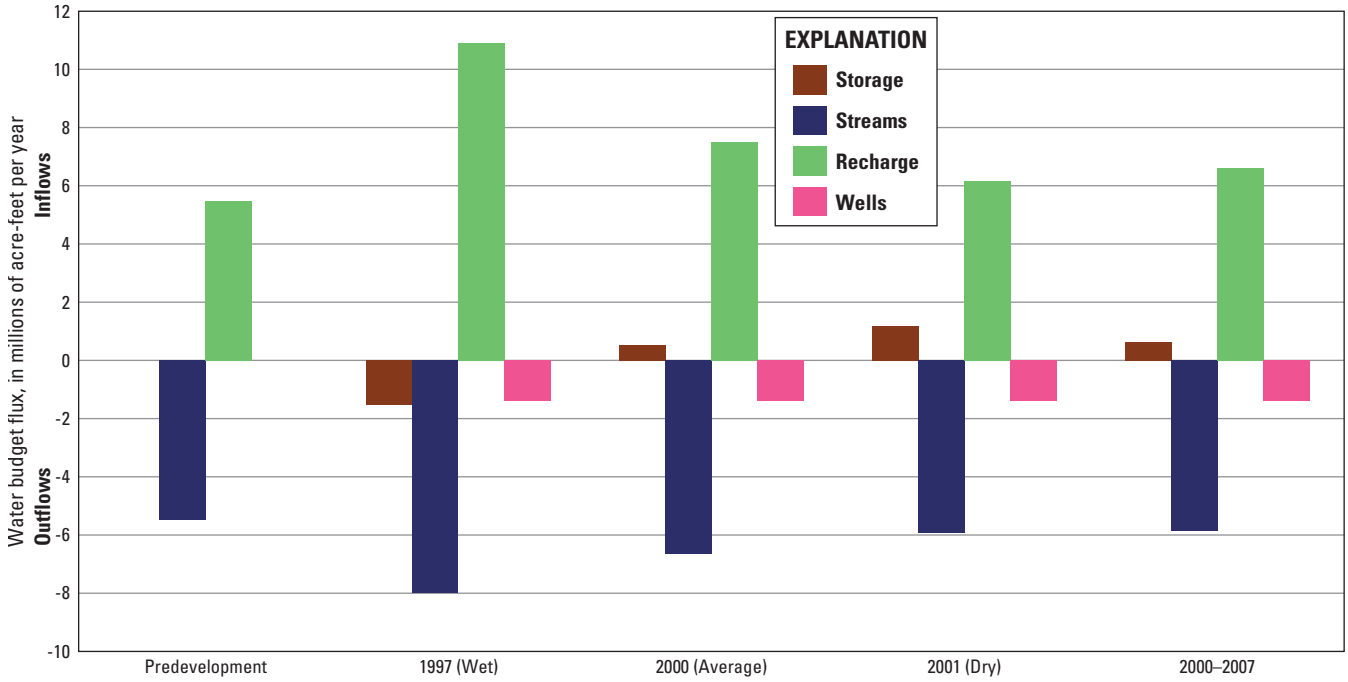

Figure 33. Simulated annual water-budget flux for predevelopment, wet (1997), average (2000), and dry (2001) years, and current conditions (2000–2007), Columbia Plateau Regional Aquifer System, Idaho, Oregon, and Washington.

These 3 years captured the hydrologic variability present in the model domain and were representative of the current groundwater pumping and recharge from irrigation. The net annual budgets for each of the three representative years showed that recharge was the largest water-budget component and dominated the inflows to the system (fig. 33). Groundwater recharge ranged from about 6.2 million acre-ft in 2001 to 10.9 million acre-ft in 1997, an increase of about 76 percent. For the average year (2000), recharge was within 2 percent of the mean annual recharge for 1950–2007. For the wet year (1997), outflows to storage greatly exceeded inflows from storage, resulting in an increase of groundwater in storage of 1.5 million acre-ft. For the dry year (2001), with less recharge and additional effects of pumping (wells), the difference is an outflow of groundwater in storage of about 1.2 million acre-ft.

The simulated water budgets for predevelopment, select wet, average, and dry years, and current conditions (2000–2007) demonstrate the role of human development of the water resources on the groundwater system (fig. 33). The predevelopment stress period was steady-state and therefore, no change in storage was simulated. Recharge in predevelopment conditions was derived solely from precipitation and was balanced by outflows from the groundwater system to streams. Although recharge increased from predevelopment to current conditions due to irrigation, streamflow gradually decreased as groundwater extraction from wells captured more streamflow and induced inflows from storage.

Simulated Effects of Pumping, Commingling Wells, and Irrigation Recharge

In order to evaluate the influence of different drawdown mechanisms, simulated changes in water levels were divided into three components: (1) commingling, (2) pumping, and (3) irrigation recharge. The effects of commingling wells, pumping wells, and irrigation for the Wanapum unit are shown in figures 34*A*–*C*. The changes due to commingling (fig. 34*A*) were simulated using commingling wells with zero pumping and recharge computed using the Bauer-Vaccaro regression equation (no extra recharge from irrigation sources). The changes due to pumping (fig. 34*B*) were estimated as the total drawdown (fig. 31) minus the drawdown simulated assuming zero pumping (recharge and commingling wells were the same for the two runs). The changes due to irrigation recharge (fig. 34*C*) were computed as the drawdown simulated assuming zero pumping minus the drawdown-from-commingling wells. This method of computation ensures that the sum of the component drawdowns equals the total drawdown (fig. 31).

In figures 34*A*–*C*, negative values indicate areas of buildup or rising water levels and positive numbers indicate areas of declining water levels. Assessment of the three scenarios shows a few general findings:

(1) The pumping component was usually positive (declining water levels) and recharge from the irrigation component was usually negative (raising water levels). Minor departures from this pattern are associated with the method of computing drawdown and water-level rise (thickness weighted averaging of cells that are not dry).

(2) The effects of commingling wells show water-level declines in some parts of the aquifers and rises in others. Commingling wells would mostly cause water-level rises in the Wanapum unit, if there was no pumping or change in recharge. This pattern is consistent with the downward gradient in the upper CRBG on the Palouse Slope.

(3) Generally, pumping dominated water-level changes, followed by irrigation enhanced recharge as facilitated by commingling pathways. Commingling was a larger factor in upland, structurally complex areas where hydraulic-head gradients are naturally high. This pattern is similar to the pattern determined by Burns and others (2012a) in Mosier, Oregon, and could be an important factor on the Palouse Slope.

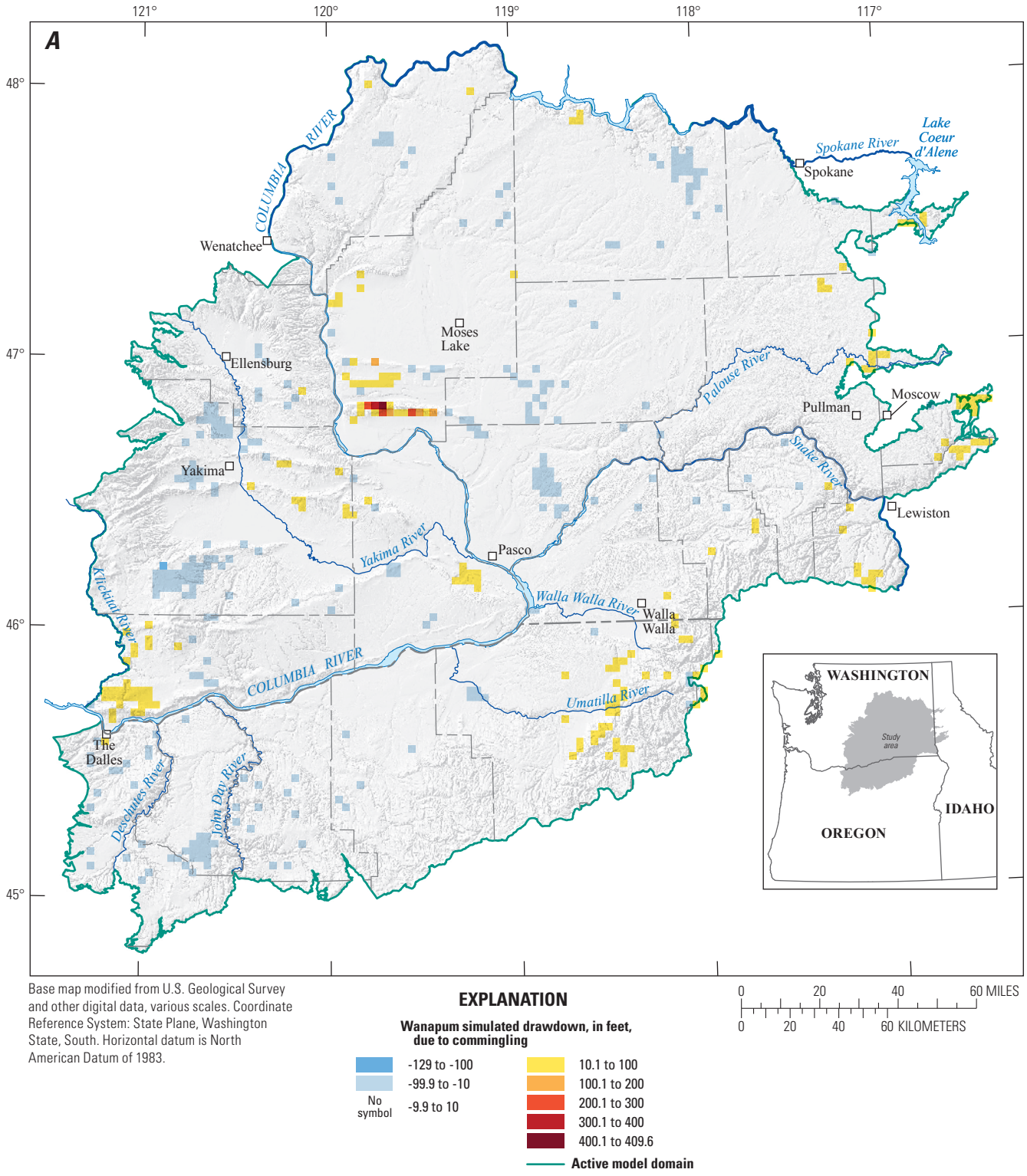

Figure 34. Simulated effects of (*A*) commingling wells only (no pumping); (*B*) pumping wells only (no commingling); and (*C*) groundwater recharge from irrigation in the Wanapum basalt unit, Columbia Plateau Regional Aquifer System, Idaho, Oregon, and Washington.

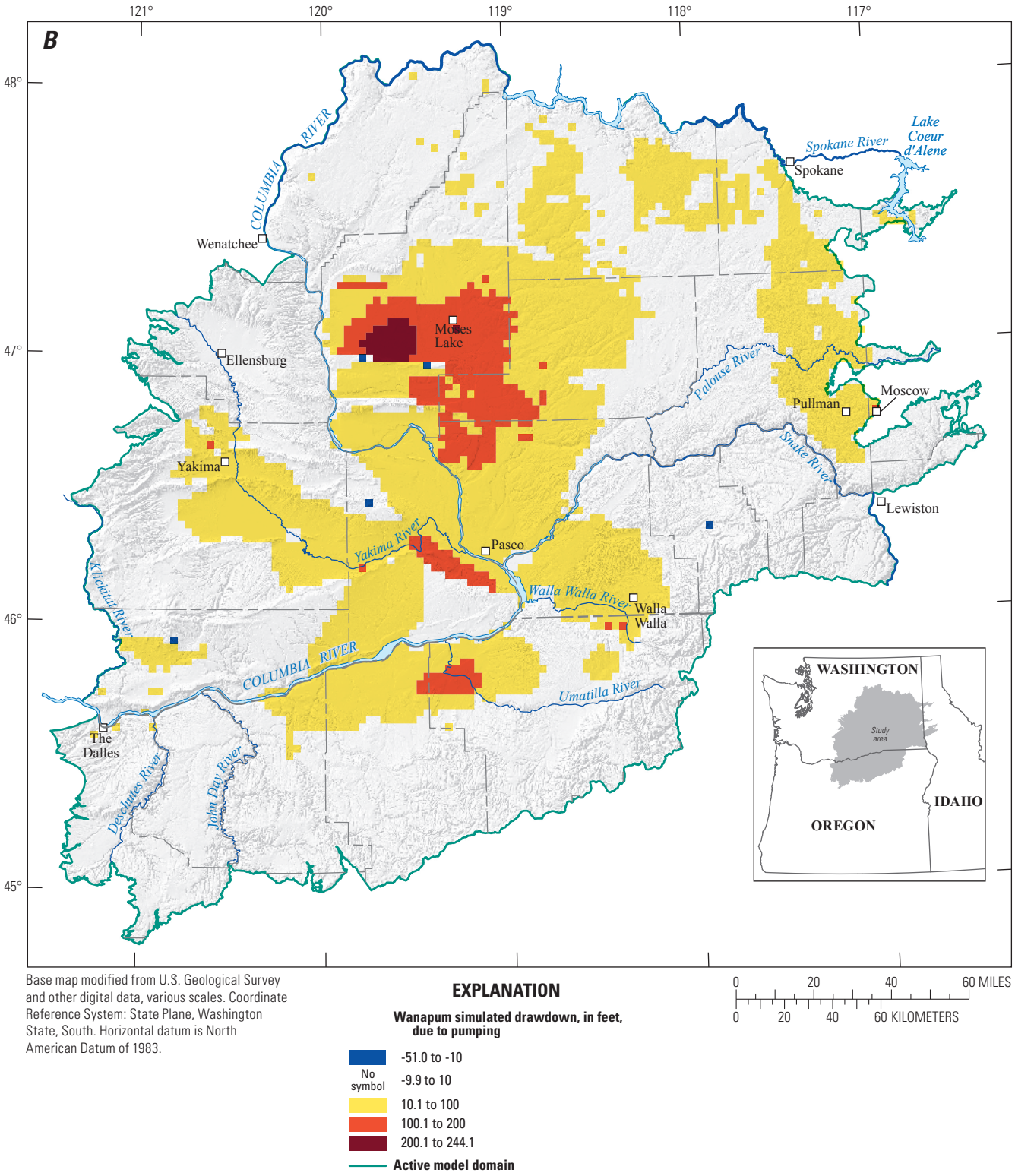

Base map modified from U.S. Geological Survey and other digital data, various scales. Coordinate Reference System: State Plane, Washington State, South. Horizontal datum is North American Datum of 1983.

Figure 34.—Continued

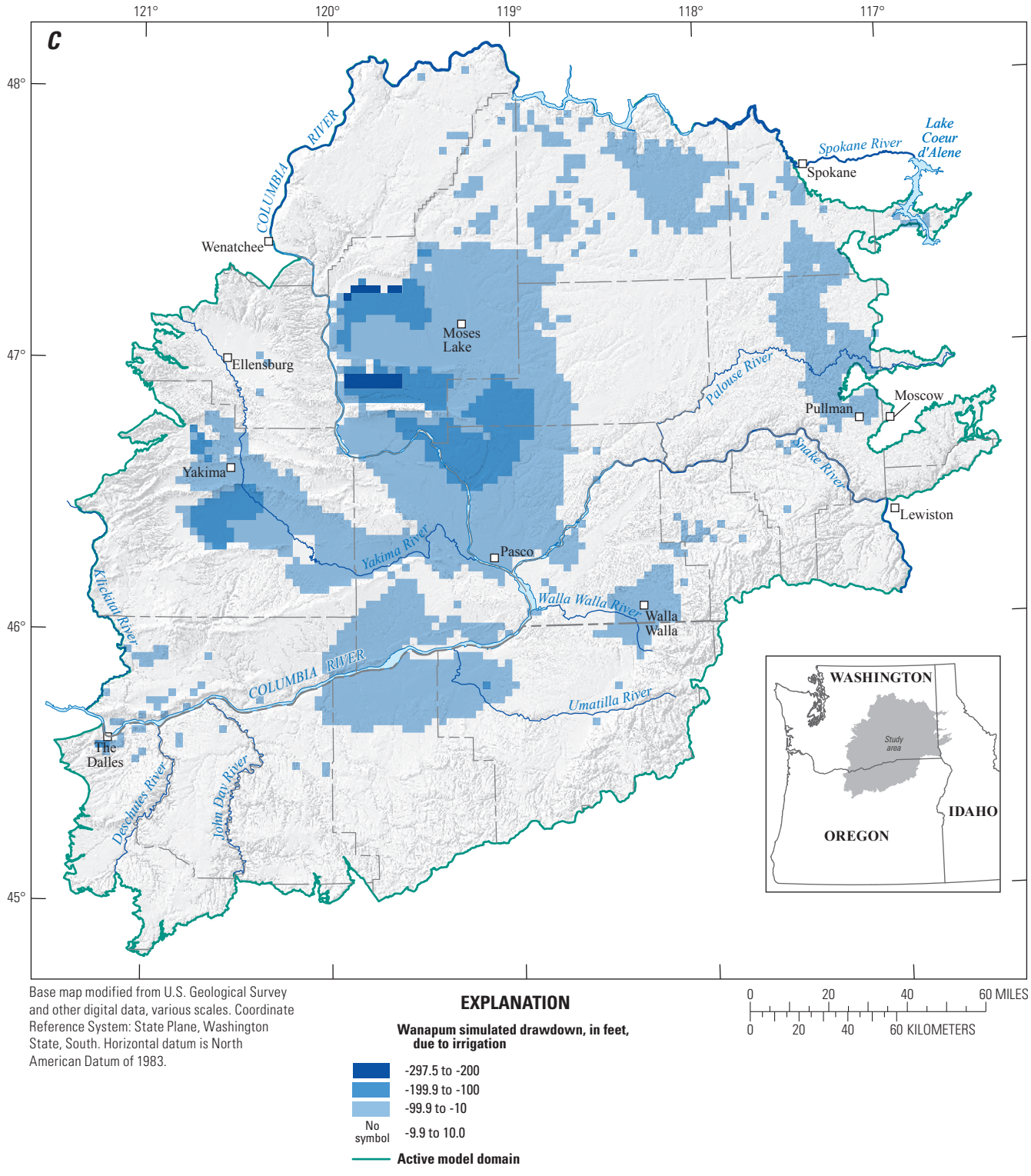

Figure 34.—Continued

Major Findings From Numerical Simulation of Groundwater Flow

The goals of the study of the CPRAS were to (1) characterize the hydrologic status of the system, (2) identify trends in groundwater storage and use, and (3) quantify groundwater availability. The simulation model was designed for evaluating and testing the conceptual model of the system defined in previous phases of the study and for evaluation of groundwater availability. In the process of accomplishing these goals, a new or improved understanding of certain aspects of the flow system was reached. Major findings from the groundwater-flow model include:

- **The use of many thin layers improve representation of vertical gradients and discrete connectivity with surface features**. This allowed for a simple representation of the permeability distribution and fewer barriers to horizontal flow. For example, the major hydraulic barrier on the Palouse Slope possibly is a linear drainage feature (erosional intersection of deeper CRBG lavas at a geologic fold) causing local changes in potentiometric surface.

- **Hydraulic heads in individual aquifers are controlled by drainage features**. Frequently, CRBG units dip at a steeper angle than the land surface. As a result, CRBG aquifers that are not exposed at land surface near the center of the basin can be exposed in upland river and stream cuts. When the rate of groundwater leakage from parts of the aquifer below the stream cut contact is lower than the recharge rate, then the aquifer fills to the altitude of the contact. In this way, a single aquifer may have old, slow moving groundwater below the discharge altitude and much younger faster-moving water filling and draining the altitudes above the spill points. The altitude controlling the head in an aquifer commonly is associated with an anticlinal fold or other geologic structure that allows connection of the aquifer with an erosional cut.

- **Horizontal-flow barriers are important for representing some hydraulic features**. These barriers can result from folds, faults, and depositional variability. Horizontal-flow barriers can vary with depth, being present in either shallow or deep units only. Deep barriers are formed by geologic structures that predate deposition of younger units. Shallow barriers may result from thrust faulting, depositional variability, and complex geometrical deformation occurring during folding and faulting. In order to understand flow barriers, more spatially and temporally dense head data may be required.

- **Water-level changes in CRBG aquifers are the result of pumping, commingling, and changes in recharge**. In areas with large-scale surface-water irrigation projects and commingling wells, model simulation results demonstrate that water-level declines are partially mitigated as recharge flows into deeper aquifers through commingling wells. In areas with little surface-water irrigation recharge, commingling is expected to result in water-level declines in higher head units as water flows from these units into lower head units.

  - The simulation results identify the effects of the simulated processes, but because this analysis was not accompanied by an uncertainty analysis, the magnitude of the effects is not well constrained.

  - Preliminary analyses indicate that commingling may vary by region.

  - Although not investigated as part of this groundwater availability study, there may be water-quality implications related to mitigation of water-level declines by surface-water recharge (for example, transport of nutrients and pesticides into deep aquifers).

- **Sufficient data do not exist to determine the possibility that hydraulic conductivity decreases with depth**. Hansen and others (1994) suggested that hydraulic conductivity decreases at depth due to overburden pressure and secondary mineralization. Because most of the data are collected above 2,000 ft below land surface, and because most of the active flow system is above this depth, the simulation results were similar, indicating that current data are insufficient to distinguish between the two competing models. Future research could be directed toward distinguishing between the two models, if desired predictions are determined to be sensitive to the difference.

- **Automated parameter estimation tends to overestimate vertical hydraulic conductivity of the CRBG units**. In areas where commingling has substantially equilibrated heads between aquifers, few water-level measurements represent predevelopment conditions, so hydraulic conductivity is overestimated (also identified by Burns and others, 2012a). In areas where vertical gradients exist, but commingling results in highly-variable water-level measurements , the use of a least-squares objective function resulted in overestimation of vertical hydraulic conductivity as the parameter estimation process seeks to fit the center-of-mass of the data, rather than the outliers that likely

represent the true magnitude of the vertical gradients largely unaffected by commingling. Future research should include novel approaches to constrain estimates of the vertical hydraulic conductivity.

- **Groundwater pumping increased substantially since the 1970s–1980s; this increase resulted in declining water levels at depth and decreased base flows over much of the study area**. The effects of pumping are mitigated somewhat by the increase of surface-water irrigation, especially in the shallow Overburden unit (Konikow, 2013), and commingling wells in some areas.

- **During dry to average years, groundwater pumping causes a net loss of groundwater in storage**. Current levels of groundwater pumping exceed recharge during all but the wettest of years.

Summary

A three-dimensional numerical model of groundwater flow was constructed for the Columbia Plateau Regional Aquifer System (CPRAS), Idaho, Oregon, and Washington, to evaluate and test the conceptual model of the system and to evaluate groundwater availability. The model described in this report can be used as a tool by water-resource managers and other stakeholders to quantitatively evaluate proposed alternative management strategies and assess the long-term availability of groundwater. The numerical simulation of groundwater flow in the CPRAS was conducted with support from the Groundwater Resources Program of the U.S. Geological Survey Office of Groundwater.

The model was constructed using the U.S. Geological Survey modular three-dimensional finite-difference groundwater-flow model, MODFLOW-NWT. The model used 3 kilometer (9,842.5 foot) grid cells that subdivided the model domain by 126 rows and 131 columns. Vertically, the model domain was subdivided into six geologic model units: the Overburden, Saddle Mountains Basalt, Mabton Interbed, Wanapum Basalt, Vantage Interbed, and Grande Ronde Basalt. The geologic units in the model were represented with 100 model layers. Soil-water balance modeling was used to estimate irrigation pumping during 1985–2007 as another component of the CPRAS availability study. These estimates were supplemented with pumping estimates for municipal, industrial, residential, and all other uses. The pumping estimates from previous studies were used to estimate pumping during 1920–84. Use of the multi-node well package for MODFLOW allowed representation of both groundwater pumping and cross-connection of aquifers through open well boreholes (commingling). Predevelopment groundwater recharge was estimated using gridded estimates of annual precipitation during 1895–2007. Recharge estimates from surface-water and groundwater irrigation application were extracted from soil-water balance modeling. The Columbia River, major tributaries, and all other surface-water features are included in the model as either river cells or drain cells.

Two separate models were constructed to simulate groundwater flow in the CPRAS: a steady-state predevelopment model representing conditions before large-scale pumping and irrigation altered the system, and a transient model representing the period 1900–2007. Calibration used an iterative approach of automated parameter-estimation techniques (steady-state predevelopment model) and traditional trial-and-error (transient model) methods. The total number of observations used in the steady-state and transient model calibrations was 10,525 and 46,460 water levels, respectively, and 50 base-flow estimates for both models.

The model simulates the shape, slope, and trends of the potentiometric surface that generally is consistent with mapped water levels. For the transient model, the mean and median difference between simulated minus measured hydraulic heads is -10 and 4 ft, respectively, with a standard deviation of 164 ft over a 5,648 ft range of measured heads. The residuals for the simulation period show that 52 percent of the simulated heads exceeded measured heads with a median residual value of 43 ft, and 48 percent were less than measured heads with a median residual value of -76 ft.

The CPRAS model was constructed to derive components of the groundwater budget and help understand the interactions of stresses, such as recharge, groundwater pumping, and commingling wells on the groundwater and surface-water system. Through these processes, the model can be used to identify trends in groundwater storage and use, and quantify groundwater availability. The annual groundwater budgets show several trends over the simulation period. Groundwater pumping was negligible until the 1950s and began to increase significantly during the 1970s and 1980s. Recharge was highly variable due to the interannual variability of precipitation, but began to increase in the late 1940s due to the increase in irrigation projects. Streamflow gains and net storage followed recharge closely, but the loss of groundwater in storage increased and stream base flow decreased as groundwater pumping increased.

The simulation model was used to evaluate and test the conceptual understanding of the system defined in previous phases of the study and to evaluate groundwater availability. In the process of accomplishing these goals, a new or improved understanding of certain aspects of the flow system was reached. Some of the major findings from the groundwater-flow model include:

1. The use of many thin layers improved representation of vertical gradients and discrete connectivity with surface features;

2. Hydraulic heads in individual aquifers are controlled by drainage features;

3. Horizontal flow barriers are important for representing some hydraulic features;

4. Water-level changes in Columbia River Basalt aquifers are the result of commingling, pumping, and irrigation recharge, with groundwater pumping having the greatest effect on water levels, followed by irrigation enhanced recharge;

5. Groundwater pumping has increased substantially since the 1970s–1980s and this increase has resulted in declining water levels at depth and decreasing base flows over much of the study area; and

6. During dry to average precipitation years, groundwater pumping causes a net loss of groundwater in storage. Groundwater pumping presently exceeds recharge during all but the wettest of years.

References Cited

Anderman, E.R., and Hill, M.C., 2000, MODFLOW-2000—The U.S. Geological Survey Modular Ground-Water Model-Documentation of the Hydrogeologic-Unit Flow (HUF) Package: U.S. Geological Survey Open-File Report 2000-342, 89 p., http://pubs.er.usgs.gov/usgspubs/ofr/ofr00342.

Anderson, M.R., and Woessner, W.W., 1992, Applied groundwater modeling simulation of flow and advective transport: San Diego/New York/Boston/London/Sydney/Tokyo/Toronto, Academic Press, Inc., 381 p.

Barker, R.A., 1979, Computer simulation and geohydrology of a basalt aquifer system in the Pullman-Moscow Basin, Washington and Idaho: Washington Department of Ecology Water-Supply Bulletin 48, 119 p.

Bauer, H.H., and Hansen, A.J., 2000, Hydrology of the Columbia Plateau Regional Aquifer System, Washington, Oregon, and Idaho: U.S. Geological Survey Water-Resources Investigations Report 96-4106, 61 p., http://pubs.er.usgs.gov/usgspubs/wri/wri964106.

Bauer, H.H., and Vaccaro, J.J., 1990, Estimates of ground-water recharge to the Columbia Plateau regional aquifer system, Washington, Oregon, and Idaho, for pre development and current land-use conditions: U.S. Geological Survey Water-Resources Investigations Report 88-4108, 37 p., http://pubs.er.usgs.gov/usgspubs/wri/wri884108.

Bergeron, M.P., Freshly, M.D., Last, G.V., and Mitchell, P.J., 1986, Development of the Hanford three-dimensional ground-water flow model: Richland, Wash., Battelle Pacific Northwest Laboratory, draft report, 14 p.

Bureau of Reclamation, 1999, Yakima River Basin Water Enhancement Project, Washington, Final Programmatic Environmental Impact Statement: Yakima, Wash., U.S. Department of Interior, Bureau of Reclamation, Pacific Northwest Region, Upper Columbia Area Office, 197 p.

Burns, E.R., Morgan, D.S., Lee, K.K., Haynes, J.V., and Conlon, T.D., 2012a, Evaluation of long-term water-level declines in basalt aquifers near Mosier, Oregon: U.S. Geological Survey Scientific Investigations Report 2012–5002, 134 p.

Burns, E.R., Morgan, D.S., Peavler, R.S., and Kahle, S.C., 2011, Three-dimensional model of the geologic framework for the Columbia Plateau Regional Aquifer System, Idaho, Oregon, and Washington: U.S. Geological Survey Scientific Investigations Report 2010-5246, 44 p., http://pubs.usgs.gov/sir/2010/5246/.

Burns, E.R., Snyder, D.T., Haynes, J.V., and Waibel, M.S., 2012b, Groundwater status and trends for the Columbia Plateau Regional Aquifer System, Washington, Oregon, and Idaho: U.S. Geological Survey Scientific Investigations Report 2012–5261, 52 p.

Calkins, F.V., 1905, Geology and water resources of a portion of east-central Washington: U.S. Geological Survey Water-Supply Paper 118, 96 p.

Cline, D.R., 1984, Ground-water levels and pumpage in east-central Washington, including the Odessa - Lind area, 1967 to 1981: Washington State Department of Ecology, Water-Supply Bulletin No. 55, 34 p.

Cline, D.R., and Collins, C.A., 1992, Ground-water pumpage from the Columbia Plateau, Washington and Oregon, 1945 to 1984: U.S. Geological Survey Water-Resources Investigations Report 90-4085, 31 p., 5 pls., http://pubs.er.usgs.gov/publication/wri904085.

Davies-Smith, A., Bolke, E.L., and Collins, C.A., 1988, Geohydrology and digital simulation of the ground-water flow system in the Umatilla Plateau and Horse Heaven Hills area, Oregon and Washington: U.S. Geological Survey Water-Resources Investigations Report 87-4268, 72 p., http://pubs.er.usgs.gov/usgspubs/wri/wri874268.

Doherty, J.E., 2010, PEST, Model-independent parameter estimation—User manual (5th ed., with additions): Brisbane, Australia, Watermark Numerical Computing, variously paged.

Doherty, J.E., and Hunt, R.J., 2010, Approaches to highly parameterized inversion—A guide to using PEST for groundwater-model calibration: U.S. Geological Survey Scientific Investigations Report 2010–5169, 59 p., http://pubs.usgs.gov/sir/2010/5169/.

Drost, B.W., Ely, D.M., and Lum, W.E., 1999, Conceptual model and numerical simulation of the ground-water-flow system in the unconsolidated sediments of Thurston County, Washington: U.S. Geological Survey Water-Resources Investigations Report 99-4165, 106 p., http://pubs.usgs.gov/wri/wri994165/.

Drost, B.W., Whiteman, K.J., and Gonthier, J.B., 1990, Geologic framework of the Columbia Plateau aquifer system, Washington, Oregon, and Idaho: U.S. Geological Survey Water-Resources Investigations Report 87-4238, 10 p., http://pubs.er.usgs.gov/publication/wri874238.

Ely, D.M., Bachmann, M.P., and Vaccaro, J.J., 2011, Numerical simulation of groundwater flow for the Yakima River Basin aquifer system, Washington: U.S. Geological Survey Scientific Investigations Report 2011-5155, 90 p., http://pubs.usgs.gov/sir/2011/5155/.

Faunt, C.C., Blainey, J.B., Hill, M.C., D'Agnese, F.A., and O'Brien, G.M., 2010, Transient numerical model, chapter F *of* Belcher, W.R. ed., Death Valley regional groundwater flow system, Nevada and California—Hydrogeologic framework and transient groundwater flow model: U.S. Geological Professional Paper 1711, p. 257–344. (Also available at http://pubs.usgs.gov/pp/1711/.)

Faunt, C.C., Hanson, R.T., Belitz, Kenneth, Schmid, Wolfgang, Predmore, S.P., Rewis, D.L., and McPherson, Kelly, 2009, Numerical model of the hydrologic landscape and groundwater flow in California's Central Valley, chapter C *of* Faunt C.C., ed., Groundwater availability of the Central Valley aquifer, California: U.S. Geological Survey Professional Paper 1766, p. 121–212, http://pubs.usgs.gov/pp/1766/.

Gannett, M.W., and Lite, K.E., Jr., 2004, Simulation of regional ground-water flow in the upper Deschutes Basin, Oregon: U.S. Geological Survey Water-Resources Investigations Report 03–4195, 84 p.

Hansen, A.J., Vaccaro, J.J., and Bauer, H.H., 1994, Ground-water flow simulation of the Columbia Plateau regional aquifer system, Washington, Oregon, and Idaho: U.S. Geological Survey Water-Resources Investigations Report 91-4187, 101 p., 15 pls., http://pubs.er.usgs.gov/usgspubs/wri/wri914187.

Harbaugh, A.W., 2005, MODFLOW-2005—The U.S. Geological Survey modular groundwater model—The ground-water flow process: U.S. Geological Survey Techniques and Methods 6-A16, variously paged, http://pubs.usgs.gov/tm/2005/tm6A16/.

Hill, M.C., 1998, Methods and guidelines for effective model calibration: U.S. Geological Survey Water-Resources Investigations Report 98-4005, 90 p.

Hsieh, P.A., and Freckleton, J.R., 1993, Documentation of a computer program to simulate horizontal-flow barriers using the U.S. Geological Survey's modular three-dimensional finite-difference ground-water flow model: U.S. Geological Survey Open-File Report 92-477, 32 p., http://pubs.er.usgs.gov/publication/ofr92477.

Jones, M.A., and Vaccaro, J.J., 2008, Extent and depth to top of basalt and interbed hydrogeologic units, Yakima River basin aquifer system, Washington: U.S. Geological Survey Scientific Investigations Report 2008-5045, 22 p., http://pubs.usgs.gov/sir/2008/5045/.

Jones, M.A., Vaccaro, J.J., and Watkins, A.M., 2006, Hydrogeologic framework of sedimentary deposits in six structural basins, Yakima River basin, Washington: U.S. Geological Survey Scientific Investigations Report 2006-5116, 24 p., http://pubs.usgs.gov/sir/2006/5116/.

Kahle, S.C., Morgan, D.S., Welch, W.B., Ely, D.M., Hinkle, S.R., Vaccaro, J.J., and Orzol, L.L., 2011, Hydrogeologic framework and hydrologic budget components of the Columbia Plateau Regional Aquifer System, Washington, Oregon, and Idaho: U.S. Geological Survey Scientific Investigations Report 2011–5124, 66 p., http://pubs.usgs.gov/sir/2011/5124/.

Kahle, S.C., Olsen, T.D., and Morgan, D.S., 2009, Geologic setting and hydrogeologic units of the Columbia Plateau Regional Aquifer System, Washington, Oregon, and Idaho: U.S. Geological Survey Scientific Investigations Map 3088, 1 sheet, http://pubs.usgs.gov/sim/3088/.

Kinnison, H.B., and Sceva, J.E., 1963, Effects of hydraulic and geologic factors on streamflow of the Yakima River Basin, Washington: U.S. Geological Survey Water-Supply Paper 1595, 134 p., http://pubs.er.usgs.gov/usgspubs/wsp/wsp1595.

Konikow, L.F., 2013, Groundwater depletion in the United States (1900–2008): U.S. Geological Survey Scientific Investigations Report 2013−5079, 63 p., http://pubs.usgs.gov/sir/2013/5079.

Konikow, L.F., Hornberger, G.Z., Halford, K.J., and Hanson, R.T., 2009, Revised multi-node well (MNW2) package for MODFLOW ground-water flow model: U.S. Geological Survey Techniques and Methods 6–A30, 67 p.

Lindholm, G.F., and Vaccaro, J.J., 1988, Region 2, Columbia Lava Plateau, *in* Back, William, Rosenshein, J.S., and Seaber, P.R., eds., Hydrogeology, v. O-2—The geology of North America: Boulder, Colo., Geological Society of America, p. 37–50.

Lum, W.E., II, Smoot, J.L., and Ralston, D.R., 1990, Geohydrology and numerical model analysis of groundwater flow in the Pullman-Moscow area, Washington and Idaho: U.S. Geological Survey Water-Resources Investigations Report 89-4103, 73 p., http://pubs.er.usgs.gov/usgspubs/wri/wri894103.

Magirl, C.S., and Olsen, T.D., 2009, Navigability potential of Washington rivers and streams determined with hydraulic geometry and a geographic information system: U.S. Geological Survey Scientific Investigations Report 2009–5122, 22 p., http://pubs.usgs.gov/sir/2009/5122/.

Newcomb, R.C., 1965, Geology and ground-water resources of the Walla Walla River Basin, Washington-Oregon: Washington Division of Water Resources, Water-Supply Bulletin 21, 151 p., accessed January 31, 2011, at http://pubs.er.usgs.gov/publication/70047774.

Newcomb, R.C., 1969, Effect of tectonic structure on the occurrence of ground water in the basalt of the Columbia River Group of The Dalles area, Oregon and Washington: U.S. Geological Survey Professional Paper 383-C, 33 p., 1 pl., http://pubs.er.usgs.gov/publication/pp383C.

Niswonger, R.G., Panday, Sorab, and Ibaraki, Motomu, 2011, MODFLOW-NWT, A Newton formulation for MODFLOW-2005: U.S. Geological Survey Techniques and Methods 6–A37, 44 p.

Packard, F.A., Hansen, A.J., Jr., and Bauer, H.H., 1996, Hydrogeology and simulation of flow and the effects of development alternatives on the basalt aquifers of the Horse Heaven Hills, south-central Washington: U.S. Geological Survey Water-Resources Investigations Report 94-4068, 92 p., 2 pls., http://pubs.er.usgs.gov/publication/wri944068.

Parker, G.L., and Storey, F.B., 1916, Water powers of the Cascade Range, Part III—Yakima River Basin: U.S. Geological Survey Water Supply Paper 369, 169 p., 16 pls., http://pubs.er.usgs.gov/publication/wsp369.

Piper, A.M., 1932, Geology and ground-water resources of the Dalles region, Oregon: U.S. Geological Survey Water-Supply Paper 659-B, p. 107–189.

Porcello, J., Kindsey, K., Tonkin, M., Muffels, C., and Karanovic, M., 2010, Groundwater model development process for the Columbia Basin Ground Water Management Area of Adams, Franklin, Grant, and Lincoln Counties, Washington: Prepared by the Columbia Basin Ground Water Management Area of Adams, Franklin, Grant and Lincoln Counties, variously paged.

PRISM Climate Group, 2004, PRISM Spatial Climate Datasets: Corvallis, Oregon State University, accessed October 1, 2009, at http://www.prismclimate.org.

Reidel, S.P., Johnson, V.G., and Spane, F.A., 2002, Natural gas storage in basalt aquifers of the Columbia Basin, Pacific Northwest USA—A guide to site characterization: Richland, Wash., Pacific Northwest National Laboratory, variously paged, accessed November 3, 2010, at http://www.pnl.gov/main/publications/external/technical_reports/PNNL-13962.pdf.

Reilly, T.E., Dennehy, K.F., Alley, W.M., and Cunningham, W.L., 2008, Ground-water availability in the United States: U.S. Geological Survey Circular 1323, 70 p., http://pubs.usgs.gov/circ/1323/.

Schwennsen, A.T., and Meinzer, O.E., 1918, Ground water in Quincy Valley, Washington: U.S. Geological Survey Water-Supply Paper 425-E, p. 131–161.

Senay, G.B., Budde, M., Verdin, J.P., and Melesse, A.M., 2007, A coupled remote sensing and simplified surface energy balance approach to estimate actual evapotranspiration from irrigated fields: Sensors, v. 7, p. 979–1000.

Simley, J.D., and Carswell, Jr., W.J., 2009, The National Map—Hydrography: U.S. Geological Survey Fact Sheet 2009-3054, 4 p.

Simons, W.D., 1953, Irrigation and streamflow depletion in Columbia River basin above The Dalles, Oregon: U.S. Geological Survey Water Supply Paper 1220, 126 p., 1 pl., http://pubs.er.usgs.gov/usgspubs/wsp/wsp1220.

Sinclair, K.A., and Pitz, C.F., 1999, Estimated baseflow characteristics of selected Washington rivers and streams: Washington State Department of Ecology, Water-Supply Bulletin No. 60, 181 p.

Sloto, R.A., and Crouse, M.Y., 1996, HYSEP—A computer program for streamflow hydrograph separation and analysis: U.S. Geological Survey Water Resources Investigation Report 96-4040, 46 p.

Smith, G.O., 1901, Geology and water resources of a portion of Yakima County, Washington: U.S. Geological Survey Water-Supply Paper 55, 68 p.

Snyder, D.T., and Haynes, J.V., 2010, Groundwater conditions during 2009 and changes in groundwater levels from 1984 to 2009, Columbia Plateau Regional Aquifer System, Washington, Oregon, and Idaho: U.S. Geological Survey Scientific Investigations Report 2010–5040, 12 p., http://pubs.usgs.gov/sir/2010/5040/.

State of Washington Office of Financial Management, 2014, Washington's Rank in the Nations Agriculture—2013 Data Book: State of Washington Office of Financial Management, accessed March 21, 2014, at http://www.ofm.wa.gov/databook/pdf/databook.pdf.

Stearns, R.T., 1942, Hydrology of lava-rock terranes, chap. XV, *in* Meinzer, O.E., ed., Hydrology: New York, McGraw-Hill, 712 p.

Tanaka, H.H., Hansen, A.J., Jr., and Skrivan, J.A., 1974, Digital-model study of ground-water hydrology, Columbia Basin Irrigation Project area, Washington: State of Washington Department of Ecology Water-Supply Bulletin 40, 60 p.

Taylor, G.C., Jr., 1948, Ground water in the Quincy Basin, Wahluke Slope, and Pasco Slope subareas of the Columbia Basin Project, Washington: U.S. Geological Survey Open-File Report, 182 p.

Tolan, T.L., Reidel, S.P., Beeson, M.H., Anderson, J.L., Fecht, K.R., and Swanson, D.A., 1989, Revisions to the estimates of the areal extent and volume of the Columbia River Basalt Group, *in* Reidel, S.P., and Hooper, P.R., eds., Volcanism and tectonism in the Columbia River flood-basalt province: Boulder, Colo., Geological Society of America Special Paper 239, p. 1-20, doi: 10.1130/SPE239-p1.

Troutman, B.M., 1985, Errors and parameter estimation in precipitation-runoff modeling 2—Case Study: Water Resources Research, v. 21, no. 8, p. 1,214–1,222.

U.S. Department of Agriculture, 2007, Census of agriculture—2007 census publications: U.S. Department of Agriculture, accessed June 16, 2009, at http://www.agcensus.usda.gov/Publications/2007/Online_Highlights/Rankings_of_Market_Value/Washington/index.asp.

U.S. Geological Survey, 2004, National hydrography dataset—Watershed boundary dataset: U.S. Geological Survey database, accessed March 13, 2014, at http://nhd.usgs.gov/index.html.

Vaccaro, J.J., 1986, Plan of study for the regional aquifer-system analysis, Columbia Plateau, Washington, northern Oregon, and northwestern Idaho: U.S. Geological Survey Water-Resources Investigations Report 85-4151, 25 p.

Vaccaro, J.J., 1999, Summary of the Columbia Plateau Regional Aquifer-System Analysis, Washington, Oregon, and Idaho: U.S. Geological Survey Professional Paper 1413-A, 51 p.

Vaccaro, J.J., Jones, M.A., Ely, D.M., Keys, M.E., Olsen, T.D., Welch, W.B., and Cox, S.E., 2009, Hydrogeologic framework of the Yakima River Basin aquifer system, Washington: U.S. Geological Survey Scientific Investigations Report 2009–5152, 106 p., http://pubs.usgs.gov/sir/2009/5152/.

Vermeul, V.R., Bergeron, M.P., Cole, C.R., Murray, C.J., Nichols, W.E., Scheibe, T.D., Thorne, P.D., Waichler, S.R., and Xie, Y., 2003, Transient inverse calibration of the site-wide groundwater-flow model (ACM-2)—FY03 progress report: Richland, Wash., Pacific Northwest National Laboratory, PNNL-14398, variously paged.

Vermeul, V.R., Cole, C.R., Bergeron, M.P., Thorne, P.D., and Wurstner, S.K., 2001, Transient inverse calibration of site-wide groundwater model to Hanford Operational Impacts from 1943 to 1996—Alternative conceptual model considering interaction with uppermost basalt confined aquifer: Richland, Wash., Pacific Northwest National Laboratory, PNNL-13623, variously paged.

Waring, G.A., 1913, Geology and water resources of a portion of south-central Washington: U.S. Geological Survey Water-Supply Paper 316, 46 p.

Weiss, Emanuel, 1982, A computer program for calculating relative-transmissivity input arrays to aid model calibration: U.S. Geological Survey Open-File Report 82-447, 18 p.

Whiteman, K.J., Vaccaro, J.J., Gonthier, J.B., and Bauer, H.H., 1994, The hydrogeologic framework and geochemistry of the Columbia Plateau Regional Aquifer System in Washington, Oregon, and Idaho: U.S. Geological Survey Professional Paper 1413-B, 73 p.

Wurstner, S.K., Thorne, P.D., Chamness, M.A., Freshley, M.D., and Williams, M.D., 1995, Development of a three-dimensional groundwater model of the Hanford Site unconfined aquifer system—FY 1995 status report: Richland, Wash., Pacific Northwest Laboratory, PNL-10886, variously paged.

Publishing support provided by the U.S. Geological Survey
Publishing Network, Tacoma Publishing Service Center

For more information concerning the research in this report, contact the
Director, Washington Water Science Center
U.S. Geological Survey
934 Broadway, Suite 300
Tacoma, Washington 98402
http://wa.water.usgs.gov

ISSN 2328-0328 (online)
http://dx.doi.org/10.3133/sir20145127